REVIEW

Meteorological Research Enabled by Rapid-Scan Radar Technology

DAVID J. BODINE[a,b] AND CASEY B. GRIFFIN[c]

[a] School of Meteorology, University of Oklahoma, Norman, Oklahoma
[b] Advanced Radar Research Center, University of Oklahoma, Norman, Oklahoma
[c] State University of New York at Brockport, Brockport, New York

(Manuscript received 21 November 2022, in final form 4 October 2023, accepted 11 October 2023)

ABSTRACT: The scientific community has long acknowledged the importance of high-temporal-resolution radar observations to advance science research and improve high-impact weather prediction. Development of innovative rapid-scan radar technologies over the past two decades has enabled radar volume scans of 10–60 s compared to 3–5 min with traditional parabolic dish research radars and the WSR-88D radar network. This review examines the impact of rapid-scan radar technology, defined as radars collecting volume scans in 1 min or less, on atmospheric science research spanning different subdisciplines and evaluates the strengths and weaknesses of the use of rapid-scan radars. In particular, a significant body of literature has accumulated for tornado and severe thunderstorm research and forecasting applications, in addition to a growing number of studies of convection. Convection research has benefited substantially from more synchronous vertical views, but could benefit more substantially by leveraging multi-Doppler wind retrievals and complementary in situ and remote sensors. In addition, several years of forecast evaluation studies are synthesized from radar testbed experiments, and the benefits of assimilating rapid-scan radar observations are analyzed. Although the current body of literature reflects the considerable utility of rapid-scan radars to science research, a weakness is that limited advancements in understanding of the physical mechanisms behind observed features have been enabled. There is considerable opportunity to bridge the gap in physical understanding with the current technology using coordinated efforts to include rapid-scan radars in field campaigns and expanding the breadth of meteorological phenomena studied.

SIGNIFICANCE STATEMENT: Recently developed rapid-scan radar technologies, capable of collecting volumetric (i.e., three-dimensional) measurements in 10–60 s, have improved temporal sampling of weather phenomena. This review examines the impact of these radar observations from the past two decades on science research and emerging operational capabilities. Substantial breadth and impact of research is evident for tornado research and forecasting applications, in addition to documentation of other rapidly evolving phenomena associated with deep convection, such as tornadoes, hail, lightning, and tropical cyclones. This review identifies the strengths and weaknesses of how these radars have been used in scientific research to inform future studies, emerging from the increasing availability and capability of rapid-scan radars. In addition, this review synthesizes research that can benefit future operational radar decisions.

KEYWORDS: Severe storms; Mesoscale systems; Radars/Radar observations; Numerical weather prediction/forecasting

1. Introduction

Important technological developments in weather radar, such as Doppler and dual-polarization capabilities (e.g., Brown et al. 1971; McCormick and Hendry 1975; Doviak and Zrnić 1993; Wurman et al. 2021), have provided key observing capabilities and enabled important advancements in many atmospheric science subdisciplines, ranging from studies of high-impact weather phenomena to cloud and microphysical processes (e.g., Byers and Braham 1948; Ligda 1950; Marshall et al. 1955; Wurman et al. 1996; Vivekanandan et al. 1999; Wakimoto and Srivastava 2003; Wurman et al. 2021; Bluestein et al. 2022). A major limitation of radar observations is that traditional scanning radars may take 10–20 s to collect a single horizontal scan called a plan-position indicator (PPI) or vertical scan called a range–height indicator (RHI). To obtain a volume scan, comprising of PPIs at increasing elevation angles, traditional radars can take anywhere from 2 to 7 min to complete depending on the number of angles selected (typically 10–15) (e.g., National Research Council 2002; Kosiba et al. 2013b; Miller et al. 2020). Tornadoes are an obvious example where slow volume scan times insufficiently sample the phenomena. Tornadoes can develop in <30 s and, in some instances, have a full life cycle of less than 1 min (e.g., Bluestein et al. 2003a). In addition, the evolution of deep convective clouds or the generation of hail and severe winds require volumetric observations at time scales of 1 min or less (e.g., Carbone et al. 1985; Zrnić et al. 2007; Heinselman et al. 2008; Isoda et al. 2018). Acknowledging these observational

Corresponding author: David J. Bodine, bodine@ou.edu

DOI: 10.1175/MWR-D-22-0324.1

limitations, decadal surveys and National Science Foundation–led workshops have recognized that rapid-scan radar systems must be prioritized to advance scientific understanding of high-impact weather phenomena (Bluestein et al. 2014; Geerts et al. 2018; National Academies of Science, Engineering, and Medicine 2018). The evident gap in temporal sampling and technological advancements spurred new rapid-scan radar technology for basic science and operational research in the 2000s and 2010s (Wurman and Randall 2001; Zrnić et al. 2007; Weber et al. 2007; Bluestein et al. 2010; Pazmany et al. 2013; Isom et al. 2013; Yoshikawa et al. 2013; Kurdzo et al. 2017; Weber et al. 2021).

In addition to the basic research motivation for higher-temporal-resolution radar observations, it has long been recognized that the current operational radar network in the United States has inadequate temporal resolution (4–7-min volume scan times) to capture and predict the development of many severe weather phenomena (National Research Council 2002; Zrnić et al. 2007). Phased array radars (PARs) can address this temporal sampling limitation by electronically forming and steering a radar beam. Specifically, PARs use hundreds or thousands of small antennas to synthesize a radar beam without requiring mechanical motion of the antenna. With the operational radar network requiring replacement by 2040 (NOAA 2020), NOAA began testing PAR technology in the late 2000s to evaluate its capabilities and limitations in a future operational radar network using the National Weather Radar Test bed (NWRT) PAR (Weber et al. 2007; Zrnić et al. 2007). This research has explored whether reduced volume scan times can improve operational warning performance (e.g., Heinselman et al. 2012, 2015; Bowden et al. 2015) and benefit short-term numerical weather prediction (NWP) forecasts through data assimilation (e.g., Yussouf and Stensrud 2010; Supinie et al. 2017).

Although rapid-scan technology is still maturing, an initial body of over 100 publications have been published to date. It is important to determine from these publications whether rapid-scan radar technology has facilitated much-anticipated advancements in scientific understanding and operational capability. Specifically, have faster observations elucidated physical processes that were previously undetected or undersampled by slower scanning radar systems? Additionally, has rapid-scan technology improved key operational warning and numerical weather prediction performance metrics?

To address these key questions, this study provides a critical review of the science contributions enabled by rapid-scan radar technology over the past two decades. Although recent papers have captured a vision for future PAR science research (Kollias et al. 2022), reviewed PAR technology (Palmer et al. 2022), and described NOAA-supported, operational PAR research (Weber et al. 2021), a critical review of rapid-scan radar science research across a broad range of topics has yet to be conducted. In this review, the most and least effective approaches to using rapid-scan radars are noted, as well as the impacts of technological limitations. This study will illuminate major scientific gaps where rapid-scan radars have been underutilized. Approximately half of the papers reviewed here deal with the subject of tornadoes or supercells, whereas most other studies have focused on other severe hazards or convective processes. The large emphasis on supercells is unsurprising given the number of high-impact phenomena that evolve on very short time scales within severe convective storms. However, the imbalance in publications illustrates the scientific gaps arising from the underutilization of PARs outside of severe storm research, particularly for nonconvective weather applications (e.g., boundary layer processes, nonconvective precipitation).

The scope of this review is limited to scientific studies using rapid-scan radar observations, herein defined as radars collecting volume scans in 1 min or less. The upper limit was chosen due to the ubiquity of 1-min data in operational testbeds, whereas many research applications require faster volumetric scans than 1 min. In a few instances, rapidly collected observations from radars scanning at a single-elevation angle or volumetric sector scans are explored, where the goal of these studies was to examine the benefits of rapid-scan technology prior to it being broadly available. As an example, the Collaborative Adaptive Sensing of the Atmosphere (CASA) radar network employed PPI and targeted sector scans to obtain 1-min volume scans (McLaughlin et al. 2009; Brotzge et al. 2010; Mahale et al. 2012). In addition to studies documenting very fast changes (e.g., tens of seconds), studies leveraging rapid-scan data to finely resolve features evolving on longer time scales (e.g., <5–10 min) will be discussed since traditional scanning radars only marginally resolve this evolution with two to three volume scans (Koch et al. 1983; Carbone et al. 1985; Trapp and Doswell 2000; Majcen et al. 2008).

This review is organized into the following sections. A brief review of rapid-scan radar technologies used in the scientific studies is presented in section 2. Section 3 examines scientific discoveries of rapidly evolving tornado characteristics during various stages of the tornado life cycle. In section 4, the broader applications of rapid-scan radars to mesoscale convective processes, including hailstorms, damaging winds, flash flooding, lightning, and tropical cyclones are discussed. The improvements in three-dimensional wind retrievals are examined in section 5. In section 6, the potential benefits of rapid-scan radar data to improve operational forecasts are reviewed, including warning performance evaluations and numerical weather prediction experiments. The review concludes with a summary and discussion of the successes and limitations of rapid-scan radar research to date (section 7).

2. Rapid-scan radar systems used in science research

Different types of rapid-scan radar systems have been developed for science and operational research applications. In this section, an introduction to these radar systems and associated technologies that enable the rapid-scan observations are provided. The strengths and weaknesses of the different radar technologies are also examined.

A summary of the specifications of the rapid-scan radar systems discussed in this study are provided in Table 1, including the type of technology, polarization, frequency band, beamwidth, and volume scan times. Most of these radar systems employ PAR technology, and the reader is referred to Zrnić et al. (2007), Weber et al. (2021), and Palmer et al. (2022) for

TABLE 1. Specifications of rapid-scan radar systems. Volume scan time is defined as the time it takes to collect at least 10 elevation angles. For the AIR and NWRT PAR, sector scans were collected rather than PPIs.

Radar system	Antenna type	Technology type	Polarization	Frequency band	Beamwidth (azimuth, elevation)	Volume scan time
Rapid DOW	PAR	Frequency-based, electronic steering	Single	X	0.9°, 0.9°	10–20 s
NWRT PAR	PAR	Phase-based steering, electronic steering	Single	S	1.5°, 1.5°	40–60 s
MWR-05XP	PAR	Phase-based steering, electronic steering	Single	X	1.8°, 2.0°	5–10 s
RaXPol	Parabolic dish	Frequency hopping	Dual	X	1.0°, 1.0°	20–30 s
AIR	PAR	Imaging	Single	X	1.0°, 1.0°	5–10 s
PAWR (Japan)	PAR	Imaging	Single	X	1.0°, 1.0°	10–30 s

a more detailed discussion of PARs. One exception is the Rapid X-band Polarimetric (RaXPol) radar (Pazmany et al. 2013), which uses fast mechanical steering of a parabolic dish antenna. For volume scan times, which do not have a universal definition, a volume scan is defined as the time necessary to complete at least 10 elevation angles in a PPI, or in the case of AIR and NWRT PAR, 90°–180° sector scans.

The first mobile phased-array weather observations were collected using the Rapid Doppler on Wheels (DOW) in 2003. The Rapid DOW is a radar that employs a vertically aligned array of slotted waveguide antennas. The transmitter operates over a wide range of frequencies (9.3–9.7 GHz) within X band to steer the radar beam electronically in elevation while rotating mechanically in azimuth (Wurman and Randall 2001; Wurman et al. 2021). Specifically, the use of different frequencies changes the phase of the transmitted wave at each antenna, thus altering the elevation angle of the radar beam through constructive and destructive wave interference. Using such frequency steering, the Rapid DOW collects single-polarization volumetric observations at up to six elevation angles in 5–10 s.

The first rapid-scan radar used for operational network testing was the NWRT PAR located at a fixed site in Norman, Oklahoma (Weber et al. 2007; Zrnić et al. 2007), which became operational in 2003 and was developed through partnerships among government, industry, and academia. Operating at S band, the NWRT PAR electronically steers the radar beam in azimuth and elevation by introducing phase delays at each of its 4352 elements. Single-polarization volumetric 90° sector scans were collected as fast as every 40 s (Table 1). Using a similar phase-based steering approach, the Mobile Weather Radar 2005 X-band (MWR-05XP; Bluestein et al. 2010) was a single-polarization, mobile radar that electronically steers a pencil beam in elevation while rotating in azimuth.[1] Compared to the Rapid DOW and other rapid-scan radar systems, a notable disadvantage is that the beamwidths for the NWRT PAR and MWR-05XP are 1.5–2 times larger.

Whereas these first PARs electronically steered a pencil beam, imaging radars employ a different approach to collect rapid observations. Specifically, imaging radars transmit a wider or "spoiled" beam in one or two dimensions and then employ multiple narrow beams on receive to fill the illuminated area. In contrast, previous PARs and parabolic dish radars transmit and receive with the same radar beam pattern. For example, a typical pencil beam radar's transmit or receive beamwidth is 1° × 1° in azimuth and elevation, whereas an imaging radar's transmit beamwidth could be 10° or 20° in elevation and 1° in azimuth. In the imaging radar case, multiple beams are formed simultaneously on receive using digital beamforming by applying different combinations of complex weights to the received data (Capon 1969; Skolnik 2001). Multiple receive beams obviate the need to steer the radar beam mechanically or electronically in time, providing even higher temporal resolution than PARs that steer a pencil beam between sequential pulses or dwells.

Leveraging imaging technology, the Atmospheric Imaging Radar (AIR) and X-band weather radar (PAWR) collected the first imaging radar observations of weather in the early 2010s. The AIR was a mobile, X-band radar that employed imaging using a 20°-wide spoiled beam on transmit in the vertical plane (Isom et al. 2013; Nai et al. 2013). The PAWR is a fixed-site radar that employs a 10°-wide spoiled beam and uses digital beamforming to obtain a native 1.0° beamwidth in azimuth and elevation based on antenna aperture (Yoshikawa et al. 2013). With both imaging systems, an arbitrary number of 1.0° beamwidth receive beams (typically oversampled at 0.5°) can be formed within a vertical column, eliminating any gaps in vertical coverage.

While the previous PAR systems improved temporal resolution, they lacked dual-polarization capabilities since dual-polarization PAR technology was not yet sufficiently mature. To address the challenge of obtaining accurate, rapid-scan, polarimetric measurements, the Rapid X-band Polarimetric (RaXPol) radar was developed and became operational in 2011 (Pazmany et al. 2013). RaXPol is a mobile, traditional parabolic dish radar that combines very fast azimuthal rotation (180° s^{-1}) of a parabolic dish antenna with frequency hopping, a technique that changes the transmit frequency between successive pulse pairs to obtain independent measurements (e.g., ~5–10 separate frequencies depending on scan mode). Frequency hopping enables radar measurements to be obtained within a shorter dwell, and thus allows RaXPol to employ fast pedestal rotation. Using this approach, RaXPol has provided the first extensive rapid-scan, polarimetric radar datasets for science research (e.g., Snyder and Bluestein 2014; Bluestein et al. 2015).

[1] Electronic backscanning was used to maintain the same beam position in azimuth, even as the radar rotates mechanically in azimuth. This was done to minimize beam smearing that otherwise occurs as the radar mechanically rotates during data collection.

Although these systems greatly improve temporal resolution compared to common parabolic dish radars, notable limitations must be considered. Most fine-scale rapid-scan systems have beamwidths comparable to traditional, pencil-beam radars, particularly those systems specifically designed for science research (e.g., Rapid DOW, AIR, RaXPol, PAWR). However, many of the phased arrays were obtained from military surplus (NWRT PAR, MWR-05XP), and thus they have wider beamwidths since the radar designs were not specifically tailored to science research. Additionally, the PAR systems in Table 1 have reduced capability of detecting weak signals (low sensitivity) and increased sidelobe contamination (i.e., from signals outside the main beam) compared to parabolic dish antennas. In particular, imaging systems such as the AIR and PAWR suffer the most substantial sidelobe contamination and reduction in sensitivity. As a result of relatively poor sensitivity, clear-air studies using these rapid-scan radar systems have been relatively limited.

All of the aforementioned systems except RaXPol transmit and receive only one polarization, precluding extensive studies of microphysical processes that leverage polarimetric observations to obtain more detailed information about hydrometeor characteristics (e.g., Kumjian and Ryzhkov 2010; Kennedy and Rutledge 2011; Kumjian 2013; Chandrasekar et al. 2013; Kumjian et al. 2022). Accurate polarimetric PAR data are difficult to obtain due to increased cross-polarization contamination[2] as the radar electronically scans at azimuth and elevation angles away from where the center of the array is pointing (i.e., broadside). Contamination occurs because the horizontally and vertically polarized beams become less vertically and horizontally oriented, respectively, and therefore are less orthogonal to one another due to beam geometry as the radar scans off broadside (Zhang et al. 2011).

Although not the focus of this study, several dual-polarization PARs have been recently deployed for operational radar network testing, including the Advanced Technology Demonstrator (ATD; Torres and Wasiewlewski 2022) and Horus (Yeary et al. 2021) in the United States, MP-PAWR in Japan (Asai et al. 2021), and XPAR in China (Wu et al. 2018). Within the United States, a future operational PAR network is expected to have dual-polarization capability (NWS 2015; Weber et al. 2021). To date, these operational dual-polarization PAR studies have largely focused on validation and signal processing (e.g., calibration, scanning techniques) and have limited contribution to fundamental research. Only one mobile dual-polarization PAR is fully complete at this time, SKYLER (Kollias et al. 2018), and it has been used more recently in field campaigns since 2022.

Industry partners worldwide have played a crucial role in the development of these new dual-polarization PARs. For example, Toshiba, Inc. was central to the design of the PAWR and MP-PAWR, Lockheed Martin has played a critical role with NWRT-PAR, Raytheon designed the SKYLER radar, and numerous industry partners have helped continued development of the ATD. Continued collaboration between academia, government, and industry will be crucial for greater utility and accessibility to PARs in the future.

[2] Cross-polarization contamination is a leaked radar signal from horizontal to vertical polarization (or vice versa) during transmission or reception.

3. Tornadoes

Tornadoes have been the most extensively studied phenomena with rapid-scan radars. Rapid-scan tornado research was readily motivated by the tornado's short advective time scales (e.g., Bluestein et al. 2010), and early observations documenting missed evolution with coarse temporal sampling (e.g., Wurman 2002; Bluestein et al. 2003b,a). In this section, the impact of rapid-scan radars on tornado research is examined through each stage of the tornado's life cycle. First, section 3a examines how rapid-scan radars have been used to differentiate tornadogenesis modes, identify storm-scale processes affecting tornadogenesis, and measure rapid secondary tornado intensification periods. Next, section 3b examines how rapidly evolving storm-scale phenomena affect tornado maintenance and explores short-time-scale intensity changes associated with waves and subvortices. Finally, the contribution of rapid-scan radars to understanding of tornado dissipation is discussed in section 3c.

Before discussing these scientific findings, some limitations to radar estimation of tornado intensity are discussed. Tornado intensity is quantified primarily by measuring the difference between the maximum and minimum radial velocities (ΔV) within the tornadic vortex signature (TVS; e.g., Donaldson 1970; Brown et al. 1971, 2005). The TVS magnitude depends on the radar's spatial sampling, primarily the azimuthal component. Coarse spatial sampling leads to underestimates of TVS magnitude, and small changes in beam position impact TVS magnitude (Brown et al. 2005). Another challenge in estimating tornado intensity is obtaining measurements in the lowest few tens of meters where the strongest winds occur in a tornado (Kosiba and Wurman 2013; Snyder and Bluestein 2014). Finally, Doppler radars sample the motion of scatterers rather than the air itself, so debris can introduce wind speed biases of up to tens of meters per second (Dowell et al. 2005; Nolan 2012). These biases may have considerable impact on sensitive analyses such as dual-Doppler or make comparisons of tornado intensity between separate tornadoes difficult (e.g., at different ranges) (Toth et al. 2013; Kingfield and LaDue 2015). However, subjective conclusions on vertical and temporal trends in TVS magnitude are unlikely to be significantly impacted.

a. *Tornadogenesis and tornado intensification*

Prior to the advent of rapid-scan radars, two modes of tornadogenesis were identified based on the vertical progression of the TVS. Trapp et al. (1999) identified and developed criteria for descending and non-descending TVSs in WSR-88D observations. Within these two categories, they found a nearly even split between descending and non-descending TVSs. Descending TVSs were attributed to the dynamic pipe effect (DPE; Leslie 1971; Trapp and Davies-Jones 1997), involving an existing midlevel mesocyclone with a dynamically induced

TABLE 2. Summary of tornadogenesis observations from rapid-scan radars, including the spatial sampling and minimum and maximum altitudes of the radar observations (at time of tornadogenesis), the directionality of the TVS (in the lowest 1 km AGL), and presence of a preceding low-level vortex. For directionality, upward/downward is used where directionality depended on the criteria used. The asterisk denotes an instance where two rapid-scan radars independently observed the same tornado.

Publication	Tornado case	Spatial sampling	Min and max observed altitude	Direction	Preceding low-level vortex?
French et al. (2013)	24 May 2008	530 m	0.3 km, 5.8 km	Not downward	Unknown
French et al. (2013)	5 Jun 2009	570 m	0.3 km, 6.2 km	Upward	Yes
French et al. (2013)*	24 May 2011	680 m	0.4 km, 13.8 km	Upward (above 2.5 km AGL)	Unknown
Houser et al. (2015)*	24 May 2011	140 m	0.6 km, 2.5 km	Simultaneous	Yes
Bluestein et al. (2019)	31 May 2013	160 m	0 km, 3.1 km	Simultaneous	Yes
Adachi and Mashiko (2020)	12 Oct 2019	70 m	0.1 km, 1.3 km	Upward/downward	Yes
Houser et al. (2022)	25 May 2012	220 m	0.2 km, 3.7 km	Upward/downward	Yes
Houser et al. (2022)	25 May 2012	90 m	0.1 km, 1.5 km	Upward	Yes
Houser et al. (2022)	27 May 2015	120 m	0 km, 1.2 km	Simultaneous	Yes
Houser et al. (2022)	27 May 2015	120 m	0 km, 1.2 km	Simultaneous	Yes
Houser et al. (2022)	27 May 2015	100 m	0 km,1.1 km	Upward/downward	Yes
Houser et al. (2022)	27 May 2015	100 m	0 km, 1.1 km	Simultaneous	Yes
Houser et al. (2022)	22 May 2016	260 m	0 km, 5.1 km	Simultaneous	No

pressure deficit that forces convergence and intensification of rotation at progressively lower altitudes. Non-descending TVSs were hypothesized to develop from near-simultaneous convergence of angular momentum over a deep layer or upward advection of vertical vorticity (Wicker and Wilhelmson 1995; Tanamachi et al. 2012).

Experiments with the DOWs in the 1990s and 2000s employed volumetric sector scans to collect observations about every 1 min (Wurman and Gill 2000; Wurman 2002; Alexander and Wurman 2005; Wurman et al. 2007), providing a higher temporal resolution of tornadogenesis compared to the WSR-88Ds. In an examination of five TVSs, Alexander (2010) observed that TVSs formed nearly simultaneously in the lowest 1 km above ground level (AGL). Although these observations showed a near-simultaneous intensification of the TVS, Alexander (2010) remarked that higher-temporal-resolution observations [$\mathcal{O}(10)$ s] were needed to assess possible upward or downward directionality.

Rapid-scan radar observations (10–20-s volumes) in the 2010s have reexamined the vertical development of TVSs on temporal scales required to properly resolve tornadogenesis. In this paper, tornadogenesis is defined by the development of a strong TVS from the surface through at least 1 km AGL. However, differences in radar sampling of tornadoes leads to different thresholds of tornado intensity at the time of tornadogenesis, and there is no agreed-upon definition to what constitutes the beginning and end of tornadogenesis. The first rapid-scan study of tornadogenesis was conducted by French et al. (2013), using MWR-05XP data. Of the twelve unique tornadoes documented in the literature, nine instances of upward or simultaneous TVS formation were noted and three instances of descending TVS mode were observed (Table 2). Figure 1a illustrates an example of non-descending tornadogenesis where rotational intensity increases to the tornado threshold simultaneously in the lowest 2 km above radar level (ARL) in the minute prior to tornadogenesis (black line). Figure 1b illustrates the clearest case of descending tornadogenesis. In this instance, rotational intensity reaches the tornado threshold in the ~500-m column near 1 km ARL (box A) and this column descends to the surface over a period of 2–3 min. However, the illustrated case of descending tornadogenesis is dependent on the definition of the tornado threshold because prior to descending tornadogenesis, a subtornadic vortex ascends from near the surface up to 1 km. In fact, all three instances of the descending TVS mode in the literature suggest the possibility of non-descending tornado formation depending on the rotational thresholds used to define the tornado (Adachi and Mashiko 2020; Houser et al. 2022).

From the evidence presented, these three cases show limited support for a descending TVS in the lowest 1 km. First, testing of different rotational intensity parameters led to ambiguous directionality of the TVS. For example, in the two possible descending cases from Houser et al. (2022) identified using ΔV, a pseudovorticity-based estimate of vortex intensity, indicated an *upward* tornadogenesis mode. In the other possible descending TVS case (Adachi and Mashiko 2020), only ΔV was examined. In addition, even with 20–30-s temporal sampling, the descent of the TVS from 1 to 2 km to the surface (e.g., where tornado formation occurs) happened within one or two volume scans. Thus, the descent was at best coarsely observed (25 May 2012 in Houser et al. 2022; Adachi and Mashiko 2020) or not directly observed (27 May 2015; Houser et al. 2022), and higher-temporal-resolution observations are necessary (<10-s volumes) to assess if descending TVS intensification is occurring.

With these caveats in mind, do these observations of descending TVSs support DPE? The original numerical simulation studies of the DPE found that tornadogenesis occurred over 5–20 min and it initiated from the midlevel mesocyclone between 2 and 6 km (Smith and Leslie 1979; Trapp and Davies-Jones 1997). In contrast, tornadogenesis in the reviewed cases occurred much faster (<2 min by our estimation). Additionally, any possible downward intensification of the TVS began at less than 1 km AGL in two of the three descending TVS cases, as opposed to the altitude of the midlevel mesocyclone. Thus, a DPE-like mechanism, as it was originally proposed,

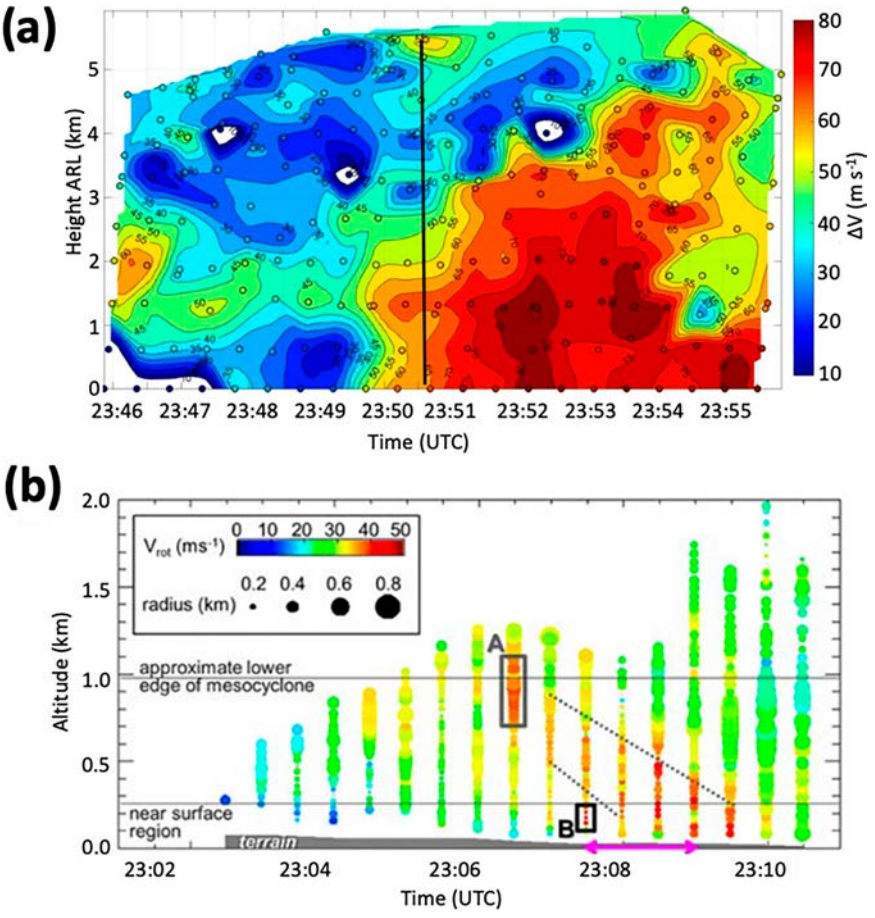

FIG. 1. Examples of the time–height evolution of rotational intensity (ΔV) to illustrate different modes of non-descending and descending tornadogenesis: (a) filled contours of ΔV (m s^{-1}) demonstrating a two-step non-descending tornadogenesis mode with near-simultaneous vertical TVS formation in the lowest 2–3 km around 2350 UTC (black line), followed by upward intensification above 3 km AGL after 2352 UTC and (b) filled circles of ΔV (m s^{-1}) with size of circles representing vortex radius (km) illustrating tornado intensification (2306–2310 UTC) starting near 1 km AGL in box A and descending between the dashed lines toward the surface. The plot in (a) is adapted from Houser et al.'s (2022) Fig. 7 and the plot in (b) is adapted from Adachi and Mashiko's (2020) Fig. 3.

does not explain the rapid formation of tornadoes. In addition, there is limited support that tornadogenesis initiates with the midlevel mesocyclone, documented in possibly one out of six unique cases with observations above 2 km. A physical mechanism has not yet been proposed for tornadogenesis in a rapidly descending mode from the low-level mesocyclone, but must explain descent rates of 15–50 m s^{-1}.

In addition to rapid-scan radar evidence, recent high-resolution simulation studies of supercells have found that tornado formation proceeds in a simultaneous or upward manner with no evidence of slow (or rapid) intensification occurring in a downward manner (Dahl et al. 2014; Dahl 2015; Markowski 2016; Orf et al. 2017; Rotunno et al. 2017). A key limitation of numerical simulations of tornadoes identifying DPE was the use of limited-domain simulations without a parent supercell, and thus storm-scale vorticity generation and updraft characteristics were prescribed through boundary and initial conditions rather than being developed by a parent storm. High-resolution supercell simulations have primarily identified tornadogenesis mechanisms resulting from processes in the lowest 1 km AGL, including tilting of low-level horizontal vorticity (e.g., from streamwise vorticity currents or frictionally generated vorticity) and stretching of vertical vorticity as dynamic lifting by the low-level mesocyclone increases. Rapid-scan radar observations generally corroborate the importance of a rapidly intensifying low-level mesocyclone (2–3 min) that increases dynamic lifting prior to tornadogenesis occurring in a non-descending manner (e.g., French et al. 2013; Houser et al. 2015; Bluestein et al. 2019).

Another important contribution of rapid-scan radar observations of tornadogenesis is documenting the shallow nature of tornadogenesis in some instances. In at least four cases

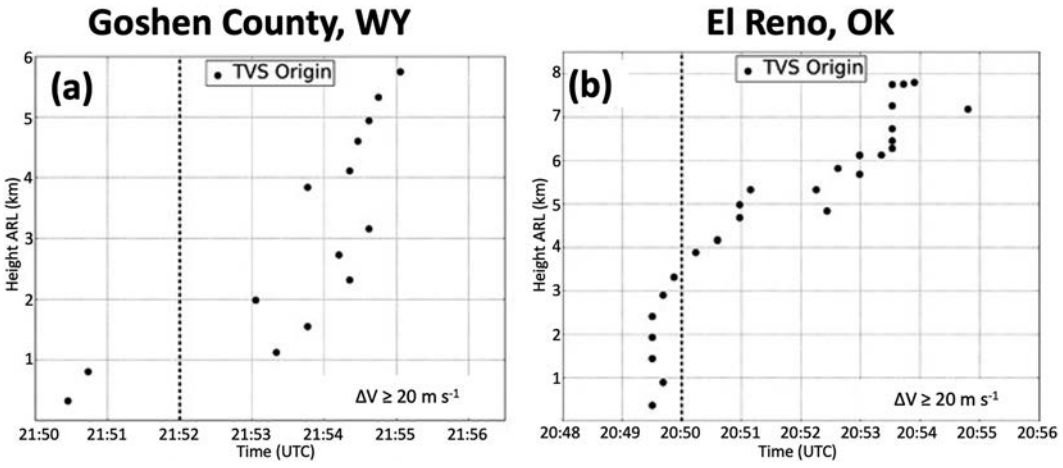

FIG. 2. Time–height series of the initial time vortex intensity met the baseline TVS criteria ($\Delta V > 20$ m s^{-1}) in (a) the 5 Jun 2009 Goshen County tornado and (b) the 24 May 2011 El Reno, Oklahoma, tornado. Vertical dashed lines indicate the approximate time of tornadogenesis in each case. The Goshen County case illustrates slow upward tornadogenesis, whereas the El Reno case illustrates simultaneous tornadogenesis followed by upward deepening of tornado-intensity rotation. Figure adapted from French et al.'s (2013) Figs. 11 and 13.

(French et al. 2013; Bluestein et al. 2019; Houser et al. 2022), tornadogenesis occurred through a shallow depth (<1–2 km). A delayed, deep intensification followed shallow tornadogenesis in three of these cases whereas some of the 27 May 2015 tornadoes in Houser et al. (2022) remained confined to the boundary layer. Two contrasting examples are shown in a time-height plot of the initial TVS appearance in Fig. 2, with the Goshen County tornado exhibiting a delayed, deep intensification above 1 km AGL, whereas the 24 May 2011 El Reno tornado intensified through 3 km AGL simultaneously. The environmental profile of buoyancy was hypothesized to modify tornado behavior in these cases. For example, the level of free convection (LFC) was noted to divide slower and more rapid tornado intensification in French et al. (2013) and Houser et al. (2015). To address these environmental factors and near-tornado buoyancy effects on tornadogenesis behavior, in situ observations collected contemporaneously with rapid-scan radars are needed.

Although the fastest tornado-scale features are marginally resolved, high-temporal observations are capable of fully resolving storm-scale evolution contributing to tornadogenesis. Using rapid-scan polarimetric data, Tanamachi and Heinselman (2016) found that midlevel updrafts merged with the primary updraft in as little as 2–3 min, and the mergers may have aided tornadogenesis by widening the updraft. Rapid-scan observations also provided the first observational account of a nonoccluding cyclic mesocyclone mode of tornadogenesis (Adlerman and Droegemeier 2002, 2005) where the decaying tornado moves ahead of the mesocyclone and subsequent intensification of a new, subtornadic vortex occurs in the original tornado location (Houser et al. 2015). This mode contrasts with the traditional conceptual model of cyclic tornadogenesis in which the tornado decays in a rearward position and a new mesocyclone and tornado form in a forward position (e.g., Burgess et al. 1982; Dowell and Bluestein 2002a,b). The use of rapid-scan radars to examine the impacts of storm-scale boundaries and momentum surges was also illustrated by capturing increased convergence along merging rear-flank gust fronts for the same storm (Tanamachi et al. 2015) and tornadogenesis along an internal momentum surge (Bluestein et al. 2016).

Shortly after tornadogenesis in some long-lived tornadoes, a second rapid intensification period was often observed. Several studies noted an initial period of 2–6 min where minimal intensification occurs, followed by rapid intensification of tens of meters per second in ΔV as little as 30 s (Kosiba et al. 2013b; Houser et al. 2015; Bluestein et al. 2019; Wienhoff et al. 2020; Satrio et al. 2021). In rapid-scan cases with deep observations (>2 km AGL), secondary intensification occurs simultaneously through 3+ km in Houser et al. (2015) and appears to occur in Bluestein et al. (2019) prior to the end of data collection. This low-level intensification occurred contemporaneously with an erosion of the stable-layer bifurcation in TVS magnitude. In this case, we hypothesize that persistent low-level dynamic lifting may contribute to the erosion of the stable layers, and subsequent increases in low-level convergence contribute to secondary intensification.

Although secondary rapid intensification has been documented, few physical mechanisms have been proposed to explain why secondary intensification occurs. In observations (French et al. 2015; Seimon et al. 2016) and high-resolution numerical simulations (Orf et al. 2017; Orf 2019) of the 24 May 2011 El Reno supercell, two tornadoes wrap around each other and merge in an upward manner. During the merger, both observations and simulations show a large change in tornado intensity (about 30 m s^{-1} in ΔV and 35 m s^{-1} in model surface winds) and diameter. Given that secondary tornado intensification has received insufficient attention, additional work is needed to clearly identify the physical mechanisms underlying rapid intensification. Tornado mergers, for example, are unlikely to explain most instances of secondary tornado

intensification. However, tornado mergers with subtornadic vorticity areas (Tanamachi et al. 2013) could contribute to discrete increases in intensity.

Rapid-scan radar studies have provided insight into the characteristics of tornadogenesis and tornado intensification, helping to refute the dynamic pipe effect. Given the limited evidence for DPE and more broadly, the unclear importance of TVS directionality to tornadogenesis mechanisms, future rapid-scan radar studies should focus their efforts on process-based studies of tornadogenesis and testing emerging hypotheses from high-resolution numerical simulations. Recent numerical modeling studies and field campaigns, such as the Targeted Observations by Radars and UASs (TORUS), have examined the structure of the streamwise vorticity current (SVC) within the forward-flank downdraft (FFD) and its potential role in intensification of the low-level mesocyclone and tornadogenesis (Orf et al. 2017; Murdzek et al. 2020; Schueth et al. 2021; Finley et al. 2023). However, other recent numerical simulations have more robustly shown that low-level mesocyclones primarily ingest environmental streamwise vorticity from storm inflow in the lowest 500 m rather than the FFD (Coffer et al. 2023). To provide observational testing of the Coffer et al. (2023) results, rapid-scan radar studies, contextualized by detailed sampling of inflow to characterize environmental streamwise vorticity (e.g., lidar or sensitive Doppler radars), could be conducted to compare low-level mesocyclone and tornado evolution with numerical simulations. Shallow, rapid scans with lidar or sensitive, higher-resolution Doppler radars (e.g., Ka-band radars) could be combined with rapid-scan, volumetric radar observations to characterize the time evolution of near-surface vorticity and its degree of organization to evaluate another recent simulation-based hypothesis that coherent organization of vorticity sources is not required for tornadogenesis (Fischer and Dahl 2022; Parker 2023).

Multi-Doppler analyses enable more process-based studies by quantifying vorticity budgets or circulation or examining parcel trajectories (e.g., Dowell and Bluestein 2002b; Wurman et al. 2007; Markowski et al. 2012b; Kosiba et al. 2013b; Murdzek et al. 2020), particularly in concert with large-scale field campaigns with thermodynamic measurements (e.g., Wurman et al. 2012). However, these dual-Doppler studies had 2-min temporal sampling that only marginally resolves intensification to tornado strength occurring in ~1–2 min or less and may contain considerable errors in trajectories (e.g., Dahl et al. 2012). Owing to limited synchronous deployment of the few rapid-scan radar systems, which are inherently difficult to coordinate, rapid-scan multi-Doppler analyses of tornadoes are scarce. Thus, increased coordination between research groups to acquire rapid-scan multi-Doppler data are needed, particularly within large-scale field campaigns. To test the previously discussed numerical simulation-based hypotheses and better understand the limitations of rapid-scan radar observations, radar simulations of numerical models should inform single- or multi-Doppler observational approaches. For example, sampling issues (Brown et al. 1978; Wood and Brown 1997; Brown et al. 2005; French et al. 2014) may preclude sufficient low-level observations. Moreover, dual-Doppler analyses further degrade spatial resolution from single-Doppler observations, which may make capturing the smallest features (e.g., subtornado scale) difficult or impossible to properly sample with the current technology. A more detailed discussion of recent improvements in dual-Doppler accuracy facilitated by rapid-scan radar observations as well as remaining limitations can be found in section 5.

b. *Tornado maintenance and mature tornado evolution*

Tornado maintenance requires a delicate balance of tornado positioning relative to sources of vorticity and the ability to tilt and stretch vorticity. Long-lived, strong tornadoes tend to reside beneath the primary updraft, within regions of strong near-surface convergence, and with sustained access to external sources of high-angular-momentum air (Marquis et al. 2012). Additionally, relatively buoyant outflow is also observed near strong, long-lived tornadoes (Markowski 2002; Weiss et al. 2015), and these tornadoes often reside at the intersection of the rear-flank and forward-flank gust fronts while maintaining access to buoyant inflow air with favorable positioning within the mesocyclone (Dowell and Bluestein 2002a,b).

Rapid-scan radar observations have advanced understanding of tornado maintenance by minimizing advection and evolution between vertical measurements of tornado intensity and positioning that can change on time scales as fast as 10 s (French et al. 2014; Kurdzo et al. 2015; Mahre et al. 2018; McKeown et al. 2020). These capabilities have been leveraged to examine whether a persistent TVS in the mesocyclone is necessary to maintain a tornado. French et al. (2014) found that a continuous TVS within the mesocyclone was not required to maintain a strong tornado, whereas Wienhoff et al. (2020) noted that the difference between long-lived, strong tornadoes and weak, short-lived tornadoes was the presence of a TVS within the mesocyclone. In addition, Wienhoff et al. (2020) examined how rapid changes (1–2 min) in mesocyclone-relative position of the tornado affect tornado maintenance. In several weak tornado cases (Wienhoff et al. 2020), increased displacement of the tornado from the low-level mesocyclone resulted from momentum surges and instigated rapid tornado decay. In contrast, strong and violent tornadoes persisted through changes in tornado–mesocyclone-relative positioning (Mahre et al. 2018; McKeown et al. 2020), perhaps due to wider and more intense updrafts (Marion et al. 2019; French and Kingfield 2021). Momentum surges, as inferred by rapid successions of ejected tornado debris (1 min), may also prevent tornado occlusion and subsequent decay by restoring the tornado to a favorable position within the mesocyclone (Kurdzo et al. 2015).

During the mature stage of a tornado, rapid changes in tornado intensity and damage are observed. Some intensity changes exhibit periodic behavior (Fig. 3), evidenced by ΔV oscillations from 5 m s^{-1} (Wurman et al. 2013) to in excess of 20 m s^{-1} (French et al. 2014; Mahre et al. 2018). In most instances, the period of oscillation (Fig. 3b) was between 30 and 100 s (Bluestein et al. 2003b; Wurman et al. 2013; French et al. 2014; Mahre et al. 2018), which required observations every ~10 s to properly resolve them. Periodicities have been observed primarily near the surface (<500 m) (French et al. 2014;

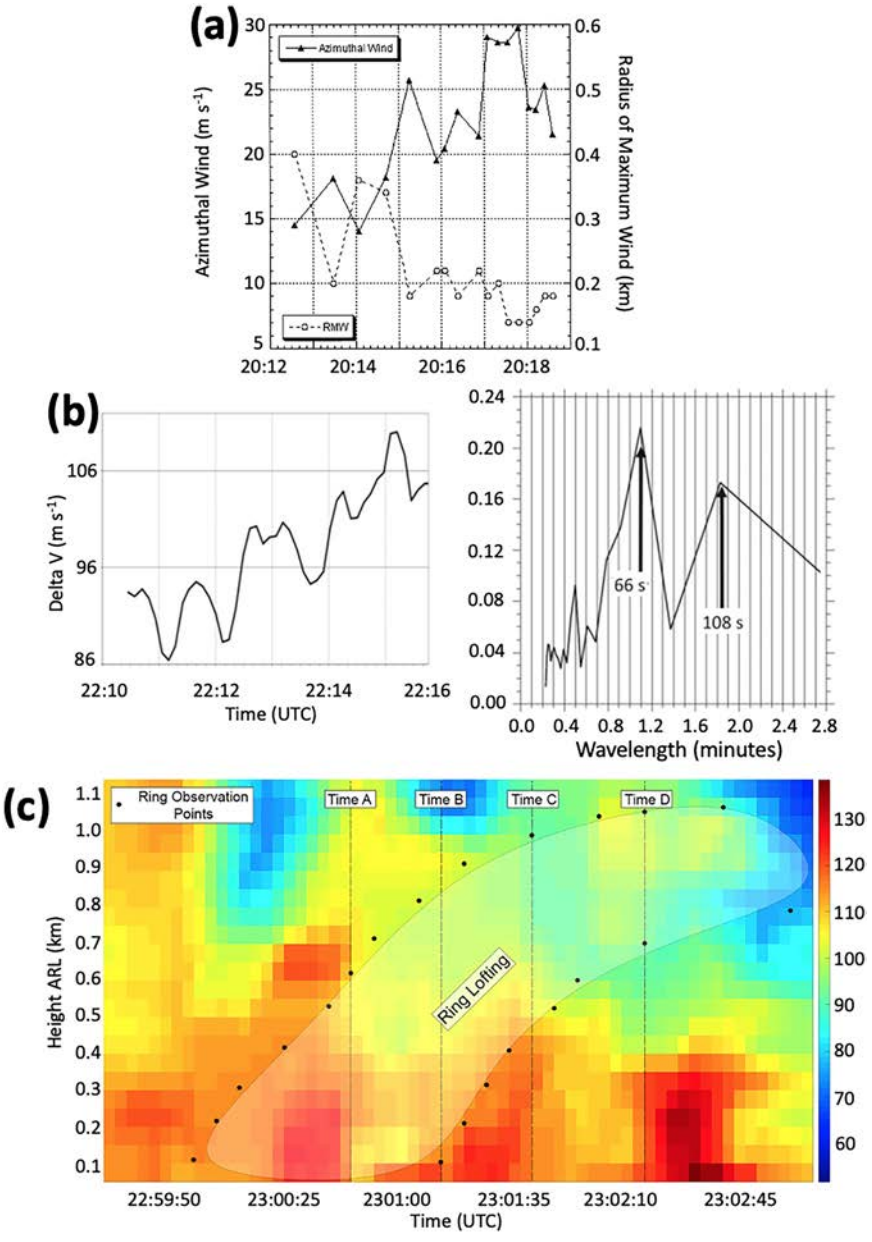

FIG. 3. Time series of rotational intensity (m s^{-1}) in mature tornadoes. (a) Rotational intensity is plotted in solid black. (b) A time series of rotation intensity is plotted on the left with the corresponding Fourier transform included on the right. (c) A time–height analysis is provided. The plot in (a) is adapted from Bluestein et al.'s (2003b) Fig. 3, the plot in (b) is adapted from Wurman et al.'s (2013) Fig. 7, and the plot in (c) is adapted from Mahre et al.'s (2018) Fig. 11

Mahre et al. 2018), but substantial periodicities have been noted aloft (>2 km) with smaller near-surface oscillations (French et al. 2014). Few studies have commented on the lack of periodicities. However, McKeown et al. (2020) noted no periodic intensity oscillations throughout the mature stage of a long-lived tornado despite observing periodic oscillations in tornado positioning relative to the mesocyclone. But the temporal sampling rate precluded detection of periods shorter than ~50 s.

Several oscillation mechanisms have been proposed to explain tornado periodicities. However, a conclusive mechanism has yet to be identified. Rapid sector scans from a W-band radar revealed periodicities and showed an inverse relationship between tornado intensity and diameter, consistent with angular momentum conservation (Bluestein et al. 2003b). Although the underlying cause of these radial displacements was not determined, a possible cause is vertically propagating centrifugal waves that modulate tornado diameter and intensity,

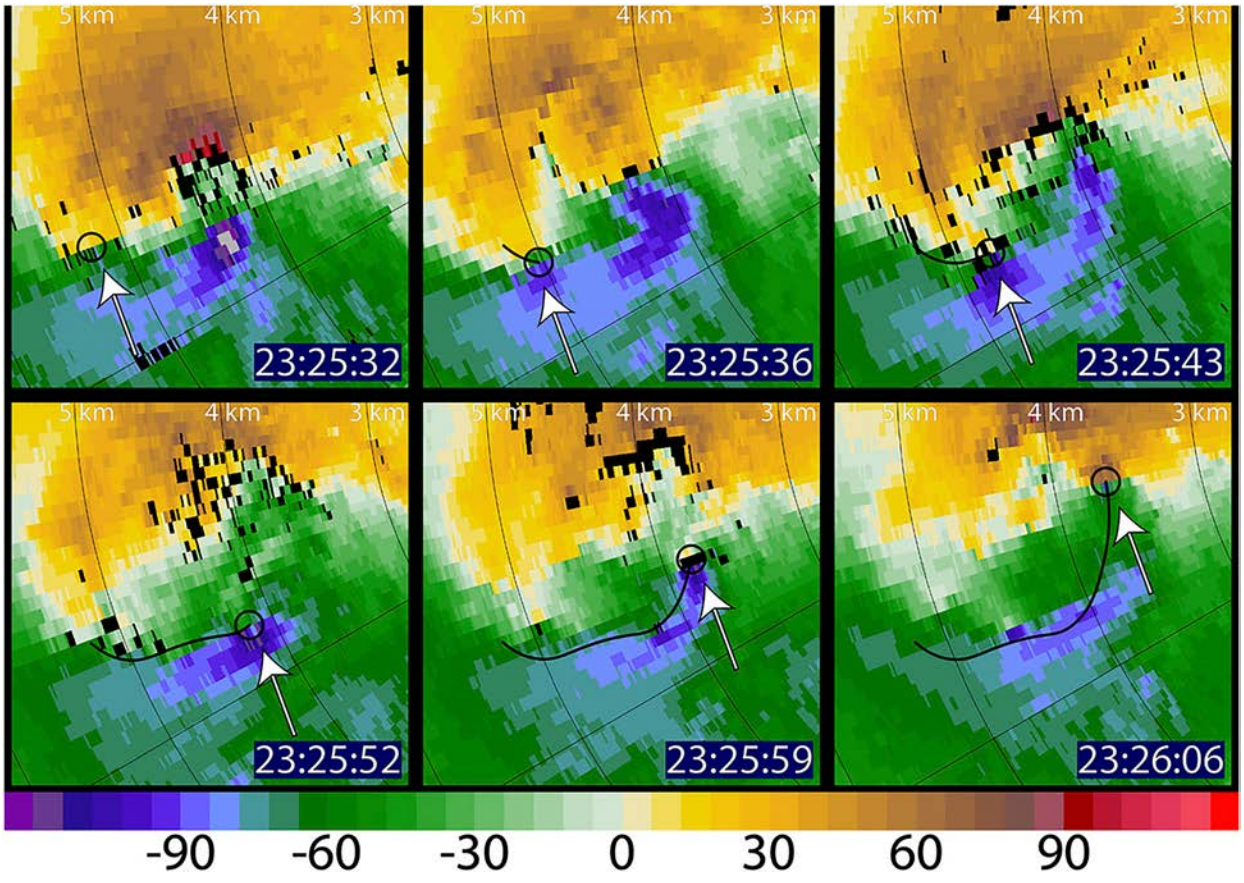

FIG. 4. Time series of 31 May 2013 El Reno, Oklahoma, RaXPol Doppler velocity (m s^{-1}) PPI observations at (top left to top right) 3°, 5°, and 1° and (bottom left to bottom right) 5°, 1°, and 4° elevation angles. The subvortex is annotated with the black circle and its track is shown by the black curve. Figure from Bluestein et al.'s (2018) Fig. 2.

as illustrated in theoretical numerical solutions (Dahl 2021). The best evidence of vertically propagating waves was found in Houser et al. (2016), where they identified ascending wave-like structures using the polarimetric debris signature. Although there were fluctuations in ΔV [Fig. 3c in Houser et al. (2016)], it was not clear that the fluctuations correspond to a particular frequency. Next, vortex Rossby waves may also introduce periodicities with superimposed, long-wavelength perturbations in the tornado's flow (Bluestein et al. 2003b; Wurman et al. 2013). However, it has yet to be explained how Vortex Rossby waves introduce time-dependent variations in ΔV, but could occur as a consequence of time-dependent radar observing geometry and spatial undersampling. Finally, tornado subvortices, small vortices within a multiple-vortex tornado, while generating small-scale perturbations in tornado winds and damage (Lewellen et al. 2000; Wurman 2002; Nolan 2012; Snyder and Bluestein 2014; Wurman et al. 2014), typically have life cycles of <30 s (Bluestein et al. 2018) and appear unlikely to explain the observed intensity oscillations with periods near 100 s. Very rapid-scan, volumetric observations (<10 s) of azimuthally and vertically propagating waves are needed to quantify phase speeds and changes in tornado intensity and diameter with height. To identify oscillation mechanisms, quantitative intercomparisons between wave speeds and velocity perturbations from analytical solutions of azimuthally and vertically propagating waves and radar observations could be employed, in addition to radar simulation studies using high-resolution numerical models of tornadoes.

Although tornado subvortices may not explain periodic intensity oscillations, rapidly collected radar observations have helped to better understand subvortex behavior. Rapid, sector scans every 4–5 s (Wurman 2002) and rapid PPIs every 2 s (Bluestein et al. 2018) have been used to document that subvortices may retrograde, or translate azimuthally at a lower velocity than the mean azimuth velocity. These rapid-scan radar studies provided the first observational evidence of retrograding behavior of subvortices documented by vortex chamber and simulation studies (Ward 1972; Lewellen et al. 1997). Using rapid PPIs, the first full life cycle view of subvortices was captured by Bluestein et al. (2018), who identified that short-lived and long-lived subvortices lasted 8 and 34 s, respectively, on average. An example of a tracked subvortex in a sequence of PPIs is shown in Fig. 4. Subvortices formed within the radius of maximum wind, primarily in the left-rear quadrant, and typically did not complete more than one revolution of the tornado before dissipating in the right-forward or left-forward quadrants,

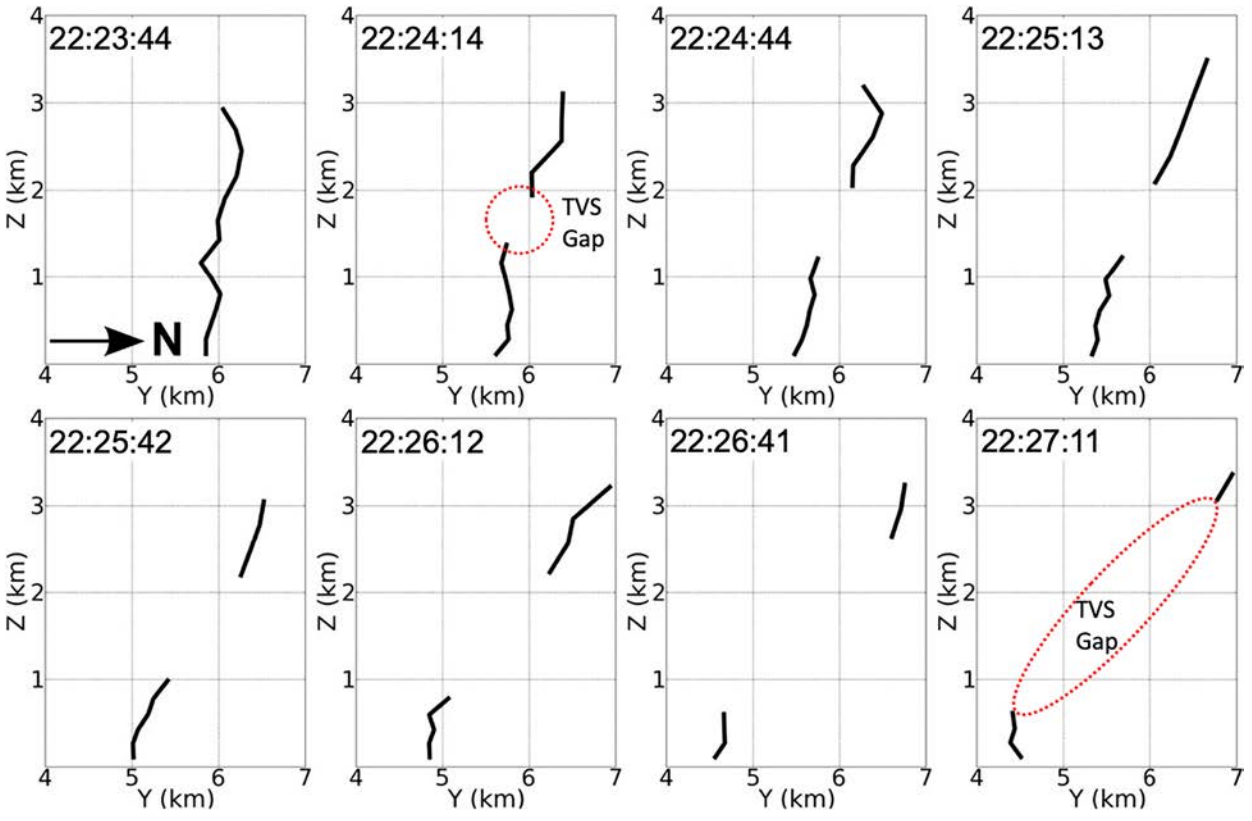

FIG. 5. Vertical cross section of the Goshen County TVS position over a 3-min period, shown every 30 s during tornado dissipation. The inside-out weakening starts with a gap in the TVS profile first at 1.5–2 km, progressively extending to higher and lower altitudes and becoming increasingly tilted. The TVS gap is highlighted by the dashed red circle at 2224:14 and 2227:11 UTC. Figure adapted from French et al.'s (2014) Fig. 19.

similar to numerical simulations (Lewellen et al. 1997). A key distinction between short- and long-lived subvortices is that long-lived subvortices moved inward toward the tornado center with time, whereas short-lived subvortices remained close to their original radius. In contrast, an interior tornado subvortex in a larger tornado/multivortex mesocyclone moved radially outward during a rapid increase in the overall number of subvortices occurring over 40 s (Wurman et al. 2014).

Although rapid-scan radars have documented potentially important short time-scale phenomena that impact tornado maintenance and intensity, several barriers remain to fully understand the underlying physical processes and their overall importance. Advancements in understanding are limited by coarse spatial sampling of a hundred to a few hundreds of meters, depending on beamwidth and range. Thus, small-scale structures in tornadoes such as higher-wavenumber oscillations, vertically propagating waves, and subvortices are, at best, coarsely resolved. Although relatively uncommon, close-range observations of large-diameter tornadoes (>1 km) provide the best opportunity to examine these processes. However, finer-scale measurements are needed, perhaps by developing rapid-scan radars with narrow beamwidths or using rapid sectors or single-elevation PPIs with existent millimeter-wavelength radars (Weiss 2009).

c. *Tornado dissipation*

Storm-scale processes leading to the occlusion of the mesocyclone and tornado dissipation are well-documented (e.g., Lemon and Doswell 1979), involving increased negatively buoyant storm outflow that disrupts the balance between inflow and outflow (Dowell and Bluestein 2002b) and initiates tornado dissipation by reducing convergence of angular momentum and vorticity stretching (e.g., Dowell and Bluestein 2002b; Marquis et al. 2012). In this review "decay" is used to describe the weakening of the rotational intensity of an ongoing tornado, whereas "dissipation" is used to describe the termination of a tornado-strength vortex. Rapidly collected volume scans have improved understanding of tornado-scale decay initiated by storm-scale processes. The first study to examine tornado decay using a rapid-scan radar (MWR-05XP) was French et al. (2014). French et al. (2014) made the first observations of the late tornado life cycle using rapid-scan radars. They documented two instances of an "inside-out" weakening of the tornado where the tornado weakened upward and downward from an initial altitude of 1.5–2 km (Fig. 5), near the LFC. French et al. (2014) suggest that weakening at the LFC might occur first in response to near-surface buoyancy decreasing during an occlusion. In addition, the TVS exhibited differential motion below and above the first altitude where the TVS weakened. One limitation of the French et al. (2014) study was

TABLE 3. Summary of tornado dissipation cases, including observed directionality, duration of decay, starting height of decay or dissipation, and presence of differential motion above and below the dissipation height. Cases where differential motion was not examined or was uncertain is denoted as unknown, and it is labeled as N/A for the simultaneous case. Spatial resolution and altitudes are computed at time of initial decay.

Publication	Tornado case	Spatial resolution	Min and max obs alt	Dissipation behavior	Duration of decay	Decay starting height	Differential TVS motion
French et al. (2014)	5 Jun 2009	240 m	0.1 km, 2.6 km	Inside out	4–5 min	1.5–2.0 km	Yes
French et al. (2014)	19 May 2010	250 m	0.1 km, 5.1 km	Inside out	8 min	1.5–2.0 km	Yes
French et al. (2014)	25 May 2010	310 m	0.1 km, 6.4 km	Downward, upper part unknown	3 min	1.5–2.0 km	Unknown
Houser et al. (2015)	24 May 2011	270 m	1.1 km, 4.8 km	Simultaneous, followed by inside out	30 s	2.5 km (not LFC)	Unknown
Bluestein et al. (2016)	23 May 2008	500 m	0.3 km, 5.5 km	Inside out	1 min	750 m	Yes
Griffin et al. (2019)	27 May 2015	100 m	0.1 km, 1.9 km	Downward, upper part unknown	2–3 min	1.25–2+ km	Unknown
McKeown et al. (2020)	9 May 2016	210 m	0.2 km, 2.1 km	Simultaneous below 1.5 km	15 min	1.5–2 km	N/A
Wienhoff et al. (2020)	24 May 2016	190 m	<0.1 m, 1.9 km	Initial weakening aloft	~90 s	Unknown	Unknown

the relatively coarse resolution preventing analysis at the tornado scale, thus making the distinction between decay and dissipation in this case ambiguous.

The majority of eight subsequent case studies have documented similar tornado decay to French et al. (2014). These cases are summarized in Table 3 (French et al. 2014; Houser et al. 2015; Tanamachi et al. 2015; Bluestein et al. 2016; Griffin et al. 2019; Wienhoff et al. 2020).[3] Seven of the eight cases either exhibit inside-out decay or a possibly undersampled version of inside-out decay where downward weakening is observed in the low levels but the upper levels of the TVS are not documented. Contrasting observations of inside-out decay, McKeown et al. (2020) documented that tornado dissipation either occurred simultaneously within the lowest 2 km for higher thresholds of ΔV; or, for lower thresholds, tornado dissipation happened first between 1.5 and 2 km AGL and nearly simultaneously in the observed 2 km AGL layer thereafter. For the inside-out or downward cases, decay was not sensitive to the choice of ΔV threshold.

Although the majority of tornadoes in the literature broadly behave similarly, close-range, rapid-scan observations reveal nuanced differences in tornado dissipation (e.g., lowest 1 km AGL). During dissipation, Griffin et al. (2019) noted that the tornado's wind speeds in the lowest 400 m AGL weakened simultaneously, which slightly preceded the weakening of wind speeds in the adjacent layer above (2206:22–2207:27 UTC; Fig. 6). Simultaneous, rapid changes in tornado tilt occurred at 400–700 m AGL, beneath the initial dissipation level and exhibited the slowest rate of decay (Griffin et al. 2019). Following initial decay, the tornado dissipated rapidly upward 1 min later (2207:27–2208:48 UTC; Fig. 6).

During tornado dissipation, a common observation is that the tornado moves rearward in a storm-relative sense, resulting in increased displacement between the tornado and mesocyclone (Wakimoto and Martner 1992; Dowell and Bluestein 2002a,b; Nixon and Allen 2021). A possible explanation for the nuanced differences in dissipation modes is that dissipation during cyclic mesocyclogenesis can occur in an occluding (Burgess et al. 1982; Dowell and Bluestein 2002a,b) or non-occluding manner (Adlerman and Droegemeier 2002, 2005). Rapid-scan observations first documented non-occluding mesocyclogenesis (French et al. 2014; Houser et al. 2015; Tanamachi et al. 2015) that were only previously identified in numerical simulations (Adlerman and Droegemeier 2005). In both French et al. (2014) and Houser et al. (2015), the tornado vortex was displaced ahead or to the right of storm motion, as shown in Fig. 7, causing dissipation since the tornado no longer resided beneath the parent updraft. Inside-out decay was observed for both occluding and non-occluding mesocyclogenesis cases. French et al. (2014) and Houser et al. (2015) both

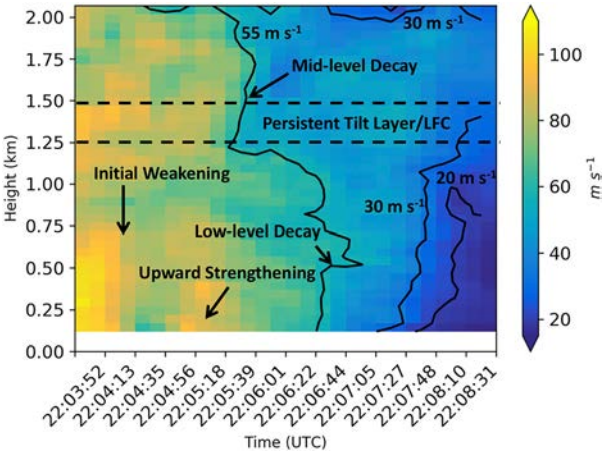

FIG. 6. Time–height plot of ΔV during the 27 May 2015 Canadian, TX, tornado observed by the AIR. Figure from Griffin et al.'s (2019) Fig. 5.

[3] Tornadogenesis decay mode for Bluestein et al. (2016) is based on the authors' analysis of Bluestein et al.'s (2016) Fig. 11 and not the original authors' discussion.

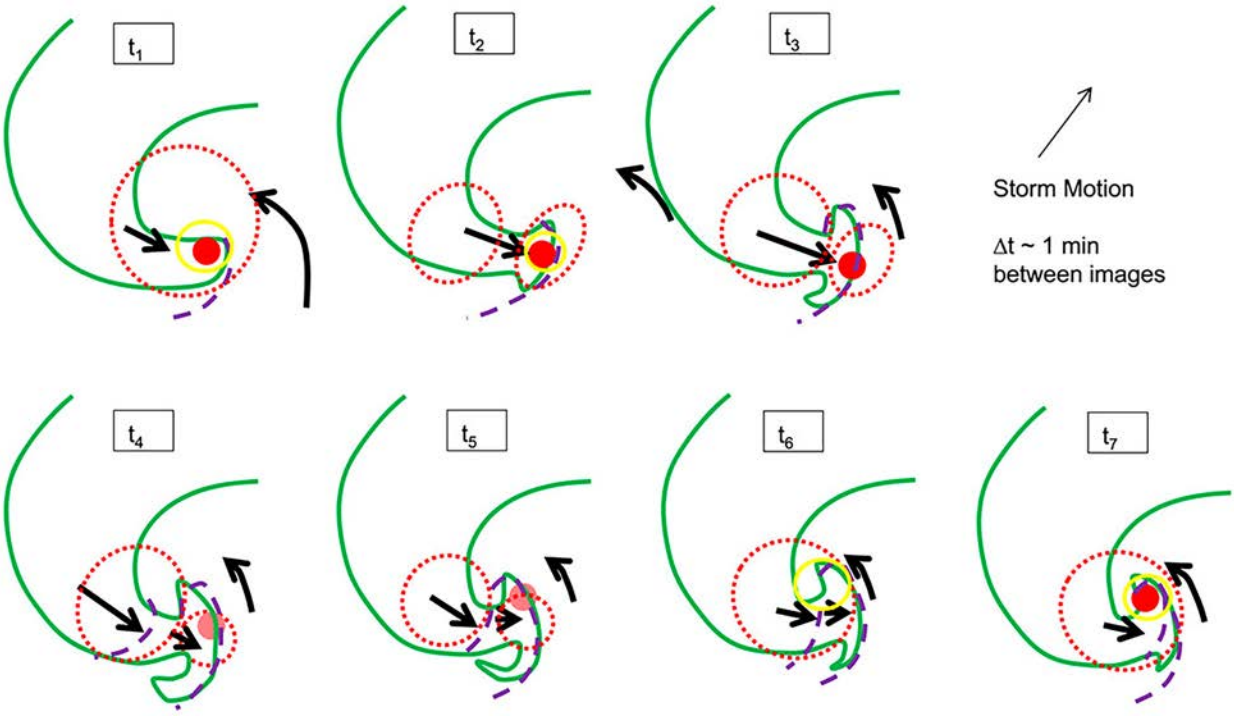

FIG. 7. Conceptual model of non-occluding mesocyclogenesis based on RaXPol observations, shown with 1-min time steps. The red dot shows the location of the tornado, the pink dot indicates the location of the subtornadic vortex, the black arrows denote the horizontal winds, and the yellow and red circles show the low-level and midlevel mesocyclone, respectively. Figure from Houser et al.'s (2015) Fig. 15.

found non-occluding cyclic mesocyclone dissipation, whereas Griffin et al. (2019) identified classic occlusion with the low-level vortex moving rearward within the supercell. Although the non-occluding sample size is small [Houser et al. (2015) in Table 3], we hypothesize that non-occluding mesocyclogenesis may result in faster tornado decay because it more rapidly displaces the tornado from the mesocyclone. Future research should seek to clarify the connection between storm-scale processes and decay mechanisms (inside-out or simultaneous), including what controls the height of tornado decay and highly varied duration of tornado dissipation.

4. Broader applications to deep convection

Although there have been numerous studies on supercells and tornadoes, many phenomena within deep convection evolve on short time scales. In this section we will examine how rapid-scan radars have been used for science applications involving hail and damaging winds (section 4a), lightning (section 4b), deep convection tracking and flash flood potential (section 4c), and tropical cyclones (section 4d). Although fewer studies have been done in these areas, these studies provide an important first examination of a broader spectrum of research opportunities and operational applications created by detecting these rapidly evolving features and motivate subsequent discussion of future research opportunities in these topic areas.

a. Hail and damaging winds

Hailstorms cause over $10 billion in damage each year (e.g., Allen et al. 2020), and weather radars are extensively used for issuing operational warnings of hailstorms. The benefits of rapid-scan observations for hail were first illustrated using data collected with the single-polarization NWRT PAR. In one 3-min period for a significant hail event, NWRT PAR observations showed that echo intensity increased from 30 to 55 dBZ and the storm top height increased from 5 to 9 km AGL. In the subsequent 3–4 min, the maximum reflectivity exceeded 70 dBZ and a three-body scatter spike became evident (Heinselman et al. 2008). In addition, Heinselman et al. (2012) identified a bounded region of high reflectivity that descended from 6 km to the surface in 7 min during a wet microburst. Tracking such features required both high-temporal-resolution and dense vertical observations as illustrated by the local WSR-88D, which sometimes missed the onset of hailfall (Newman and Heinselman 2012). Examining Maximum Estimated Size of Hail (MESH) output from the NWRT PAR, the maximum hail sizes were observed to increase and decrease by as much as 7 cm within 7-min periods (e.g., 2240 UTC in Fig. 8; Witt et al. 2018). However, verification studies have found that MESH has little correlation with hail size (e.g., Ortega et al. 2009; Ortega 2018; Murillo and Homeyer 2019), and thus these MESH changes may reflect integrated reflectivity changes and not necessarily changes in hail size. With operational prototype S-band PARs (e.g., ATD), future research can examine if polarimetric radar algorithms of hail-size categories (e.g.,

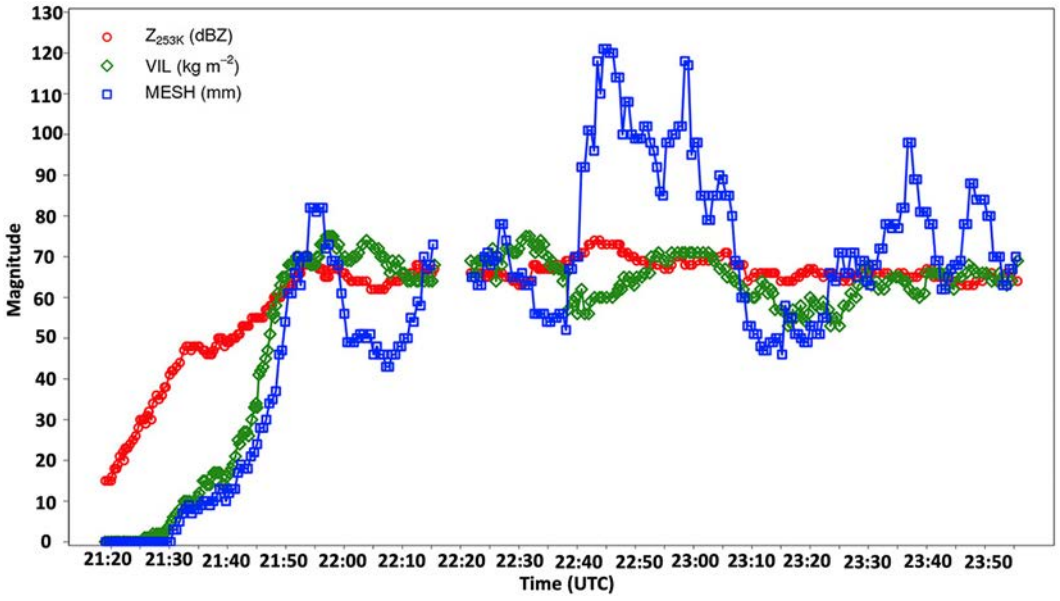

FIG. 8. Time series plot of MESH (blue line), vertical integrated liquid (VIL; green line), and radar reflectivity factor at 253 K (red line). MESH increases by about 7 cm in a 5-min period centered around 2240 UTC. Figure from Witt et al.'s (2018) Fig. 6.

Ryzhkov et al. 2013; Ortega et al. 2016) observe similar high temporal variations and if these variations correlate with surface hail observations.

Improving on early single-polarization radars, polarimetric observations more clearly discriminate between areas of hail and other types of hydrometeors (Vivekanandan et al. 1999; Straka et al. 2000). Using rapid-scan, polarimetric data collected with volumetric sector scans, polarimetric signature evolution has been examined using KOUN (Kumjian et al. 2010; Tanamachi and Heinselman 2016; Kuster et al. 2019), a WSR-88D radar in Norman, Oklahoma. In a tornadic supercell case, Tanamachi and Heinselman (2016) showed that rapid-scan observations captured the descent of large hail, characterized by near-zero Z_{DR} and low ρ_{HV}, over six volume scans compared to three with the WSR-88D (Fig. 9). The hail signature disrupted the structure of the Z_{DR} arc, a region of high Z_{DR} along the forward-flank downdraft (e.g., Kumjian and Ryzhkov 2008, 2009; Dawson et al. 2014), reducing its areal coverage (Tanamachi and Heinselman 2016; Witt et al. 2018). These observations differed from an earlier KOUN rapid-scan study (Kumjian et al. 2010), in which a Z_{DR} arc was disrupted by a region of small drops rather than hail during an occlusion cycle. In addition to hailfall, polarimetric radar signatures can be related to updraft characteristics (Kumjian et al. 2014; Snyder and Ryzhkov 2015), such as the height or width of Z_{DR} columns. Z_{DR} columns are vertical turrets of positive Z_{DR} comprised of lofted raindrops above the environmental freezing level (Conway and Zrnić 1993; Kumjian and Ryzhkov 2008). In the largest sample size study to date, Kuster et al. (2019) analyzed 50 storms using rapid-scan KOUN data and found that detection of the maximum in Z_{DR} column and radar reflectivity core height provided the best lead time for hail onset, consistent with modeling studies that identified a 10–15-min lead time between Z_{DR} column height and hail reaching the surface (Kumjian et al. 2014).

Forecasting severe wind events requires detection of precursor signatures that occur at different altitudes and must be tracked vertically in time. In particular, microburst detection often relies on the detection of descending reflectivity features, midlevel radial convergence (Wilson et al. 1984; Roberts and Wilson 1989), as well as Z_{DR} column signatures (Kuster et al. 2019). Descending reflectivity cores are localized, columnar maxima in reflectivity (Wakimoto and Bringi 1988), often observed 4–10 min prior to downburst formation (e.g., one to two WSR-88D volumes). Rapid-scan data facilitate their detection and subsequent tracking of their descent through a vertical column (Heinselman et al. 2008; Adachi et al. 2016; Kuster et al. 2016). Midlevel convergence signatures, a precursor to downbursts, can be short-lived (e.g., <90 s) and can precede the onset of strong surface winds or the development of mesovortices by as little as 1 min (Adachi et al. 2016; Kuster et al. 2016; Newman and Heinselman 2012). In addition to convergence signatures, Kuster et al. (2019) also found that the peak Z_{DR} column height provided skill in anticipating severe wind events using trends in column size and height that was greatly aided by improved scan-to-scan consistency of rapid-scan radar data that minimized storm evolution between observations.

Although the reviewed hail and wind research has documented rapid changes in precursor signatures, rapid-scan, dual-polarization radars could be better leveraged to provide more vertically dense observations, covering near-surface to storm top, while still improving volume scan times (e.g., 30 elevations in 60 s). For hail research, such observations would improve

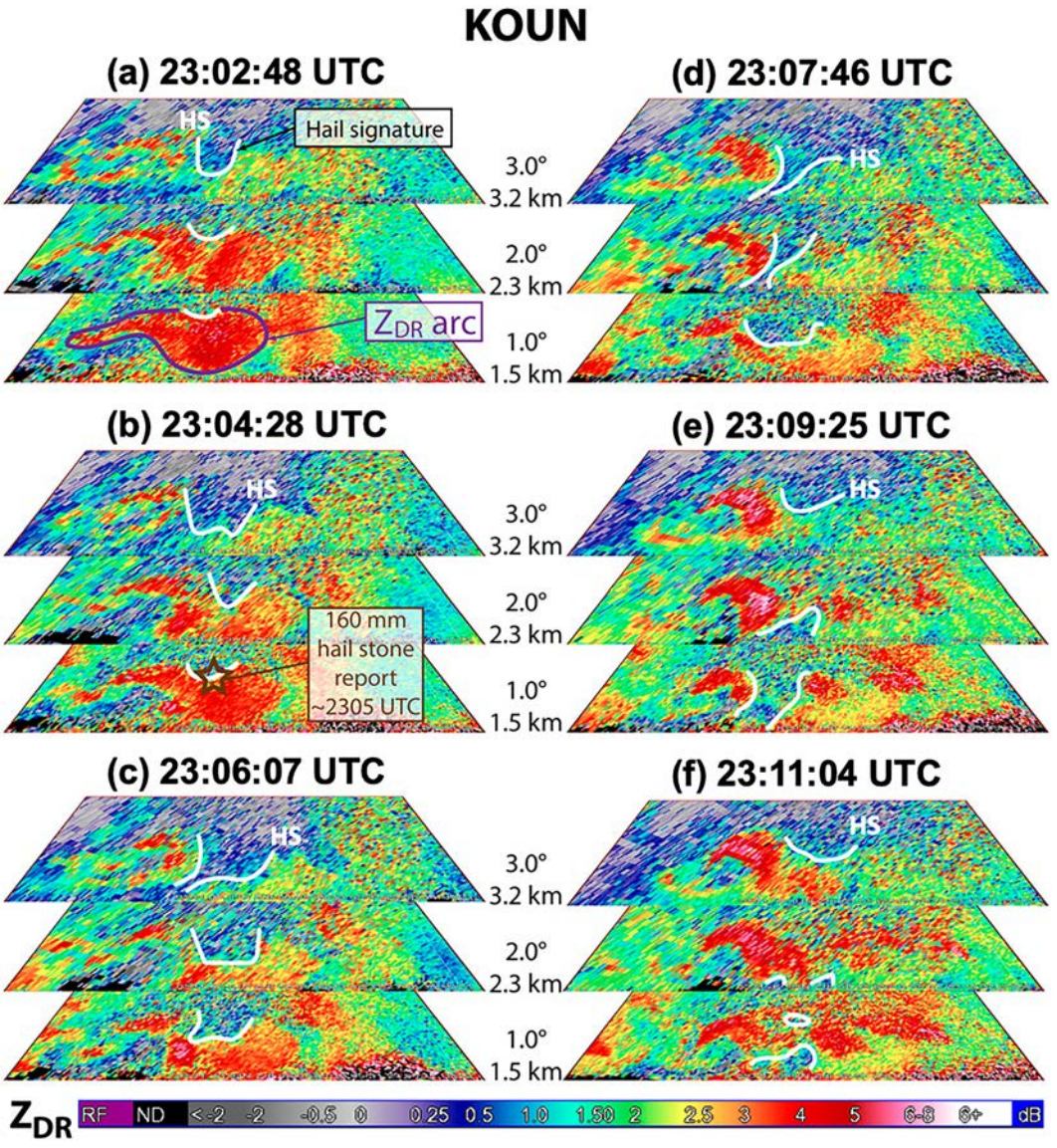

FIG. 9. KOUN observations of Z_{DR} at 1.0°, 2.0°, and 3.0° elevation from (a) 2302 to (f) 2311 UTC 31 May 2013, illustrating the descent of the hail signature and disruption of the Z_{DR} arc. Figure adapted from Tanamachi and Heinselman's (2016) Fig. 4.

understanding of hail formation, trajectories, and its relationship with convective updrafts (Adams-Selin and Ziegler 2016; Dennis and Kumjian 2017; Kumjian et al. 2021), while simultaneously observing hail fallout and documenting along-track variability of hail sizes for intercomparisons with advancing in situ hail measurements (Blair et al. 2017; Giammanco et al. 2017; Soderholm et al. 2020). By correlating polarimetric signatures and on-ground reports that are infrequent in time and space, rapid-scan observations enabled more precise correlation between polarimetric radar signatures and giant hail occurrences (Witt et al. 2018). Rapid-scan polarimetric observations could improve understanding of the roles of hydrometeor loading and latent heating to downburst generation (e.g., Srivastava 1987; Wakimoto and Bringi 1988), particularly when combined with rapid-scan, dual-Doppler to measure downdraft and subsequent wind speeds.

b. *Lightning*

The processes that lead to cloud electrification and discharge occur on very short time scales, with flash rates of hundreds per minute in intense thunderstorms (e.g., Williams et al. 1989; Schultz et al. 2009; Calhoun et al. 2013) and rapid increases in lightning are often associated with severe storms (Williams et al. 1999; Schultz et al. 2009, 2015; Chronis et al. 2015) and increases in convective mass and ice particle fluxes (Deierling et al. 2008; Bruning and MacGorman 2013; Schultz et al. 2015). Lightning mapping arrays (LMAs) afford the capability to acquire subsecond sampling of electrical discharges. However,

intercomparisons with parabolic dish radar scans are difficult since they only provide a snapshot of corresponding three-dimensional storm structure every 3–5 min, making it difficult to link storm microphysics and dynamics to electrification. The difference in sampling frequency between LMAs and radars have been lessened by sacrificing radar spatial coverage using fixed radar beam positions with subsecond temporal sampling or RHIs collected every 10–20 s (Hendry and McCormick 1976; Caylor and Chandrasekar 1996).

Parabolic dish radars with dual-polarization capability have shown that ice crystals, up to a few millimeters in diameter, become increasingly vertically aligned as the electric field strengthens and ice crystals become horizontally aligned after lightning discharge (Weinheimer and Few 1987). Such changes can occur on time scales as short as 1 s (Hendry and McCormick 1976; Caylor and Chandrasekar 1996), but can also occur more gradually over time scales of 10–30 s in other cases (Caylor and Chandrasekar 1996; Krehbiel et al. 1996; Biggerstaff et al. 2017). In contrast to parabolic dish radars, imaging radars can be used to provide subsecond RHIs or three-dimensional observations in less than 10 s. Initial experiments are underway to collect these data with imaging systems (Wang et al. 2023; Yu et al. 2023), which can be used to expand upon previous work in one- or two-dimensions to elucidate the three-dimensional structure of aligned ice and its response to electric field changes at more appropriate time scales. A potential barrier to using imaging radars to examine ice alignment signatures is that the anvil region containing these ice crystals has lower reflectivity compared to lower altitudes, and thus the higher sidelobe levels and reduced sensitivity of imaging systems may yield lower data quality than traditional radars.

The principal contribution of rapid-scan radars to lightning studies to date has been to examine inferred updraft and downdraft motions and their relationship to time-evolving charge and microphysical structure. Ice crystals and graupel obtain different charge in mixed-phase updraft regions through rebounding collisions in the presence of supercooled liquid water (Takahashi 1978; Saunders 2008; Deierling et al. 2008). Rapid-scan radar studies have focused on fluxes of ice crystals and graupel in the mixed-phase region of thunderstorms and subsequent charge separation due to differential sedimentation of these ice species. Using the NWRT PAR (Emersic et al. 2011) in Oklahoma and the PAWR (Yoshida et al. 2017; Moroda et al. 2022) in Japan, observations of single- and multicell storms showed that ascending regions of high reflectivity coincided with a collocated ascending region of increased lightning discharge inferred from radiation sources. The rate of ascent of echo tops was associated with the ascent rate of the positive-charge layer inferred by lightning discharges measured by LMA data (Emersic et al. 2011; Yoshida et al. 2017; Moroda et al. 2022) and is illustrated in Fig. 10. This figure shows a developing convective cell with a core of reflectivity exceeding 50 dBZ ascending from 4 to 10 km ARL in approximately 7 min. Concurrent LMA data on the left indicate an initial ascent of a lower positive and negative charge layer and the development of an upper positive charge layer as the reflectivity core reaches its maximum altitude. Lightning discharges occurring in the upper portion of the ascending reflectivity core are hypothesized to result from noninductive charging from ice crystals and graupel (Moroda et al. 2022).

Significant scientific advancements have followed the deployment of LMAs or similar three-dimensional lightning mapping networks in recent years (Goodman et al. 2005; MacGorman et al. 2005; Bruning and MacGorman 2013), but rapid-scan radar technology has only been used to observe kinematic processes with comparable temporal resolution on rare occasions. Methodology developed using traditional radars to investigate the relationship between lightning activity or charge structure and updraft intensity (Stough et al. 2022), turbulence kinetic energy (Souza and Bruning 2021), and three-dimensional microphysical trajectories (Chmielewski et al. 2020) could be reproduced in the future with rapid-scan radars for shorter time scales and with three-dimensional-storm scale observation. Compared to the millimeter-wavelength radar systems used in the TKE studies, existing rapid-scan radars are limited to cross-beam spatial sampling of a few hundred meters, which are sufficient to resolve eddy-scale processes at ≥1-km scale that affect charge structure (Brothers et al. 2018), but not finer-scale turbulence resolved by existing millimeter-wavelength radars (<300 m).

c. *Deep convection tracking and flash flood potential*

Weather radars are uniquely capable of detecting and tracking localized regions of heavy precipitation, which cause flash flooding, one of the leading causes of weather-related fatalities in the United States (Ashley and Ashley 2008). Rapid-scan radars are necessary to track and document the evolution of heavily precipitating cells that, on average, last between 5 and 15 min (Isoda et al. 2018; Wen et al. 2021; Moroda et al. 2021). Although cells can be detected by slower scanning radars, PARs allow 10–15 volumes within cell lifetimes to finely capture evolution. In Isoda et al. (2018), PAR observations showed a rapidly developing cell with >55-dBZ reflectivity in less than 3 min from first echo detection (Fig. 11). Moroda et al. (2021) documented and tracked the individual life cycles of convective cores and precipitating regions within a multicell storm, finding that the majority of cells produced heavy rainfall at the surface within 9–15 min of initial echoes aloft. Future research with rapid-scan, dual-polarization radars could improve storm tracking and vertical sampling to better capture the microphysical differences resulting in varied pathways to precipitation formation and intensities, for example, to explain the substantial differences seen in storm longevity and rainfall rates (Fridlind et al. 2019; Jensen et al. 2022).

Rainfall rates locally exhibit high temporal and spatial variability (Nystuen 1998; Krajewski et al. 2003) that impact flash flood potential and streamflow. Using KOUN rapid sector-scan data to explore the utility of high-temporal-resolution radar observations, Wen et al. (2021) found that although all radar-derived streamflow algorithms underestimate streamflow compared to situ measurements, 5-min radar data produced 10% less discharge compared to 1-min data. More degraded 30- and 60-min radar estimates of streamflow were 33% and 43% less, respectively. However, the impact of rapid-scan data is most evident when identifying flash flood events. Using 1-min data as truth, Wen et al. (2021) also found that 5-min

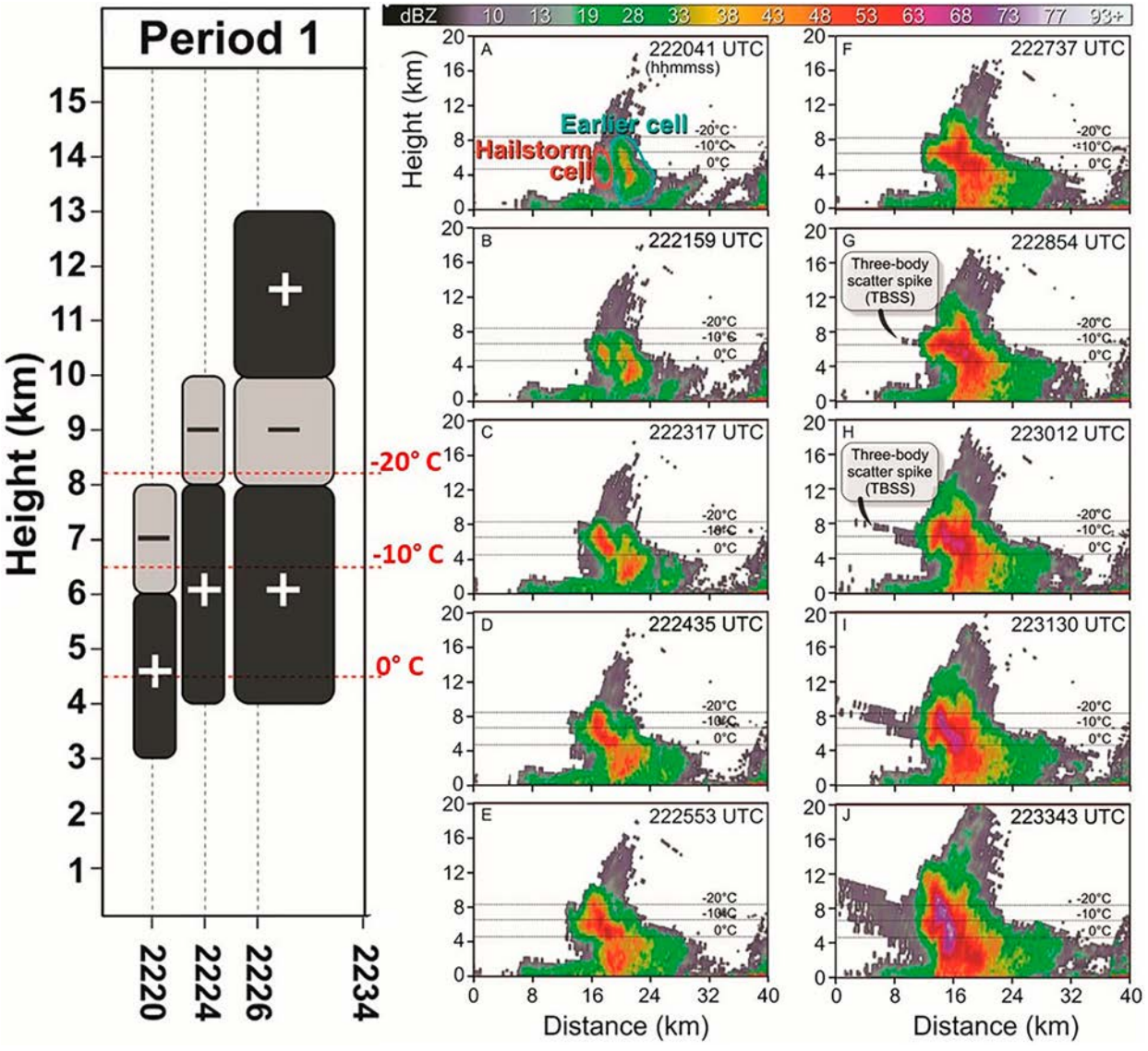

FIG. 10. (left) Charge structure inferred from lighting discharges measured by the Oklahoma LMA and (right) NWRT PAR, showing the concurrent evolution of the vertical charge structure and a rapidly developing new cell between 2220 and 2226 UTC. In the left column, the charge structure with red lines indicating environmental temperatures is displayed. In the right column, radar vertical cross sections of radar reflectivity (dBZ) are displayed with black lines corresponding to the same environmental temperatures as on the left. Adapted from Emersic et al.'s (2011) Figs. 3 and 5.

data missed over half of flash flooding events defined by a discharge threshold. The temporal resolution of radar data had the greatest impact when observing rainfall over small drainage basins, and temporally degraded data impacted discharge rates even more than spatial degradation. Because these observations were limited to Oklahoma, additional research is needed to quantify these benefits in different climatic regions and over different basin characteristics.

d. Tropical cyclones

High-temporal-resolution radar research has attempted to bridge the gap between the time and space scales of motions resolved by in situ surface observations and WSR-88D, which is necessary to examine heterogeneous causes of damage within tropical cyclones. Small-scale features, such as boundary layer rolls, contribute to localized perturbations in background flow and downward transport of high-angular-momentum air (Wurman and Winslow 1998; Morrison et al. 2005). Using 12-s single-elevation PPI observations, DOW Doppler velocity perturbations on the order of 10 m s^{-1} have been correlated with the observed fluctuations in measured surface wind speeds as illustrated in Fig. 12 (Kosiba et al. 2013a). In addition to boundary layer rolls, short-time-scale fluctuations in wind speed have

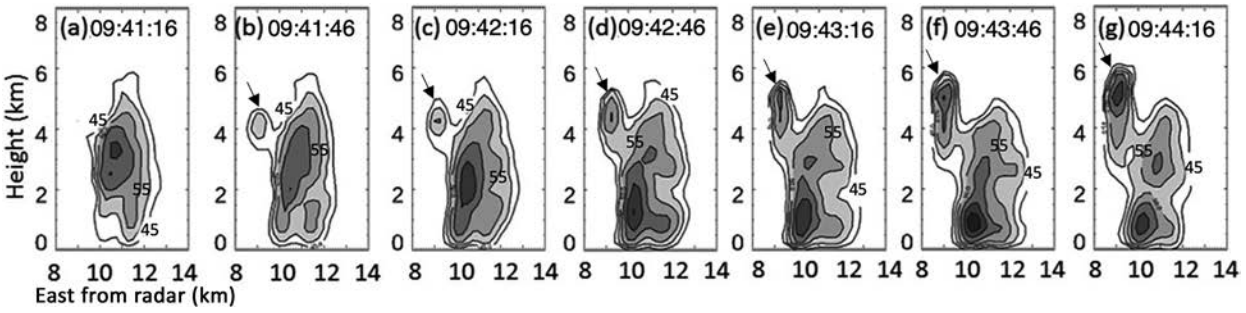

FIG. 11. Vertical cross sections of radar reflectivity factor through isolated thunderstorms near Osaka, Japan, on 26 Jul 2012, observed by the PAWR. Observations are shown every 30 s from 0941 to 0944 UTC, and the contour increment is 5 dB*Z*. The first filled contour has 45 dB*Z*, and the darker shadings increase by 5 dB*Z*. A rapidly intensifying new cell develops upwind between 4 and 6 km AGL in a period of 3 min and is denoted by the black arrow in each panel. Figure from Isoda et al.'s (2018) Fig. 6.

been observed along the periphery of convective bands (Alford et al. 2020).

Mesoscale vortices associated with vortex Rossby waves within the hurricane eyewall also perturb the observed near-surface wind field (Montgomery and Kallenbach 1997). Four distinct mesoscale vortices were observed within the eyewall of Hurricane Harvey, each with diameters ranging from 2 to 11 km and amplitudes of 15–20 m s^{-1} relative to the background flow (Wurman and Kosiba 2018). Rapid-scan observations facilitated the tracking of the Rossby waves and identified that they translated at approximately half the background wind speed (32 versus 55–70 m s^{-1}). Tornado-scale vortices were also observed during Hurricane Harvey, lasting from 60 to 240 s and producing peak gusts that lasted for less than 10 s (Wurman and Kosiba 2018).

Although some studies documented characteristics of tornado-scale vortices, vortex Rossby waves, and the hurricane boundary layer, the use of rapid, single-elevation analyses precluded deeper understanding, such as examining the formation and dissipation of tornado-scale vortices or the three-dimensional structure of boundary layer rolls. Additionally, recent studies (e.g., Wingo and Knupp 2016; Fernández-Cabán et al. 2019; Alford et al. 2019) have documented the three-dimensional wind fields of vortex Rossby waves and investigated how they may contribute to localized near-surface wind extrema. These studies were limited by using at least one WSR-88D radar to create

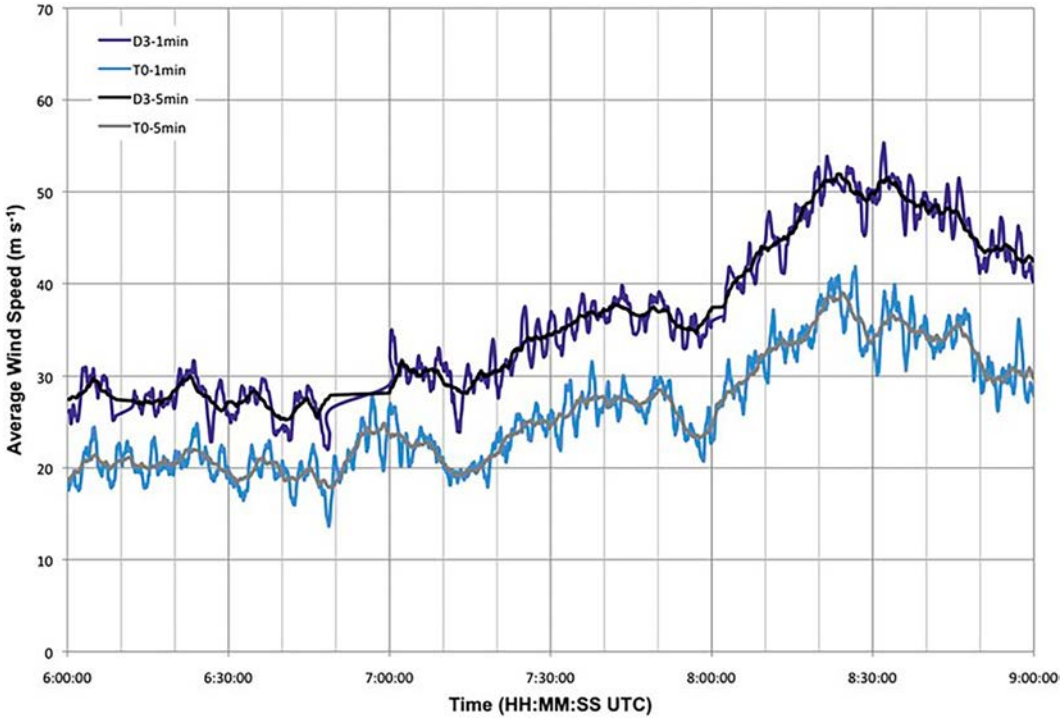

FIG. 12. Time series of 1- and 5-min average wind speeds from DOW (purple) and in situ measurements (blue) during Hurricane Rita. Dow measurements are from ~100 m ARL. Figure from Kosiba et al.'s (2013a) Fig. 7.

dual-Doppler analyses. Rapid-scan dual-Doppler analyses could improve the accuracy of analyses by minimizing time differences between contributing volume scans and help bridge the gap for investigating the evolution of mesoscale features on time scales closer to the wind gusts that may contribute to the greatest damage.

5. Improvements in wind retrievals

Three-dimensional wind retrievals are critical to understanding the dynamics of thunderstorms and the formation of severe hazards. Errors in three-dimensional wind retrievals can often be significant (Ray et al. 1980; Dowell and Shapiro 2003; Gao et al. 2004; Potvin et al. 2012a,b; Oue et al. 2019). Two common sources of error are nonlinear advection and evolution of observed phenomena that occurs between volumetric samples and the related errors in vertical velocity estimates that arise from vertical integration of mass continuity using a poorly sampled low-level wind field and temporally displaced observations. To remedy these errors, the addition of the vertical vorticity equation as a dynamical constraint has been explored (Shapiro et al. 2009) as well as spatially variable advection correction (Shapiro et al. 2010a,b). Rapid-scan radar observations are necessary to adequately estimate the time rate of change of vertical vorticity and nonlinear advection and evolution of Doppler velocity fields required for these proposed techniques. In this section, the benefits of rapid-scan observations to improve wind retrievals are discussed, including multi- and single-Doppler methods.

Owing to the limited availability of rapid-scan, multi-Doppler observations necessary to calculate the time rate of change of vertical vorticity, most studies to date have focused on simulating dual-Doppler analyses from high-resolution models. Using supercell simulations, Potvin et al. (2012a) and Dahl et al. (2019) demonstrated that increasing temporal sampling from 5 to 2 min showed the greatest improvement in the accuracy of vertical velocity retrievals by up to a factor of 2, whereas finer temporal sampling than 2 min produced more modest improvement. The benefit of using rapid-scan radars for dual-Doppler analyses diminished with increasing range, likely due to the poor matching of resolved space–time scales (Dahl et al. 2019). The vertical vorticity constraint is most helpful in cases where the low-level mass flux is poorly sampled (e.g., no observations were available in the lowest 1.5 km AGL), but it still improves analyses when low-level observations are available (Potvin et al. 2012a).

Radar simulation studies further demonstrated that rapid-scan data can better estimate nonlinear advection and improve vertical sampling of the mass flux. Using simulations of mesoscale convective systems (MCSs), Oue et al. (2019) found that volume scans of 2 min or less were needed for accurate three-dimensional wind retrievals. Advection correction further improved dual-Doppler analyses for 2-min volume scans, but did not improve them for 5-min volume scans owing to substantial convective evolution. Similarly, Dahl et al. (2019) determined that advection correction based on reflectivity tracking improved analyses, but only for sub-30-s intervals. When collecting volume scans of 2 min or less, increasing the density of upper-level observations improved vertical velocity retrievals at higher altitudes that are important for understanding many convective phenomena such as hail and lightning and are often poorly sampled (Oue et al. 2019). Comparatively, denser vertical sampling was found to improve analyses more than the introduction of advection correction, but not as much as faster sampling (Oue et al. 2019).

Although most of the previous studies were done with simulated data, a few studies have performed rapid-scan, dual-Doppler analyses using observations (Wakimoto et al. 2016; Moroda et al. 2021; Gebauer et al. 2022). Using observations of a single-cell thunderstorm, including vertically pointing radar verification, Gebauer et al. (2022) found that significant errors in w were introduced when the volume scan time increased from 30 to 90 and 150 s. The use of advection correction mitigated many of the introduced errors, but the improvement diminished for shorter time scales where interscan advection is minimized. Additionally, a vertical vorticity constraint improved analyses compared to retrievals without this constraint despite adequate low-level observations. The use of the vertical vorticity constraint even improved vertical velocity estimates in single-cell thunderstorms and MCSs where magnitudes of vertical vorticity changes (and associated tendency terms) are smaller than supercell thunderstorms. However, systematic studies of differences in rapid-scan wind retrievals among convective modes are still needed.

The most extensive application of rapid-scan radars to observations is through single-Doppler wind retrievals. Using 30–60-s volumetric update rates, several observational studies showed improvement in variational, single-Doppler wind retrievals when increasing temporal sampling from 5 to 1 min or less (Shapiro et al. 2003; Qiu et al. 2013; Otsuka et al. 2016; Liou et al. 2018). Rapid, single-Doppler observations have facilitated improved kinematic estimates in cold-front (Shapiro et al. 2003), downburst (Qiu et al. 2013), supercell (Liou et al. 2018), and tornado (Kosiba and Wurman 2013) cases. Additionally, when using one rapidly scanning radar and a WSR-88D, Wienhoff et al. (2018) demonstrated that rapid and improved-accuracy multi-Doppler wind retrievals can be obtained even when only using one rapidly scanning radar and a spatially variable advection correction scheme (Shapiro et al. 2010a). Liou et al. (2018) performed an experimental intercomparison between single- and dual-Doppler wind retrievals and found a qualitatively similar spatial structure of vertical motions when using rapid-scan observations, but considerable differences in magnitudes. Although these retrieval techniques appear promising and could alleviate some challenges with multi-Doppler deployment logistics, more research is needed to evaluate their potential for qualitative and quantitative analyses.

Future field experiments are needed to more robustly determine whether single- and dual-Doppler wind estimates of three-dimensional winds improve in actual rapid-scan observations and the degree to which these benefits vary as a function of phenomena observed, scanning strategies, radar standoff range, and mismatch in temporal synchronization. More extensive validation of dual-Doppler wind syntheses

TABLE 4. Summary of PAR forecast evaluation experiments, including number and type of cases, number of forecasters, and whether POD, FAR, and lead time improved. Cases include a mix of tornado (TOR), severe wind and hail (SVR), and subsevere (NULL) events. Most experiments quantified forecast statistics relative to a control group. However, the asterisk denotes statistics computed relative to the forecaster's NWS office or region. Thus, the relative changes in forecast statistics are not included. Median lead time compared to the control group is provided in parentheses.

Study	Phenomena/No. of cases	No. of forecasters	POD improved?	FAR improved?	Lead time improved?
Heinselman et al. (2012)	1 TOR, 1 SVR	12 (6 pairs)	Unknown	No (+50%)	Yes (+12.8 min)
Heinselman et al. (2015)	2 TOR, 2 SVR	12	Yes*	Yes*	Yes*
Bowden et al. (2015)	2 SVR	12	Yes (+11%)	Yes (−10%)	Yes (+5 min)
Wilson et al. (2017b)	3 TOR, 3 SVR, 3 NULL	30	Yes (+7%)	Yes (−2%)	Yes (+3.4 min)

from vertically pointing radar observations is needed to understand quantitative differences in errors from different volume scan times and vertical sampling strategies across a spectrum of convective modes. Examination of how these errors affect derived meteorological quantities is limited, particularly from observations. Oue et al. (2019) illustrate how different volume scan times and vertical sampling strategies subsequently affect estimates of convective mass flux and updraft fraction in OSSEs, which could be further tested using observational data. Other meteorological applications are best suited for simulations because of verification limitations, such as quantifying errors in Lagrangian vorticity budgets or hail trajectories.

6. Benefits for weather forecasting

In addition to enabling science research (discussed in sections 3–5), rapid-scan radar systems are being considered to replace the existing operational WSR-88D radar network (Zrnić et al. 2007; Weber et al. 2021). Improvements in operational forecasting could emerge from forecasters using rapid-scan radar data in warning decision-making, as well as increasing the accuracy of short-term numerical weather prediction models assimilating rapid-scan data. In this section, operational PAR test bed experiments are reviewed to evaluate whether rapid-scan radar data have helped improve forecaster decision-making and warning metrics (section 6a). Then, the impact of rapid-scan radar observations on numerical weather prediction is examined (section 6b).

a. Forecaster evaluation of rapid-scan radar data

For network-wide upgrades and replacements, operational radar testbeds have proven highly beneficial for demonstrating and evaluating new radar technologies, including testbeds for Doppler (Burgess et al. 1979) and polarimetric capabilities (Scharfenberg et al. 2005). Building upon previous radar technology testbeds, a series of Phased Array Radar Innovative Sensing Experiments (PARISEs) were conducted from 2010 to 2015 to evaluate the impact of PAR data on warning performance and obtain forecaster feedback on its benefits and limitations (Heinselman et al. 2012, 2015; Bowden et al. 2015; Bowden and Heinselman 2016; Wilson et al. 2017a,b). PARISE used data collected with the NWRT PAR in Norman, Oklahoma (Zrnić et al. 2007). Although numerous benefits to operations were found in PARISE and will be summarized in this subsection, a few caveats are noted. First, owing to the fixed site, cases were only collected in Oklahoma and thus broader benefits and limitations across the United States were not evaluated. Next, compared to an envisioned operational PAR, the NWRT PAR had a larger beamwidth, poorer sensitivity, lacked dual-polarization capability, and scans were limited to a 90° volumetric sector. Compared to the NWRT PAR, a full-scale operational PAR will have enhanced capabilities, including better spatial resolution and data quality, as well as 360° coverage in azimuth.

The main experimental setup of PARISE involved testing warning performance and decision-making with 1-min PAR data compared to PAR data temporally degraded to a typical WSR-88D update rate (5 min). Forecasters with varying levels of experience were recruited from different NWS regions. Each successive PARISE involved a higher number of forecasters and larger sample sizes of PAR cases, which are briefly summarized in Table 4. The 2015 experiment had forecasters rotate through being part of the control group with 5-min data and experiment group with 1-min data, whereas earlier experiments did not involve enough cases to allow for this. In addition to quantitative evaluation of warning metrics, later experiments also sought to determine how forecasters were using rapid-scan data to make decisions through retrospective cognitive task analysis (Heinselman et al. 2015; Bowden and Heinselman 2016; Wilson et al. 2017a).

Throughout each PARISE, warning performance metrics provided a key quantitative measure of the benefits of PAR data. Specific warning statistics are presented in Table 4, covering 4 years of PARISE and 17 total PAR cases (including 6 tornado cases) involving 66 total participants. In all four experiments, the PAR group had a better warning lead time compared to the control group by an average of 3–13 min (Heinselman et al. 2012, 2015; Bowden et al. 2015; Wilson et al. 2017a,b) In addition, the PAR forecast group generally exhibited small improvements (10% or less) in probability of detection (POD) and reduced false alarm ratio (FAR) compared to the control group. Partitioning the data into tornado and severe cases (hail, wind), Wilson et al. (2017b) noted that the average warning lead time improved for tornado cases. Bowden et al. (2015) found a statistically significant improvement in lead time for severe events (5-min increase), whereas the warning lead time did not improve for the severe events examined in Wilson et al. (2017b). Although PARISE studies consistently found modest improvements in warning metrics, statistical significance in forecaster performance was reported

only in a few instances. This may be in part because the number of cases is small, particularly when subsetting tornado and severe cases. This small sample size likely resulted from the experimental design that focused on obtaining detailed qualitative feedback from forecasters about their decision-making process and replicated an operational setting, requiring travel and increased costs that limit participation.

When describing the impact of rapid-scan data on their decision-making, forecasters claimed higher confidence in their warning decisions while exhibiting greater forecast skill (Heinselman et al. 2012; Bowden et al. 2015). Forecasters in the PAR group leveraged the high-temporal-resolution data to evaluate temporal trends and vertical continuity of rotation across scans. In two cases, forecasters correctly diagnosed that the intensification and deepening of rotation was short-lived, whereas forecasters with 5-min data incorrectly issued "false alarm" tornado warnings since they were not comfortable waiting another 5 min for additional data (Bowden and Heinselman 2016). Next, forecasters reported that 1-min radar data provided them with a better ability to identify trends in storm intensity and motion (Heinselman et al. 2015; Bowden and Heinselman 2016; Wilson et al. 2017a). For example, forecasters were able to better account for deviant storm motion and adjust warning polygons accordingly. In addition, they noted an improved ability to cancel warnings when severe weather threats diminished and more readily identify subsevere hazards when deciding not to issue warnings (Bowden and Heinselman 2016). In particular, more frequent radar updates were helpful in monitoring mesocyclone trends for tornado warning decisions, perhaps explaining some improvements in warning performance.

Although high-temporal-resolution data improved warning performance and forecaster comprehension of events, an increase in data volume introduced some challenges to forecaster situational awareness. Forecasters in the PAR group reported a higher cognitive workload compared to the control group (Wilson et al. 2017b). However, after a short adjustment period, forecasters were better able to prioritize the most important data and adapt their data interrogation strategies (Bowden and Heinselman 2016; Wilson et al. 2017a). These strategies were highly individualistic, and therefore more research is needed to examine best practices for incorporating PAR data into warning operations. Because forecasters were used to 5-min updates, some recalibration to their perceived sense of time was necessary when using 1-min data. For example, forecasters needed to resist warning based on transient storm behavior and leverage the increased temporal sampling to ensure a sustained trend (Wilson et al. 2017a).

In summarizing conceptual models used by forecasters (Heinselman et al. 2015), key indicators of imminent tornadogenesis included a descending intensification of the mesocyclone. However, non-descending TVS intensification appears to be the most common mode of tornadogenesis in rapid-scan observations, as discussed in section 3a. Moreover, the descending tornadogenesis mode may be an artifact of temporal aliasing due to small, transient tornado-intensity vortices being misinterpreted as temporally continuous, descending tornado development (French et al. 2013). Thus, future research needs to examine whether forecaster conceptual models of tornadogenesis and training modules need to change for fixed-site, rapid-scan operational radars that less commonly observe tornado-scale features due to limited spatial resolution and reduced low-level coverage. For example, in recent high-resolution numerical simulations, Yao et al. (2019) noted the downward development of the mesocyclone was followed by a rapid upward intensification of the tornado, illustrating how differences in time evolution of rotational intensity may vary depending on the minimum observable scale.

Future research should also examine a larger sample size of archived PAR cases, evaluate rapid-scan cases from other regions, and compare forecaster performance using dual-polarization WSR-88D data and polarimetric PAR data, from, for example, the ATD. Additionally, analysis of precursor signatures using statistical analysis or automated algorithms would enable studies to examine whether PAR data improve the detection and lead time of precursor signatures. For example, such comparisons were done between polarimetric and conventional radar data to evaluate the comparative performance of rainfall estimation and hail detection algorithms (Scharfenberg et al. 2005). In addition, algorithms or machine learning approaches could be used to leverage trends from rapid-scan data to better identify trends in precursor signatures that traditional algorithms cannot identify (Chase et al. 2022; Sandmæl et al. 2023). Finally, rapid-scan observations from experiments outside of Oklahoma could help assess the benefits and limitations of an operational PAR network for more geographically diverse weather phenomena.

With a much larger sample size of cases and greater geographic diversity, the recent implementation of Supplemental Advantage Intravolume Low-level Scans (SAILS) may provide some insight into the operational utility of 1–2-min revisiting of low-level PPIs in a future PAR network. In SAILS mode, one to three additional lowest-elevation-angle scans are interspersed into a volume coverage pattern to capture the evolution of rapidly evolving low-level features. Evaluations of warning statistics with and without SAILS mode demonstrated that lead time, POD, and FAR for severe thunderstorm warnings, flash flood warnings, and tornado warnings improved when SAILS mode was used (Kingfield and French 2022; Cho et al. 2022). But, while SAILS mode offers an important adaptation to the capabilities of the WSR-88D network, the increased volume scan time can adversely affect the detection of hazards originating at the mid and upper-levels (e.g., hail) or inhibit radar data assimilation efforts to initiate thunderstorms not yet represented in the model (Carlin et al. 2017).

b. Numerical weather prediction

Short-term forecasts of deep convection benefit greatly from the assimilation of radar data (e.g., Sun 2005; Stensrud and Gao 2010; Sun et al. 2014; Wheatley et al. 2015; Benjamin et al. 2016). Presently, radar data assimilation intervals are limited by the WSR-88D volume scan time of ~5 min, and

the inability of the WSR-88D radars to adaptively scan high-priority targets at more frequent intervals. Thus, two pertinent questions for PARs are whether significant improvements in model performance result from rapidly assimilating radar data and whether models can maintain dynamic balance while using faster assimilation cycles (Hu and Xue 2007; Dowell et al. 2011).

Predating the availability of rapid-scan technology, early studies used Observation System Simulation Experiments (OSSEs) to address the first question and explore whether shorter data assimilation intervals improved analysis and forecast accuracy. In the first investigation of assimilation of sub-5-min radar data, only marginal improvement in error statistics was found for the first few observation cycles (Zhang et al. 2004). However, subsequent OSSE studies found improvements in forecast performance when decreasing the assimilation time from 5 to 2 min, but reduced benefits from 2 to 1 min (Xue et al. 2006; Lu and Xu 2009; Yussouf and Stensrud 2010). The greatest benefit obtained from rapid data assimilation cycles was during convection initiation (Xue et al. 2006; Yussouf and Stensrud 2010) where models struggle with suppressing spurious convection and require an appreciable number (10–15) of data assimilation cycles to accurately capture the initial analysis. Thus, assimilating data every 1 min leads to a shorter storm initiation period of about 15 min compared to 5-min data assimilation intervals requiring close to 1 h. This rapid cycling may provide considerable future benefits to short-term (e.g., Warn-on-Forecast, Rapid Refresh Forecast System, etc.) forecasting efforts (Stensrud et al. 2013; Benjamin et al. 2016; Dowell et al. 2022).

In addition to facilitating more rapid cycling, the adaptive scanning of PARs can provide targeted observations to potentially benefit model forecasts. Assessment of the impact of adaptive scanning has been done in several OSSE studies. Using adaptive sampling to increase the number of elevation angles, Yussouf and Stensrud (2010) found that model forecast error decreased for close-range storms with additional upper-level observations by 10%–25% but no reduction was observed for storms at farther ranges where additional low-level scans provided limited independent information. Using an automated approach, Kerr and Wang (2020) demonstrated that an observation targeting algorithm can further reduce model error variances by adapting radar scanning strategies based on regions with the greatest predicted error reduction. Finally, adaptive scanning techniques that assimilated clear-air observations were shown to improve supercell track and updraft helicity forecasts (Huang et al. 2020). However, there was no substantial benefit in assimilating clear-air observations every 1 min compared to 5 min.

Following OSSE studies using simulated observations, data assimilation experiments with real PAR observations were conducted to examine their impact on short-term forecasts using four-dimensional data assimilation approaches. These techniques improved model balance by better synchronizing observations with model updates and reduced computational expense and errors (Wang et al. 2013; Supinie et al. 2017). Rapidly assimilating PAR observations (1-min time intervals) provided similar results to the OSSE studies, where the greatest improvement in forecast skill occurred during the first

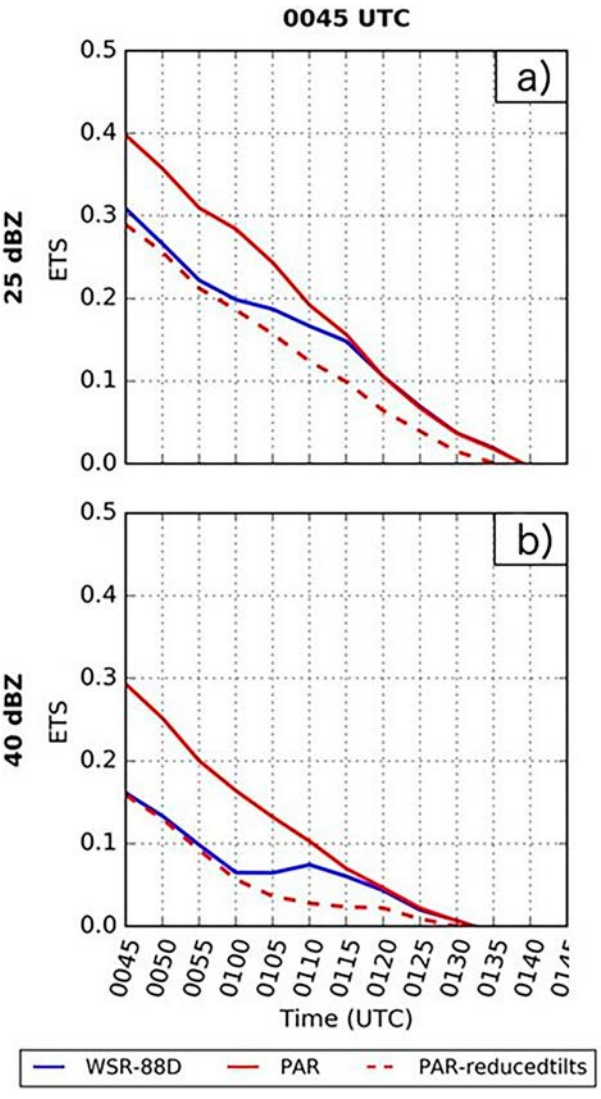

FIG. 13. Equitable threat score (ETS) for (a) 25- and (b) 40-dBZ thresholds, comparing the WSR-88D (blue solid), PAR (red solid), and PAR with fewer elevation angles (red dotted). For both thresholds, the PAR experiment shows improvement in ETS for the first 30–40 min of the forecast. Figure from Supinie et al.'s (2017) Fig. 17.

30–45 min due to faster initiation of supercell thunderstorms and mitigation of spurious convection (Supinie et al. 2017; Stratman et al. 2020). This improvement in forecast skill is demonstrated in Fig. 13, which shows equitable threat score assessments with different reflectivity thresholds. However, after the storm spin-up period, little difference in forecast skill was observed. Given this limitation, Stratman et al. (2020) proposed that adaptive cycling intervals could better leverage computational resources since 1-min cycling may not be needed at all times and locations, for example, after convection initiation. Adverse effects of assimilating radar data rapidly include stronger cold pools (Stratman et al. 2020), resulting from the coupling of microphysical fields and cold pool intensity (Dowell

TABLE 5. Characteristic temporal resolution needed to observe different phenomena with three to five samples, time period of evolution, and radar systems capable of addressing the temporal-resolution requirement.

	Optimal temporal sampling		
	<10-s volumes	<30-s volumes	<60-s volumes
Phenomena	Tornadoes Tropical cyclones Boundary layer rolls	Thunderstorm updrafts Lightning Microbursts Mesocyclones Eyewall vortices	Storm-scale microphysics Hail Flash flooding
Time period of evolution	<1 min	1–5 min	5–10 min
Radar systems	AIR MWR-05XP Rapid DOW	PAWR RaXPol	NWRT PAR DOW or KOUN (in sector mode)

et al. 2011). In addition, shortcomings in model parameterizations currently limit the benefit of sub-1-min radar data assimilation (Miyoshi et al. 2016).

Although some challenges remain to maximize the benefits of rapid cycling of PAR data, PAR data assimilation experiments have demonstrated the ability to improve short-term forecast skill (<1 h) while maintaining dynamic balance. However, the benefits of rapid radar data assimilation diminish after storm initiation, potentially a consequence of increased model imbalance due to persistent rapid cycling and diminished benefits once the observations and models have smaller differences (Guerra et al. 2022). A limitation of the studies to date is that they have focused only on the benefits of rapid data assimilation for supercell thunderstorms. Thus, a major gap is exploring whether rapid data assimilation would improve forecast skills for single cell or multicellular convection and nonconvective precipitation. Since the life cycle of single cell thunderstorms is less than 1 h, rapid cycling could improve analyses and forecasts by allowing the model to capture their full life cycle and resulting environmental changes (e.g., cold pools) that affect later forecast times. Although it is beyond the scope of this article, examining the comparative benefits and limitations of assimilating rapid-scan radar data with other observations is important to maximize computational resources and forecast performance. Assimilating all-sky irradiances complement radar observations, for example, by providing observations of early stages of convective clouds and other nonprecipitating clouds, leading to improved short-term model forecasts when combined with radar data assimilation (Zhang et al. 2018, 2019; Jones et al. 2020). In addition, joint radar and satellite data assimilation can improve the representation of boundary layer structure. Assimilation of dual-polarization estimates of planetary boundary layer (PBL) depth could improve model representation of the PBL by leveraging the higher temporal and finer vertical sampling capabilities of rapid-scan radars (Eure et al. 2023).

7. Summary and discussion

Over the past two decades, new rapid-scan radar technologies have allowed scientists to address temporal sampling gaps by collecting volumetric observations every 10–60 s. In this review, the impact of these radar systems on scientific and operationally focused research has been examined to understand where anticipated benefits were and were not obtained. We explore the impact of rapid-scan technologies and provide recommendations for future work on studied topics in section 7a. Based on overarching shortcomings, discussion of improved approaches to maximize the benefits of rapid-scan radars are presented in section 7b. This discussion focuses on how rapid-scan radars can be better integrated into field campaigns, how adaptive scanning can be better utilized, and what impactful research areas remain unexplored.

a. Impact of rapid-scan radars on science and operational applications

Examining the motivation described in the radar system papers (Wurman and Randall 2001; Zrnić et al. 2007; Bluestein et al. 2010; Isom et al. 2013; Pazmany et al. 2013), the rationale behind the development of rapid-scan radars was to study tornadoes and severe thunderstorms that have periods of evolution ranging from less than 60 s to on the order of minutes (Table 5). Subsequent research emphasized these areas heavily, particularly tornado research, as a result of user-case selection bias. Given the known rapidly evolving nature of tornadoes, the investigators leading these experimental efforts probably viewed tornado studies as best suited for initial rapid-scan data collection, in addition to aligning with their research interests and perhaps emphasis of funding opportunities. However, as a consequence of the user-case selection bias, many high-impact weather events have not been heavily emphasized in rapid-scan radar research, such as hailstorms, severe wind events, tropical cyclones, or flooding. Furthermore, rapid-scan radar studies outside of severe weather are even more limited despite considerable utility for studies of the life cycle of deep convection, precipitation studies in turbulent environments, or convective boundary layer research.

Given the heavy emphasis on severe weather data collection, it is unsurprising that the most extensive science advancements facilitated by rapid-scan radars have occurred for phenomena occurring on time scales of less than 1 min (Table 5).

One of the greatest advantages that rapid-scan radars provide for phenomena evolving on the shortest time scales is the ability to provide dense, vertical sampling while minimizing the evolution between elevation scans and successive volumes. These capabilities have been leveraged to advance scientific understanding of tornadoes by characterizing the fine-scale vertical evolution of rotation throughout a tornado's life cycle, identifying that the non-descending mode of tornadogenesis and inside-out tornado dissipation are most common.

Although these studies have quantified rotational intensity changes on 10–30-s time scales and authors do speculate on their relationships to tornadogenesis or dissipation theories, these studies were unable to robustly identify the dynamical mechanisms to explain tornado evolution. For example, what was the dynamical explanation for why tornadogenesis occurred and how was it connected to storm-scale vorticity generation? Coordinated multi-Doppler studies of tornadoes (e.g., Markowski et al. 2012a; Kosiba and Wurman 2013; Murdzek et al. 2020) using recently developed vorticity constraints would address this observational gap and will require coordination of a limited pool of rapid-scan radars within organized field experiments. In addition, intercomparisons between rapid-scan radar observations and high-resolution numerical simulations could be better utilized to explain physical mechanisms (e.g., Coffer et al. 2017; Coffer and Parker 2017; Orf et al. 2017; Orf 2019; Dahl 2021). Finally, rapid-scan radar analyses have focused exclusively on tornadoes from supercells. Thus, future research should prioritize collecting and analyzing rapid-scan radar observations of quasi-linear convective systems, tropical cyclone tornadoes, or non-supercellular tornadoes.

Research on severe hazards evolving on time scales of 1–5 min (Table 5) focused on documenting rapid changes in precursor signatures, with some qualitative commentary about physical processes. For example, brief midlevel convergence signatures have been documented preceding severe wind events and descending high-reflectivity cores were tracked in instances where a WSR-88D undersampled or completely missed hail and wind events. In addition, rapid-scan observations have aided research correlating rapidly ascending reflectivity cores with concentrated regions of lightning discharges. Similar to studies of supercells and tornadoes, the collective advancement in the understanding of physical processes has been limited. In some instances, authors note a clear need for dual-polarization capabilities or multi-Doppler retrievals of three-dimensional winds. For example, in lightning studies, the authors offered hypotheses that were not able to be tested without polarimetric observations (e.g., dry versus wet growth impacting lightning rates) or three-dimensional wind observations (e.g., correlation of developing updraft characteristics with observed charge structure).

The last part of this review examined benefits and limitations of rapid-scan radar observations to operational and numerical weather prediction forecasts for features evolving on the order of minutes (Table 5). The multiyear PAR test bed experiments provided quantitative assessments of benefits to operational warnings and excelled at qualitatively understanding how 1-min PAR data impacted forecasters' decision-making, confidence, and workload. However, there is undoubtedly an upper limit to the amount of data a forecaster can process, and therefore it is uncertain how much of a role direct human interrogation of the highest-frequency radar fields will play in future operational settings, compared to automated algorithms leveraging artificial intelligence (Stuart et al. 2022) or short-range model guidance. Nevertheless, modest improvements in operational warning performance with rapid-scan data have been found, and even increases in warning lead time of a few minutes or improvements 5%–10% in POD or FAR have been difficult to obtain since the upgrade of the nationwide network to Doppler capability (Brooks and Correia 2018). In addition, short-term forecasts of convection are improved with rapid cycling of radar data, reducing spurious convection and improving initiation of convection. Although initial results suggest benefits to operational and NWP forecasts, the total number of cases remains small and statistical significance has rarely been attained. Future forecast evaluation and NWP experiments must quantify forecast improvement across a larger and more diverse set of meteorological phenomena and geographic regions. OSSEs or analysis of field campaign observations could be used to study phenomena where test bed radar systems are not available.

b. Improving the utility of rapid-scan radar systems

Although rapid-scan radars have advanced scientific understanding of severe thunderstorms and their utility for forecasting, substantial opportunities remain to improve the utility of rapid-scan radar systems for science research. To address these shortcomings, we offer the following recommendations:

1) Collect coordinated rapid-scan, multi-Doppler and multisensor observations in field campaigns to increase physical understanding of observed phenomena.
2) Increase the use and maturity of adaptive scanning techniques that acquire dense vertical observations and targeted observations in multisensor field campaigns.
3) Discuss whether rapidly collected data added significant value over traditional observation frequencies for different meteorological phenomena.
4) Expand rapid-scan radar technology using dual-polarization and different transmit frequencies.
5) Increase the breadth of phenomena studied using rapid-scan radar, particularly for non-severe weather applications.

Arguably the most substantial advancements with rapid-scan radars will occur in concert with large-scale field campaigns where rapid-scan radar observational analyses are integrated with complementary in situ and remote sensing instrumentation. For example, radars cannot directly observe thermodynamic quantities, but such observations are critical to understanding the structure of cold pools or the influence of convective boundary layer thermodynamic variability on convection initiation and subsequent evolution. In addition, rapid-scan radars have limited ability to measure clear-air winds, and thus in situ and remote sensors (mobile mesonets, unmanned aircraft systems, lidars, wind profilers) can augment radar wind measurements by

capturing near-storm environmental winds. Rapid-scan radars could be leveraged to guide in-air and ground-based in situ instrumentation and coordinated multiplatform data collection. For example, rapid-scan radars and aircraft could target initiating convective cells to study their dynamical and microphysical evolution at fine temporal scales, with aircraft providing important in-cloud and environmental thermodynamic characteristics (e.g., humidity, temperature), as well as hydrometeor characteristics. Rapid-scan polarimetric data or retrieved three-dimensional winds could offer multiple measurements between flight penetrations to explain changes in hydrometeor distributions or convective updraft and downdraft structure.

A few notable recent examples of multiplatform field campaigns involving rapid-scan radars have provided opportunities to evaluate the added value of rapid-scan radar systems and identify improved sampling strategies. In the NASA Investigation of Microphysics and Precipitation for Atlantic Coast-Threatening Snowstorms (IMPACTS; McMurdie et al. 2022) and Experiment of Sea breeze Convection, Aerosols, and Precipitation (ESCAPE) field campaigns, SKYLER was operated in a rapid-scan volumetric sector mode, collecting observations in <1 min (Kollias et al. 2022). RaXPol participated in both of these field campaigns, but deployments often focused on slower volume scans (2–3 min) to provide high data quality while occasionally operating in a rapid-scan mode. RaXPol and SKYLER were also deployed in the Propagation, Evolution, and Rotation in Linear Storms campaign (PERiLS) on a limited basis (Schneider et al. 2023), which provided rapid-scan radar observations on quasi-linear convective systems in the Southeast United States. From these recent field campaigns, scientists should evaluate the benefits and limitations of the rapid-scan radar observations compared to other traditional radars. For example, was it more beneficial to scan slowly for better data quality or scan rapidly to characterize smaller-scale processes and fast-evolving evolving phenomena?

In addition to expanding the use of rapid-scan radars in field campaigns, future rapid-scan radar studies would benefit from greater use of adaptive scanning techniques. A benefit of adaptive scanning techniques is that meteorological phenomena can be scanned without vertical gaps. A common trade-off made in field campaigns is introducing large elevation angle gaps between PPIs in what users may consider less "important" areas (e.g., prioritizing low level scans over upper level scans) to avoid long volume scan times. Additionally, RHI scans are commonly prioritized to capture the vertical structure of deep convection or the boundary layer, but this mode requires considerable additional scan time. In contrast, PARs can acquire data with continuous vertical sampling and RHI-like views without stopping the antenna, providing a more holistic understanding of the vertical structure of meteorological phenomena while still maintaining temporal sampling < 1 min. As a result, adaptive scanning with PARs would inherently reduce user selection biases in many instances by eliminating the need for spatially limited scanning strategies.

Although adaptive scanning has been emphasized as a potential benefit to PARs (Zrnić et al. 2007), implementation of these techniques for science research has been scarce due to technological limitations. Several PARs had limited adaptive scanning capabilities, such as the AIR that was limited to imaging-only modes and the NWRT PAR and MWR-05XP that could not do imaging. However, new PAR systems will have greater flexibility to leverage multiple PAR scan modes. The complexity of developing and implementing effective adaptive scanning techniques is a challenge given the large amount of software development time required. Developing open-source software for adaptive scanning and PAR systems would help accelerate the scientific community's efforts toward achieving these goals. Given the challenge of manually determining adaptive scanning modes, machine learning or other algorithms demonstrated on parabolic dish and PARs can guide adaptive scanning (e.g., McLaughlin et al. 2009; Heinselman and Torres 2011; Nguyen and Chandrasekar 2017; Kollias et al. 2020).

A technological limitation of many rapid-scan radars discussed in this review is that these systems have only improved temporal resolution, whereas the spatial resolution was either degraded (due to high system development costs) or at best remained the same compared to traditional, parabolic-dish radars. Spatial and temporal scales are generally coupled, with smaller features typically evolving on shorter time scales (Orlanski 1975; Wurman et al. 2008). Thus, many rapid-scan studies may spatially undersample the features of interest, which could lead to erroneous conclusions. Moving from prototype rapid-scan radars that were restricted by cost or availability of military surplus options to larger aperture systems could address the technological gap. Additionally, millimeter-wavelength, rapid-scan radar may also facilitate more adequate sampling of small-scale features. Nonetheless, comparatively better spatial resolution will remain a substantial advantage of dish-based radar systems for the foreseeable future. In addition, obtaining comparable polarimetric PAR data quality to dish-based radar systems remains a challenge (e.g., Zhang et al. 2011; Orzel and Frasier 2018; Weber et al. 2021). Given the complementary strengths of traditional parabolic dish radars and PARs, and the comparatively high costs and complexity of PARs presently, both types of radar systems will continue to have important roles in science research and should be used synergistically in field campaigns.

A pressing gap in the rapid-scan radar literature has been the lack of commentary on whether rapid-scan radar observations were beneficial to advancing science. In addition to expanding the breadth of meteorological phenomena studied, future studies should emphasize where minimal additional utility or technological limitations were found. In other words, while scientists have hypothesized various time scales for different phenomena, what are the necessary time scales that are truly important for observing these phenomena and advancing scientific understanding? Rapid-scan radar observations may also already exist for many phenomena, but have not yet been analyzed (or the results have not been reported). For example, rapid-scan DOW8 observations exist from the Ontario Winter Lake effect Snow experiment (Kristovich et al. 2017; Wurman et al. 2021). Publications from these campaigns have yet to make substantial use of the rapid-scan elements of

collected data. It is unclear whether these data fail to add value to the results or if they remain unstudied.

Holistically, rapid-scan radar systems have made a substantial scientific impact on the understanding of convective processes, but the study of nonconvective processes have been limited. In addition to user bias, limited dual-polarization capabilities and sensitivity of prototype systems may have precluded the exploration of some topics, such as clear-air boundary layer studies or observations of snow. For example, Mahre et al. (2017) documented the evolution Kelvin–Helmholtz instability at the top of a cold front using 1-s RHI scans enabled by imaging, but limited sensitivity of the AIR prevented broader use for clear-air applications away from mesoscale boundaries with high insect concentrations (Wilson 1986; Wilson et al. 1994). Recently developed, dual-polarization radars with higher sensitivity than the prototype systems (Salazar et al. 2019; Asai et al. 2021; Kollias et al. 2022; Palmer et al. 2022; Torres and Wasiewlewski 2022), and the forthcoming Airborne Phased Array Radar (APAR; Vivekanandan et al. 2014; Joseph 2023) provide new opportunities to conduct first-of-its-kind, rapid-scan studies of many meteorological phenomena, particularly studies of turbulence in the convective boundary layer or in precipitating systems. For example, studies of orographic precipitation could benefit from rapidly collected observations to simultaneously capture effects of boundary layer turbulence or gravity waves on precipitation formation and hydrometeor growth. In addition, clear-air, rapid-scan observations could better quantify turbulence along mesoscale boundaries or in the convective boundary layer, and provide improved understanding of deep convection initiation mechanisms.

To conclude, the early generation of rapid-scan radars have provided appreciable insight into the characteristics of many rapidly evolving features, but research has largely been confined to convective phenomena and process-level scientific advancements have been limited by a lack of coordination with other observing platforms, as well as limited incorporation of theory and modeling. New rapid-scan technology with improved sensitivity and dual-polarization capabilities, as well as integration of rapid-scan radars in field experiments covering a greater breadth of meteorological phenomena, can enable more impactful research within the broader scientific community in the near future.

Acknowledgments. The authors are grateful for the expertise and detailed discussion of the manuscript provided by Jim Kurdzo, Katie Wilson, Corey Potvin, Addison Alford, Vanna Chmielewski, Zach Wienhoff, Patrick Skinner, Karen Kosiba, and Robert Palmer. The authors thank four reviewers and Editor David Schultz for helpful comments at the proposal stage of submission, providing high-level guidance to the manuscript. We also would like to thank the contributions of Chris Weiss, Howie Bluestein, Dusan Zrnić, and four anonymous reviewers for considerably improving the manuscript in review. In addition, we thank David Schultz for the work done overseeing the review and for providing additional guidance and thorough constructive comments. The authors thank participants in the Virtual Workshop on Atmospheric Science Applications of Ground-Based Radars for helpful discussion on the future of PAR technology. David Bodine was supported by National Science Foundation Grants AGS-1823478 and AGS-2114817. David Bodine was also partially supported by the NOAA/Office of Oceanic and Atmospheric Research under NOAA–University of Oklahoma Cooperative Agreement NA21OAR4320204, U.S. Department of Commerce.

Data availability statement. No original data were presented in this manuscript. However, interested readers may contact the authors for guidance on how to acquire datasets. For Advanced Radar Research Center (ARRC) managed radars (AIR and RaXPol), data can be acquired by contacting the lead author or submitting data requests through the ARRC's data email (data@arrc.ou.edu). Some freely downloadable datasets from the AIR are available at https://arrc.ou.edu/data.html.

REFERENCES

Adachi, T., and W. Mashiko, 2020: High temporal-spatial resolution observation of tornadogenesis in a shallow supercell associated with Typhoon Hagibis (2019) using phased array weather radar. *Geophys. Res. Lett.*, **47**, e2020GL089635, https://doi.org/10.1029/2020GL089635.

——, K. Kusunoki, S. Yoshida, K.-I. Arai, and T. Ushio, 2016: High-speed volumetric observations of a wet microburst using X-band phased array weather radar in Japan. *Mon. Wea. Rev.*, **144**, 3749–3765, https://doi.org/10.1175/MWR-D-16-0125.1.

Adams-Selin, R., and C. L. Ziegler, 2016: Forecasting hail using a one-dimensional hail growth model within WRF. *Mon. Wea. Rev.*, **144**, 4919–4939, https://doi.org/10.1175/MWR-D-16-0027.1.

Adlerman, E. J., and K. K. Droegemeier, 2002: The sensitivity of numerically simulated cyclic mesocyclogenesis to variations in physical and computational parameters. *Mon. Wea. Rev.*, **130**, 2671–2691, https://doi.org/10.1175/1520-0493(2002)130<2671:TSONSC>2.0.CO;2.

——, and ——, 2005: The dependence of numerically simulated cyclic mesocyclogenesis upon environmental vertical wind shear. *Mon. Wea. Rev.*, **133**, 3595–3623, https://doi.org/10.1175/MWR3039.1.

Alexander, C. R., 2010: A mobile radar based climatology of supercell tornado structures and dynamics. Ph.D. thesis, University of Oklahoma, 229 pp.

——, and J. Wurman, 2005: The 30 May 1998 Spencer, South Dakota storm. Part I: The structural evolution and environment of the tornadoes. *Mon. Wea. Rev.*, **133**, 72–97, https://doi.org/10.1175/MWR-2855.1.

Alford, A. A., M. I. Biggerstaff, G. D. Carrie, J. L. Schroeder, B. D. Hirth, and S. M. Waugh, 2019: Near-surface maximum winds during the landfall of Hurricane Harvey. *Geophys. Res. Lett.*, **46**, 973–982, https://doi.org/10.1029/2018GL080013.

——, J. A. Zhang, M. I. Biggerstaff, P. Dodge, F. D. Marks, and D. J. Bodine, 2020: Transition of the hurricane boundary layer during the landfall of Hurricane Irene (2011). *J. Atmos. Sci.*, **77**, 3509–3531, https://doi.org/10.1175/JAS-D-19-0290.1.

Allen, J. T., I. M. Giammanco, M. R. Kumjian, H. Jurgen Punge, Q. Zhang, P. Groenemeijer, M. Kunz, and K. Ortega, 2020:

Understanding hail in the Earth system. *Rev. Geophys.*, **58**, e2019RG000665, https://doi.org/10.1029/2019RG000665.

Asai, K., H. Kikuchi, T. Ushio, and Y. Hobara, 2021: Validation of X-band multiparameter phased-array weather radar by comparing data from Doppler weather radar with a parabolic dish antenna. *J. Atmos. Oceanic Technol.*, **38**, 1561–1570, https://doi.org/10.1175/JTECH-D-20-0213.1.

Ashley, S. T., and W. S. Ashley, 2008: Flood fatalities in the United States. *J. Appl. Meteor. Climatol.*, **47**, 805–818, https://doi.org/10.1175/2007JAMC1611.1.

Benjamin, S. G., and Coauthors, 2016: A North American hourly assimilation and model forecast cycle: The Rapid Refresh. *Mon. Wea. Rev.*, **144**, 1669–1694, https://doi.org/10.1175/MWR-D-15-0242.1.

Biggerstaff, M. I., Z. Zounes, A. A. Alford, G. D. Carrie, J. T. Pilkey, M. A. Uman, and D. M. Jordan, 2017: Flash propagation and inferred charge structure relative to radar-observed ice alignment signatures in a small Florida mesoscale convective system. *Geophys. Res. Lett.*, **44**, 8027–8036, https://doi.org/10.1002/2017GL074610.

Blair, S. F., and Coauthors, 2017: High-resolution hail observations: Implications for NWS warning operations. *Wea. Forecasting*, **32**, 1101–1119, https://doi.org/10.1175/WAF-D-16-0203.1.

Bluestein, H. B., C. C. Weiss, and A. L. Pazmany, 2003a: Mobile Doppler radar observations of a tornado in a supercell near Bassett, Nebraska, on 5 June 1999. Part I: Tornadogenesis. *Mon. Wea. Rev.*, **131**, 2954–2967, https://doi.org/10.1175/1520-0493(2003)131<2954:MDROOA>2.0.CO;2.

——, W.-C. Lee, M. Bell, C. C. Weiss, and A. L. Pazmany, 2003b: Mobile Doppler radar observations of a tornado in a supercell near Bassett, Nebraska, on 5 June 1999. Part II: Tornado-vortex structure. *Mon. Wea. Rev.*, **131**, 2968–2984, https://doi.org/10.1175/1520-0493(2003)131<2968:MDROOA>2.0.CO;2.

——, M. M. French, I. Popstefanija, R. T. Bluth, and J. B. Knorr, 2010: A mobile, phased-array Doppler radar for the study of severe convective storms: The MWR-05XP. *Bull. Amer. Meteor. Soc.*, **91**, 579–600, https://doi.org/10.1175/2009BAMS2914.1.

——, J. B. Houser, M. M. French, J. C. Snyder, G. D. Emmitt, I. PopStefanija, C. Baldi, and R. T. Bluth, 2014: Observations of the boundary layer near tornadoes and in supercells using a mobile, collocated, pulsed Doppler lidar and radar. *J. Atmos. Oceanic Technol.*, **31**, 302–325, https://doi.org/10.1175/JTECH-D-13-00112.1.

——, J. C. Snyder, and J. B. Houser, 2015: A multiscale overview of the El Reno, Oklahoma, tornadic supercell of 31 May 2013. *Wea. Forecasting*, **30**, 525–552, https://doi.org/10.1175/WAF-D-14-00152.1.

——, M. M. French, J. C. Snyder, and J. B. Houser, 2016: Doppler radar observations of anticyclonic tornadoes in cyclonically rotating, right-moving supercells. *Mon. Wea. Rev.*, **144**, 1591–1616, https://doi.org/10.1175/MWR-D-15-0304.1.

——, K. J. Thiem, J. C. Snyder, and J. B. Houser, 2018: The multiple-vortex structure of the El Reno, Oklahoma, tornado on 31 May 2013. *Mon. Wea. Rev.*, **146**, 2483–2502, https://doi.org/10.1175/MWR-D-18-0073.1.

——, ——, ——, and ——, 2019: Tornadogenesis and early tornado evolution in the El Reno, Oklahoma, supercell on 31 May 2013. *Mon. Wea. Rev.*, **147**, 2045–2066, https://doi.org/10.1175/MWR-D-18-0338.1.

——, F. H. Carr, and S. J. Goodman, 2022: Atmospheric observations of weather and climate. *Atmos.–Ocean*, **60**, 149–187, https://doi.org/10.1080/07055900.2022.2082369.

Bowden, K. A., and P. L. Heinselman, 2016: A qualitative analysis of NWS forecasters' use of phased-array radar data during severe hail and wind events. *Wea. Forecasting*, **31**, 43–55, https://doi.org/10.1175/WAF-D-15-0089.1.

——, ——, D. M. Kingfield, and R. P. Thomas, 2015: Impacts of phased-array radar data on forecaster performance during severe hail and wind events. *Wea. Forecasting*, **30**, 389–404, https://doi.org/10.1175/WAF-D-14-00101.1.

Brooks, H. E., and J. Correia Jr., 2018: Long-term performance metrics for National Weather Service tornado warnings. *Wea. Forecasting*, **33**, 1501–1511, https://doi.org/10.1175/WAF-D-18-0120.1.

Brothers, M. D., E. C. Bruning, and E. R. Mansell, 2018: Investigating the relative contributions of charge deposition and turbulence in organizing charge within a thunderstorm. *J. Atmos. Sci.*, **75**, 3265–3284, https://doi.org/10.1175/JAS-D-18-0007.1.

Brotzge, J., K. Hondl, B. Philips, L. Lemon, E. J. Bass, D. Rude, and D. L. Andra Jr., 2010: Evaluation of distributed collaborative adaptive sensing for detection of low-level circulations and implications for severe weather warning operations. *Wea. Forecasting*, **25**, 173–189, https://doi.org/10.1175/2009WAF2222233.1.

Brown, R. A., W. C. Bumgarner, K. C. Crawford, and D. Sirmans, 1971: Preliminary Doppler velocity measurements in a developing radar hook echo. *Bull. Amer. Meteor. Soc.*, **52**, 1186–1188, https://doi.org/10.1175/1520-0477(1971)052<1186:PDVMIA>2.0.CO;2.

——, L. R. Lemon, and D. W. Burgess, 1978: Tornado detection by pulsed Doppler radar. *Mon. Wea. Rev.*, **106**, 29–38, https://doi.org/10.1175/1520-0493(1978)106<0029:TDBPDR>2.0.CO;2.

——, B. A. Flickinger, E. Forren, D. M. Schultz, D. Sirmans, P. L. Spencer, V. T. Wood, and C. L. Ziegler, 2005: Improved detection of severe storms using experimental fine-resolution WSR-88D measurements. *Wea. Forecasting*, **20**, 3–14, https://doi.org/10.1175/WAF-832.1.

Bruning, E. C., and D. R. MacGorman, 2013: Theory and observations of controls on lightning flash size spectra. *J. Atmos. Sci.*, **70**, 4012–4029, https://doi.org/10.1175/JAS-D-12-0289.1.

Burgess, D. W., R. J. Donaldson Jr., T. Sieland, J. Hinkelman, D. Sirmans, K. Shreeve, K. Glover, and I. Goldman, 1979: Final report on the Joint Doppler Operational Project (JDOP) 1976–1979. NOAA Tech. Memo. ERL NSSL86, 84 pp.

——, V. T. Wood, and R. A. Brown, 1982: Mesocyclone evolution statistics. Preprints, *12th Conf. on Severe Local Storms*, San Antonio, TX, Amer. Meteor. Soc., 422–424.

Byers, H. R., and R. R. Braham Jr., 1948: Thunderstorm structure and circulation. *J. Atmos. Sci.*, **5**, 71–86, https://doi.org/10.1175/1520-0469(1948)005<0071:TSAC>2.0.CO;2.

Calhoun, K. M., D. R. MacGorman, C. L. Ziegler, and M. I. Biggerstaff, 2013: Evolution of lightning activity and storm charge relative to dual-Doppler analysis of a high-precipitation supercell storm. *Mon. Wea. Rev.*, **141**, 2199–2223, https://doi.org/10.1175/MWR-D-12-00258.1.

Capon, J., 1969: High-resolution frequency-wavenumber spectrum analysis. *Proc. IEEE*, **57**, 1408–1418, https://doi.org/10.1109/PROC.1969.7278.

Carbone, R. E., M. J. Carpenter, and C. D. Burghart, 1985: Doppler radar sampling limitations in convective storms. *J. Atmos. Oceanic Technol.*, **2**, 357–361, https://doi.org/10.1175/1520-0426(1985)002<0357:DRSLIC>2.0.CO;2.

Carlin, J. T., J. Gao, J. C. Snyder, and A. V. Ryzhkov, 2017: Assimilation of Z_{DR} columns for improving the spinup and forecast of convective storms in storm-scale models: Proof-of-

concept experiments. *Mon. Wea. Rev.*, **145**, 5033–5057, https://doi.org/10.1175/MWR-D-17-0103.1.

Caylor, I. J., and V. Chandrasekar, 1996: Time-varying ice crystal orientation in thunderstorms observed with multiparameter radar. *IEEE Trans. Geosci. Remote Sens.*, **34**, 847–858, https://doi.org/10.1109/36.508402.

Chandrasekar, V., R. Keranen, S. Lim, and D. Moisseev, 2013: Recent advances in classification of observations from dual polarization weather radars. *Atmos. Res.*, **119**, 97–111, https://doi.org/10.1016/j.atmosres.2011.08.014.

Chase, R. J., D. R. Harrison, A. Burke, G. M. Lackmann, and A. McGovern, 2022: A machine learning tutorial for operational meteorology. Part I: Traditional machine learning. *Wea. Forecasting*, **37**, 1509–1529, https://doi.org/10.1175/WAF-D-22-0070.1.

Chmielewski, V. C., D. R. MacGorman, C. L. Ziegler, E. DiGangi, D. Betten, and M. Biggerstaff, 2020: Microphysical and transportive contributions to normal and anomalous polarity subregions in the 29–30 May 2012 Kingfisher storm. *J. Geophys. Res. Atmos.*, **125**, e2020JD032384, https://doi.org/10.1029/2020JD032384.

Cho, J. Y. N., J. M. Kurdzo, B. J. Bennett, M. E. Weber, J. W. Dellicarpini, A. Locanto, and H. Frank, 2022: Impact of WSR-88D intra-volume low-level scans on severe weather warning performance. *Wea. Forecasting*, **37**, 1169–1189, https://doi.org/10.1175/WAF-D-21-0152.1.

Chronis, T., L. D. Carey, C. J. Schultz, E. V. Schultz, K. M. Calhoun, and S. J. Goodman, 2015: Exploring lightning jump characteristics. *Wea. Forecasting*, **30**, 23–37, https://doi.org/10.1175/WAF-D-14-00064.1.

Coffer, B. E., and M. D. Parker, 2017: Simulated supercells in nontornadic and tornadic VORTEX2 environments. *Mon. Wea. Rev.*, **145**, 149–180, https://doi.org/10.1175/MWR-D-16-0226.1.

——, ——, J. M. L. Dahl, L. J. Wicker, and A. J. Clark, 2017: Volatility of tornadogenesis: An ensemble of simulated nontornadic and tornadic supercells in VORTEX2 environments. *Mon. Wea. Rev.*, **145**, 4605–4625, https://doi.org/10.1175/MWR-D-17-0152.1.

——, ——, J. M. Peters, and A. R. Wade, 2023: Supercell low-level mesocyclones: Origins of inflow and vorticity. *Mon. Wea. Rev.*, **151**, 2205–2232, https://doi.org/10.1175/MWR-D-22-0269.1.

Conway, J. W., and D. S. Zrnić, 1993: A study of embryo production and hail growth using dual-Doppler and multiparameter radars. *Mon. Wea. Rev.*, **121**, 2511–2528, https://doi.org/10.1175/1520-0493(1993)121<2511:ASOEPA>2.0.CO;2.

Dahl, J. M. L., 2015: Near-ground rotation in simulated supercells: On the robustness of the baroclinic mechanism. *Mon. Wea. Rev.*, **143**, 4929–4942, https://doi.org/10.1175/MWR-D-15-0115.1.

——, 2021: Centrifugal waves in tornado-like vortices: Kelvin's solutions and their applications to multiple-vortex development and vortex breakdown. *Mon. Wea. Rev.*, **149**, 3173–3216, https://doi.org/10.1175/MWR-D-20-0426.1.

——, M. D. Parker, and L. J. Wicker, 2012: Uncertainties in trajectory calculations within near-surface mesocyclones of simulated supercells. *Mon. Wea. Rev.*, **140**, 2959–2966, https://doi.org/10.1175/MWR-D-12-00131.1.

——, ——, and ——, 2014: Imported and storm-generated near-ground vertical vorticity in a simulated supercell. *J. Atmos. Sci.*, **71**, 3027–3051, https://doi.org/10.1175/JAS-D-13-0123.1.

Dahl, N. A., A. Shapiro, C. K. Potvin, A. Theisen, J. G. Gebauer, A. D. Schenkman, and M. Xue, 2019: High-resolution, rapid-scan dual-Doppler retrievals of vertical velocity in a simulated supercell. *J. Atmos. Oceanic Technol.*, **36**, 1477–1500, https://doi.org/10.1175/JTECH-D-18-0211.1.

Dawson, D. T., II, E. R. Mansell, Y. Jung, L. J. Wicker, M. R. Kumjian, and M. Xue, 2014: Low-level Z_{DR} signatures in supercell forward flanks: The role of size sorting and melting of hail. *J. Atmos. Sci.*, **71**, 276–299, https://doi.org/10.1175/JAS-D-13-0118.1.

Deierling, W., W. A. Petersen, J. Latham, S. Ellis, and H. J. Christian, 2008: The relationship between lightning activity and ice fluxes in thunderstorms. *J. Geophys. Res.*, **113**, D15210, https://doi.org/10.1029/2007JD009700.

Dennis, E. J., and M. R. Kumjian, 2017: The impact of vertical wind shear on hail growth in simulated supercells. *J. Atmos. Sci.*, **74**, 641–663, https://doi.org/10.1175/JAS-D-16-0066.1.

Donaldson, R. J., Jr., 1970: Vortex signature recognition by a Doppler radar. *J. Appl. Meteor.*, **9**, 661–670, https://doi.org/10.1175/1520-0450(1970)009<0661:VSRBAD>2.0.CO;2.

Doviak, R. J., and D. S. Zrnić, 1993: *Doppler Radar and Weather Observations*. 2nd ed. Dover Publications, 592 pp., https://doi.org/10.1016/C2009-0-22358-0.

Dowell, D. C., and H. B. Bluestein, 2002a: The 8 June 1995 McLean, Texas, storm. Part I: Observations of cyclic tornadogenesis. *Mon. Wea. Rev.*, **130**, 2626–2648, https://doi.org/10.1175/1520-0493(2002)130<2626:TJMTSP>2.0.CO;2.

——, and ——, 2002b: The 8 June 1995 McLean, Texas, storm. Part II: Cyclic tornado formation, maintenance, and dissipation. *Mon. Wea. Rev.*, **130**, 2649–2670, https://doi.org/10.1175/1520-0493(2002)130<2649:TJMTSP>2.0.CO;2.

——, and A. Shapiro, 2003: Stability of an iterative dual-Doppler wind synthesis in Cartesian coordinates. *J. Atmos. Oceanic Technol.*, **20**, 1552–1559, https://doi.org/10.1175/1520-0426(2003)020<1552:SOAIDW>2.0.CO;2.

——, C. R. Alexander, J. M. Wurman, and L. J. Wicker, 2005: Centrifuging of hydrometeors and debris in tornadoes: Radar-reflectivity patterns and wind-measurement errors. *Mon. Wea. Rev.*, **133**, 1501–1524, https://doi.org/10.1175/MWR2934.1.

——, L. J. Wicker, and C. Snyder, 2011: Ensemble Kalman filter assimilation of radar observations of the 8 May 2003 Oklahoma City supercell: Influences of reflectivity observations on storm-scale analyses. *Mon. Wea. Rev.*, **139**, 272–294, https://doi.org/10.1175/2010MWR3438.1.

——, and Coauthors, 2022: The High-Resolution Rapid Refresh (HRRR): An hourly updating convection-allowing forecast model. Part I: Motivation and system description. *Wea. Forecasting*, **37**, 1371–1395, https://doi.org/10.1175/WAF-D-21-0151.1.

Emersic, C., P. L. Heinselman, D. R. MacGorman, and E. C. Bruning, 2011: Lightning activity in a hail-producing storm observed with phased-array radar. *Mon. Wea. Rev.*, **139**, 1809–1825, https://doi.org/10.1175/2010MWR3574.1.

Eure, K. C., P. D. Mykolajtchuk, Y. Zhang, D. J. Stensrud, F. Zhang, S. J. Greybush, and M. R. Kumjian, 2023: Simultaneous assimilation of planetary boundary layer observations from radar and all-sky satellite observations to improve forecasts of convection initiation. *Mon. Wea. Rev.*, **151**, 795–813, https://doi.org/10.1175/MWR-D-22-0188.1.

Fernández-Cabán, P. L., and Coauthors, 2019: Observing Hurricane Harvey's eyewall at landfall. *Bull. Amer. Meteor. Soc.*, **100**, 759–775, https://doi.org/10.1175/BAMS-D-17-0237.1.

Finley, C. A., M. Elmore, L. Orf, and B. D. Lee, 2023: Impact of the streamwise vorticity current on low-level mesocyclone development in a simulated supercell. *Geophys. Res. Lett.*, **50**, e2022GL100005, https://doi.org/10.1029/2022GL100005.

Fischer, J., and J. M. L. Dahl, 2022: Transition of near-ground vorticity dynamics during tornadogenesis. *J. Atmos. Sci.*, **79**, 467–483, https://doi.org/10.1175/JAS-D-21-0181.1.

French, M. M., and D. M. Kingfield, 2021: Tornado formation and intensity prediction using polarimetric radar estimates of updraft area. *Wea. Forecasting*, **36**, 2211–2231, https://doi.org/10.1175/WAF-D-21-0087.1.

——, H. B. Bluestein, I. PopStefanija, C. A. Baldi, and R. T. Bluth, 2013: Reexamining the vertical development of tornadic vortex signatures in supercells. *Mon. Wea. Rev.*, **141**, 4576–4601, https://doi.org/10.1175/MWR-D-12-00315.1.

——, ——, ——, ——, and ——, 2014: Mobile, phased-array, Doppler radar observations of tornadoes at X band. *Mon. Wea. Rev.*, **142**, 1010–1036, https://doi.org/10.1175/MWR-D-13-00101.1.

——, P. S. Skinner, L. J. Wicker, and H. B. Bluestein, 2015: Documenting a rare tornado merger observed in the 24 May 2011 El Reno–Piedmont, Oklahoma, supercell. *Mon. Wea. Rev.*, **143**, 3025–3043, https://doi.org/10.1175/MWR-D-14-00349.1.

Fridlind, A. M., and Coauthors, 2019: Use of polarimetric radar measurements to constrain simulated convective cell evolution: A pilot study with Lagrangian tracking. *Atmos. Meas. Tech.*, **12**, 2979–3000, https://doi.org/10.5194/amt-12-2979-2019.

Gao, J., M. Xue, K. Brewster, and K. K. Droegemeier, 2004: A three-dimensional variational data analysis method with recursive filter for Doppler radars. *J. Atmos. Oceanic Technol.*, **21**, 457–469, https://doi.org/10.1175/1520-0426(2004)021<0457:ATVDAM>2.0.CO;2.

Gebauer, J. G., A. Shapiro, C. K. Potvin, N. A. Dahl, M. I. Biggerstaff, and A. A. Alford, 2022: Evaluating vertical velocity retrievals from vertical vorticity equation constrained dual-Doppler analysis of real, rapid-scan radar data. *J. Atmos. Oceanic Technol.*, **39**, 1591–1610, https://doi.org/10.1175/JTECH-D-21-0136.1.

Geerts, B., and Coauthors, 2018: Recommendations for in situ and remote sensing capabilities in atmospheric convection and turbulence. *Bull. Amer. Meteor. Soc.*, **99**, 2463–2470, https://doi.org/10.1175/BAMS-D-17-0310.1.

Giammanco, I. M., B. R. Maiden, H. E. Estes, and T. M. Brown-Giammanco, 2017: Using 3D laser scanning technology to create digital models of hailstones. *Bull. Amer. Meteor. Soc.*, **98**, 1341–1347, https://doi.org/10.1175/BAMS-D-15-00314.1.

Goodman, S. J., and Coauthors, 2005: The North Alabama lightning mapping array: Recent severe storm observations and future prospects. *Atmos. Res.*, **76**, 423–437, https://doi.org/10.1016/j.atmosres.2004.11.035.

Griffin, C. B., D. J. Bodine, J. M. Kurdzo, A. Mahre, and R. D. Palmer, 2019: High-temporal resolution observations of the 27 May 2015 Canadian, Texas, tornado using the Atmospheric Imaging Radar. *Mon. Wea. Rev.*, **147**, 873–891, https://doi.org/10.1175/MWR-D-18-0297.1.

Guerra, J. E., P. S. Skinner, A. Clark, M. Flora, B. Matilla, K. Knopfmeier, and A. E. Reinhart, 2022: Quantification of NSSL Warn-on-Forecast System accuracy by storm age using object-based verification. *Wea. Forecasting*, **37**, 1973–1983, https://doi.org/10.1175/WAF-D-22-0043.1.

Heinselman, P. L., and S. Torres, 2011: High-temporal-resolution capabilities of the national weather radar testbed phased-array radar. *J. Appl. Meteor. Climatol.*, **50**, 579–593, https://doi.org/10.1175/2010JAMC2588.1.

——, D. L. Priegnitz, K. L. Manross, T. M. Smith, and R. W. Adams, 2008: Rapid sampling of severe storms by the national weather radar testbed phased array radar. *Wea. Forecasting*, **23**, 808–824, https://doi.org/10.1175/2008WAF2007071.1.

——, D. S. LaDue, and H. Lazrus, 2012: Exploring impacts of rapid-scan radar data on NWS warning decisions. *Wea. Forecasting*, **27**, 1031–1044, https://doi.org/10.1175/WAF-D-11-00145.1.

——, ——, D. M. Kingfield, and R. Hoffman, 2015: Tornado warning decisions using phased-array radar data. *Wea. Forecasting*, **30**, 57–78, https://doi.org/10.1175/WAF-D-14-00042.1.

Hendry, A., and G. C. McCormick, 1976: Radar observations of the alignment of precipitation particles by electrostatic fields in thunderstorms. *J. Geophys. Res.*, **81**, 5353–5357, https://doi.org/10.1029/JC081i030p05353.

Houser, J. L., H. B. Bluestein, and J. C. Snyder, 2015: Rapid-scan, polarimetric, Doppler radar observations of tornadogenesis and tornado dissipation in a tornadic supercell: The "El Reno, Oklahoma" storm of 24 May 2011. *Mon. Wea. Rev.*, **143**, 2685–2710, https://doi.org/10.1175/MWR-D-14-00253.1.

——, ——, and ——, 2016: A finescale radar examination of the tornadic debris signature and weak-echo reflectivity band associated with a large, violent tornado. *Mon. Wea. Rev.*, **144**, 4101–4130, https://doi.org/10.1175/MWR-D-15-0408.1.

——, ——, K. Thiem, J. Snyder, D. Reif, and Z. Wienhoff, 2022: Additional evaluation of the spatiotemporal evolution of rotation during tornadogenesis using rapid-scan mobile radar observations. *Mon. Wea. Rev.*, **150**, 1639–1666, https://doi.org/10.1175/MWR-D-21-0227.1.

Hu, M., and M. Xue, 2007: Impact of configurations of rapid intermittent assimilation of WSR-88D radar data for the 8 May 2003 Oklahoma City tornadic thunderstorm case. *Mon. Wea. Rev.*, **135**, 507–525, https://doi.org/10.1175/MWR3313.1.

Huang, Y., X. Wang, C. Kerr, A. Mahre, T.-Y. Yu, and D. Bodine, 2020: Impact of assimilating future clear-air radial velocity observations from phased-array radar on a supercell thunderstorm forecast: An observing system simulation experiment study. *Mon. Wea. Rev.*, **148**, 3825–3845, https://doi.org/10.1175/MWR-D-19-0391.1.

Isoda, F., S. Satoh, and T. Ushio, 2018: Temporal and spatial characteristics of localized rainfall on 26 July 2012 observed by phased array weather radar. *SOLA*, **14**, 64–68, https://doi.org/10.2151/sola.2018-011.

Isom, B., and Coauthors, 2013: The atmospheric imaging radar: Simultaneous volumetric observations using a phased array weather radar. *J. Atmos. Oceanic Technol.*, **30**, 655–675, https://doi.org/10.1175/JTECH-D-12-00063.1.

Jensen, M. P., and Coauthors, 2022: A succession of cloud, precipitation, aerosol, and air quality field experiments in the coastal urban environment. *Bull. Amer. Meteor. Soc.*, **103**, 103–105, https://doi.org/10.1175/BAMS-D-21-0104.1.

Jones, T. A., and Coauthors, 2020: Assimilation of *GOES-16* radiances and retrievals into the Warn-on-Forecast System. *Mon. Wea. Rev.*, **148**, 1829–1859, https://doi.org/10.1175/MWR-D-19-0379.1.

Joseph, E. D., 2023: Airborne Phased Array Radar (APAR): The next generation of airborne polarimetric Doppler weather radar. *40th Conf. on Radar Meteorology*, Minneapolis, MN, Amer. Meteor. Soc., 17.2, https://ams.confex.com/ams/40RADAR/meetingapp.cgi/Paper/430065.

Kennedy, P. C., and S. A. Rutledge, 2011: S-band dual-polarization radar observations of winter storms. *J. Appl. Meteor. Climatol.*, **50**, 844–858, https://doi.org/10.1175/2010JAMC2558.1.

Kerr, C. A., and X. Wang, 2020: Ensemble-based targeted observation method applied to radar radial velocity observations on idealized supercell low-level rotation forecasts: A proof of concept. *Mon. Wea. Rev.*, **148**, 877–890, https://doi.org/10.1175/MWR-D-19-0197.1.

Kingfield, D. M., and J. G. LaDue, 2015: The relationship between automated low-level velocity calculations from the WSR-88D and maximum tornado intensity determined from damage surveys. *Wea. Forecasting*, **30**, 1125–1139, https://doi.org/10.1175/WAF-D-14-00096.1.

——, and M. M. French, 2022: The influence of WSR-88D intravolume scanning strategies on thunderstorm observations and warnings in the dual-polarization radar era: 2011–20. *Wea. Forecasting*, **37**, 283–301, https://doi.org/10.1175/WAF-D-21-0127.1.

Koch, S. E., M. desJardins, and P. J. Kocin, 1983: An interactive Barnes objective map analysis scheme for use with satellite and conventional data. *J. Appl. Meteor.*, **22**, 1487–1503, https://doi.org/10.1175/1520-0450(1983)022<1487:AIBOMA>2.0.CO;2.

Kollias, P., D. McLaughlin, S. Frasier, M. Oue, E. Luke, and A. Sneddon, 2018: Advances and applications in low-power phased array X-band weather radars. *2018 IEEE Radar Conf. (RadarConf18)*, Oklahoma City, OK, Institute of Electrical and Electronics Engineers, 1359–1364, https://doi.org/10.1109/RADAR.2018.8378762.

——, E. Luke, M. Oue, and K. Lamer, 2020: Agile adaptive radar sampling of fast-evolving atmospheric phenomena guided by satellite imagery and surface cameras. *Geophys. Res. Lett.*, **47**, e2020GL088440, https://doi.org/10.1029/2020GL088440.

——, and Coauthors, 2022: Science applications of phased array radars. *Bull. Amer. Meteor. Soc.*, **103**, E2370–E2390, https://doi.org/10.1175/BAMS-D-21-0173.1.

Kosiba, K., and J. Wurman, 2013: The three-dimensional structure and evolution of a tornado boundary layer. *Wea. Forecasting*, **28**, 1552–1561, https://doi.org/10.1175/WAF-D-13-00070.1.

——, ——, F. J. Masters, and P. Robinson, 2013a: Mapping of near-surface winds in Hurricane Rita using finescale radar, anemometer, and land-use data. *Mon. Wea. Rev.*, **141**, 4337–4349, https://doi.org/10.1175/MWR-D-12-00350.1.

——, ——, Y. Richardson, P. Markowski, P. Robinson, and J. Marquis, 2013b: Genesis of the Goshen County, Wyoming, tornado on 5 June 2009 during VORTEX2. *Mon. Wea. Rev.*, **141**, 1157–1181, https://doi.org/10.1175/MWR-D-12-00056.1.

Krajewski, W. F., G. J. Ciach, and E. Habib, 2003: An analysis of small-scale rainfall variability in different climatic regimes. *Hydrol. Sci. J.*, **48**, 151–162, https://doi.org/10.1623/hysj.48.2.151.44694.

Krehbiel, P., T. Chen, S. McCrary, W. Rison, G. Gray, and M. Brook, 1996: The use of dual channel circular-polarization radar observations for remotely sensing storm electrification. *Meteor. Atmos. Phys.*, **59**, 65–82, https://doi.org/10.1007/BF01032001.

Kristovich, D. A. R., and Coauthors, 2017: The Ontario winter lake-effect systems field campaign: Scientific and educational adventures to further our knowledge and prediction of lake-effect storms. *Bull. Amer. Meteor. Soc.*, **98**, 315–332, https://doi.org/10.1175/BAMS-D-15-00034.1.

Kumjian, M. R., 2013: Principles and applications of dual-polarization weather radar. Part I: Description of the polarimetric radar variables. *J. Oper. Meteor.*, **1**, 226–242, https://doi.org/10.15191/nwajom.2013.0119.

——, and A. V. Ryzhkov, 2008: Polarimetric signatures in supercell thunderstorms. *J. Appl. Meteor. Climatol.*, **47**, 1940–1961, https://doi.org/10.1175/2007JAMC1874.1.

——, and ——, 2009: Storm-relative helicity revealed from polarimetric radar measurements. *J. Atmos. Sci.*, **66**, 667–685, https://doi.org/10.1175/2008JAS2815.1.

——, and ——, 2010: The impact of evaporation on polarimetric characteristics of rain: Theoretical model and practical implications. *J. Appl. Meteor. Climatol.*, **49**, 1247–1267, https://doi.org/10.1175/2010JAMC2243.1.

——, ——, V. M. Melnikov, and T. J. Schuur, 2010: Rapid-scan super-resolution observations of a cyclic supercell with a dual-polarization WSR-88D. *Mon. Wea. Rev.*, **138**, 3762–3786, https://doi.org/10.1175/2010MWR3322.1.

——, S. A. Rutledge, R. M. Rasmussen, P. C. Kennedy, and M. Dixon, 2014: High-resolution polarimetric radar observations of snow-generating cells. *J. Appl. Meteor. Climatol.*, **53**, 1636–1658, https://doi.org/10.1175/JAMC-D-13-0312.1.

——, K. Lombardo, and S. Loeffler, 2021: The evolution of hail production in simulated supercell storms. *J. Atmos. Sci.*, **78**, 3417–3440, https://doi.org/10.1175/JAS-D-21-0034.1.

——, O. P. Prat, K. J. Reimel, M. van Lier-Walqui, and H. C. Morrison, 2022: Dual-polarization radar fingerprints of precipitation physics: A review. *Remote Sens.*, **14**, 3706, https://doi.org/10.3390/rs14153706.

Kurdzo, J. M., D. J. Bodine, B. L. Cheong, and R. D. Palmer, 2015: High-temporal resolution polarimetric X-band Doppler radar observations of the 20 May 2013 Moore, Oklahoma, tornado. *Mon. Wea. Rev.*, **143**, 2711–2735, https://doi.org/10.1175/MWR-D-14-00357.1.

——, and Coauthors, 2017: Observations of severe local storms and tornadoes with the Atmospheric Imaging Radar. *Bull. Amer. Meteor. Soc.*, **98**, 915–935, https://doi.org/10.1175/BAMS-D-15-00266.1.

Kuster, C. M., P. L. Heinselman, and T. J. Schuur, 2016: Rapid-update radar observations of downbursts occurring within an intense multicell thunderstorm on 14 June 2011. *Wea. Forecasting*, **31**, 827–851, https://doi.org/10.1175/WAF-D-15-0081.1.

——, J. C. Snyder, T. J. Schuur, T. T. Lindley, P. L. Heinselman, J. C. Furtado, J. W. Brogden, and R. Toomey, 2019: Rapid-update radar observations of Z_{DR} column depth and its use in the warning decision process. *Wea. Forecasting*, **34**, 1173–1188, https://doi.org/10.1175/WAF-D-19-0024.1.

Lemon, L. R., and C. A. Doswell III, 1979: Severe thunderstorm evolution and mesocyclone structure as related to tornadogenesis. *Mon. Wea. Rev.*, **107**, 1184–1197, https://doi.org/10.1175/1520-0493(1979)107<1184:STEAMS>2.0.CO;2.

Leslie, L. M., 1971: The development of concentrated vortices: A numerical study. *J. Fluid Mech.*, **48**, 1–21, https://doi.org/10.1017/S0022112071001435.

Lewellen, D. C., W. S. Lewellen, and J. Xia, 2000: The influence of a local swirl ratio on tornado intensification near the surface. *J. Atmos. Sci.*, **57**, 527–544, https://doi.org/10.1175/1520-0469(2000)057<0527:TIOALS>2.0.CO;2.

Lewellen, W. S., D. C. Lewellen, and R. I. Sykes, 1997: Large-eddy simulation of a tornado's interaction with the surface. *J. Atmos. Sci.*, **54**, 581–605, https://doi.org/10.1175/1520-0469(1997)054<0581:LESOAT>2.0.CO;2.

Ligda, M. G. H., 1950: Lightning detection by radar. *Bull. Amer. Meteor. Soc.*, **31**, 279–283, https://doi.org/10.1175/1520-0477-31.8.279.

Liou, Y.-C., H. B. Bluestein, M. M. French, and Z. B. Wienhoff, 2018: Single-Doppler velocity retrieval of the wind field in a

tornadic supercell using mobile, phased-array, Doppler radar data. *J. Atmos. Oceanic Technol.*, **35**, 1649–1663, https://doi.org/10.1175/JTECH-D-18-0004.1.

Lu, H., and Q. Xu, 2009: Trade-offs between measurement accuracy and resolutions in configuring phased-array radar velocity scans for ensemble-based storm-scale data assimilation. *J. Appl. Meteor. Climatol.*, **48**, 1230–1244, https://doi.org/10.1175/2008JAMC2009.1.

MacGorman, D. R., W. D. Rust, P. R. Krehbiel, W. Rison, E. Bruning, and K. Wiens, 2005: The electrical structure of two supercell storms during STEPS. *Mon. Wea. Rev.*, **133**, 2583–2607, https://doi.org/10.1175/MWR2994.1.

Mahale, V. N., J. A. Brotzge, and H. B. Bluestein, 2012: An analysis of vortices embedded within a quasi-linear convective system using X-band polarimetric radar. *Wea. Forecasting*, **27**, 1520–1537, https://doi.org/10.1175/WAF-D-11-00135.1.

Mahre, A., T.-Y. Yu, R. D. Palmer, and J. M. Kurdzo, 2017: Observations of a cold front at high spatiotemporal resolution using an X-band phased array imaging radar. *Atmosphere*, **8**, 30, https://doi.org/10.3390/atmos8020030.

——, J. M. Kurdzo, D. J. Bodine, C. B. Griffin, R. D. Palmer, and T.-Y. Yu, 2018: Analysis of the 16 May 2015 Tipton, Oklahoma, EF-3 tornado at high spatiotemporal resolution using the Atmospheric Imaging Radar. *Mon. Wea. Rev.*, **146**, 2103–2124, https://doi.org/10.1175/MWR-D-17-0256.1.

Majcen, M., P. Markowski, Y. Richardson, D. Dowell, and J. Wurman, 2008: Multipass objective analyses of Doppler radar data. *J. Atmos. Oceanic Technol.*, **25**, 1845–1858, https://doi.org/10.1175/2008JTECHA1089.1.

Marion, G. R., R. J. Trapp, and S. W. Nesbitt, 2019: Using overshooting top area to discriminate potential for large, intense tornadoes. *Geophys. Res. Lett.*, **46**, 12 520–12 526, https://doi.org/10.1029/2019GL084099.

Markowski, P. M., 2002: Hook echoes and rear-flank downdrafts: A review. *Mon. Wea. Rev.*, **130**, 852–876, https://doi.org/10.1175/1520-0493(2002)130<0852:HEARFD>2.0.CO;2.

——, 2016: An idealized numerical simulation investigation of the effects of surface drag on the development of near-surface vertical vorticity in supercell thunderstorms. *J. Atmos. Sci.*, **73**, 4349–4385, https://doi.org/10.1175/JAS-D-16-0150.1.

——, and Coauthors, 2012a: The pretornadic phase of the Goshen County, Wyoming, supercell of 5 June 2009 intercepted by VORTEX2. Part I: Evolution of kinematic and surface thermodynamic fields. *Mon. Wea. Rev.*, **140**, 2887–2915, https://doi.org/10.1175/MWR-D-11-00336.1.

——, and Coauthors, 2012b: The pretornadic phase of the Goshen County, Wyoming, supercell of 5 June 2009 intercepted by VORTEX2. Part II: Intensification of low-level rotation. *Mon. Wea. Rev.*, **140**, 2916–2938, https://doi.org/10.1175/MWR-D-11-00337.1.

Marquis, J. M., Y. Richardson, P. Markowski, D. Dowell, and J. Wurman, 2012: Tornado maintenance investigated with high-resolution dual-Doppler and EnKF analysis. *Mon. Wea. Rev.*, **140**, 3–27, https://doi.org/10.1175/MWR-D-11-00025.1.

Marshall, J. S., W. Hitschfeld, and K. L. S. Gunn, 1955: Advances in radar weather. *Advances in Geophysics*, Vol. 2, Academic Press, 1–56, https://doi.org/10.1016/S0065-2687(08)60310-6.

McCormick, G. C., and A. Hendry, 1975: Principles for the radar determination of the polarization properties of precipitation. *Radio Sci.*, **10**, 421–434, https://doi.org/10.1029/RS010i004p00421.

McKeown, K. E., M. M. French, K. S. Tuftedal, D. M. Kingfield, H. B. Bluestein, D. W. Reif, and Z. B. Wienhoff, 2020: Rapid-scan and polarimetric radar observations of the dissipation of a violent tornado on 9 May 2016 near Sulphur, Oklahoma. *Mon. Wea. Rev.*, **148**, 3951–3971, https://doi.org/10.1175/MWR-D-20-0033.1.

McLaughlin, D., and Coauthors, 2009: Short-wavelength technology and the potential for distributed networks of small radar systems. *Bull. Amer. Meteor. Soc.*, **90**, 1797–1818, https://doi.org/10.1175/2009BAMS2507.1.

McMurdie, L. A., and Coauthors, 2022: Chasing snowstorms: The Investigation of Microphysics and Precipitation for Atlantic Coast-Threatening Snowstorms (IMPACTS) campaign. *Bull. Amer. Meteor. Soc.*, **103**, E1243–E1269, https://doi.org/10.1175/BAMS-D-20-0246.1.

Miller, R. L., C. L. Ziegler, and M. I. Biggerstaff, 2020: Seven-Doppler radar and in situ analysis of the 25–26 June 2015 Kansas MCS during PECAN. *Mon. Wea. Rev.*, **148**, 211–240, https://doi.org/10.1175/MWR-D-19-0151.1.

Miyoshi, T., and Coauthors, 2016: "Big data assimilation" revolutionizing severe weather prediction. *Bull. Amer. Meteor. Soc.*, **97**, 1347–1354, https://doi.org/10.1175/BAMS-D-15-00144.1.

Montgomery, M. T., and R. J. Kallenbach, 1997: A theory for vortex Rossby-waves and its application to spiral bands and intensity changes in hurricanes. *Quart. J. Roy. Meteor. Soc.*, **123**, 435–465, https://doi.org/10.1002/qj.49712353810.

Moroda, Y., K. Tsuboki, S. Satoh, K. Nakagawa, T. Ushio, and S. Shimizu, 2021: Structure and evolution of precipitation cores in an isolated convective storm observed by phased array weather radar. *J. Meteor. Soc. Japan*, **99**, 765–784, https://doi.org/10.2151/jmsj.2021-038.

——, ——, ——, ——, ——, and H. Kikuchi, 2022: Lightning bubbles caused by upward reflectivity pulses above precipitation cores of a thundercloud. *SOLA*, **18**, 110–115, https://doi.org/10.2151/sola.2022-018.

Morrison, I., S. Businger, F. Marks, P. Dodge, and J. A. Businger, 2005: An observational case for the prevalence of roll vortices in the hurricane boundary layer. *J. Atmos. Sci.*, **62**, 2662–2673, https://doi.org/10.1175/JAS3508.1.

Murdzek, S. S., P. M. Markowski, and Y. P. Richardson, 2020: Simultaneous dual-Doppler and mobile mesonet observations of streamwise vorticity currents in three supercells. *Mon. Wea. Rev.*, **148**, 4859–4874, https://doi.org/10.1175/MWR-D-20-0239.1.

Murillo, E. M., and C. R. Homeyer, 2019: Severe hail fall and hailstorm detection using remote sensing observations. *J. Appl. Meteor. Climatol.*, **58**, 947–970, https://doi.org/10.1175/JAMC-D-18-0247.1.

Nai, F., S. Torres, and R. Palmer, 2013: Adaptive beamforming for weather observations using the Atmospheric Imaging Radar. *2013 IEEE Int. Symp. on Phased Array Systems and Technology*, Waltham, MA, Institute of Electrical and Electronics Engineers, 709–713, https://doi.org/10.1109/ARRAY.2013.6731917.

National Academies of Science, Engineering, and Medicine, 2018: *Thriving on Our Changing Planet: A Decadal Strategy for Earth Observation from Space*. The National Academies Press, 716 pp., https://doi.org/10.17226/24938.

National Research Council, 2002: *Weather Radar Technology beyond NEXRAD*. The National Academies Press, 97 pp., https://doi.org/10.17226/10394.

Newman, J. F., and P. L. Heinselman, 2012: Evolution of a quasi-linear convective system sampled by phased array radar. *Mon. Wea. Rev.*, **140**, 3467–3486, https://doi.org/10.1175/MWR-D-12-00003.1.

Nguyen, C. M., and V. Chandrasekar, 2017: Electronic scan strategy for phased array weather radar using a space-time characterization model. *J. Atmos. Oceanic Technol.*, **34**, 921–938, https://doi.org/10.1175/JTECH-D-16-0021.1.

Nixon, C. J., and J. T. Allen, 2021: Anticipating deviant tornado motion using a simple hodograph technique. *Wea. Forecasting*, **36**, 219–235, https://doi.org/10.1175/WAF-D-20-0056.1.

NOAA, 2020: Report to Congress—Weather radar follow on plan: Research and risk reduction to inform acquisition decisions. NOAA Tech. Rep., 21 pp., https://www.nssl.noaa.gov/publications/par_reports/RadarFollowOnPlan_ReporttoCongress_2020June_Final.pdf.

Nolan, D. S., 2012: Three-dimensional instabilities in tornado-like vortices with secondary circulations. *J. Fluid Mech.*, **711**, 61–100, https://doi.org/10.1017/jfm.2012.369.

NWS, 2015: NOAA/National Weather Service radar functional requirements. NOAA Tech. Rep., 58 pp., https://www.roc.noaa.gov/WSR88D/PublicDocs/NOAA_Radar_Functional_Requirements_Final_Sept%202015.pdf.

Nystuen, J. A., 1998: Temporal sampling requirements for automatic rain gauges. *J. Atmos. Oceanic Technol.*, **15**, 1253–1260, https://doi.org/10.1175/1520-0426(1998)015<1253:TSRFAR>2.0.CO;2.

Orf, L., 2019: A violently tornadic supercell thunderstorm simulation spanning a quarter-trillion grid volumes: Computational challenges, I/O framework, and visualizations of tornadogenesis. *Atmosphere*, **10**, 578, https://doi.org/10.3390/atmos10100578.

——, R. Wilhelmson, B. Lee, C. Finley, and A. Houston, 2017: Evolution of a long-track violent tornado within a simulated supercell. *Bull. Amer. Meteor. Soc.*, **98**, 45–68, https://doi.org/10.1175/BAMS-D-15-00073.1.

Orlanski, I., 1975: A rational subdivision of scales for atmospheric processes. *Bull. Amer. Meteor. Soc.*, **56**, 527–530, https://doi.org/10.1175/1520-0477-56.5.527.

Ortega, K. L., 2018: Evaluating multi-radar, multi-sensor products for surface hailfall diagnosis. *Electron. J. Severe Storms Meteor.*, **13** (1), https://ejssm.com/ojs/index.php/site/article/view/69.

——, T. Smith, K. L. Manross, K. A. Scharfenberg, A. Witt, A. G. Kolodziej, and J. J. Gourley, 2009: The Severe Hazards Analysis and Verification Experiment. *Bull. Amer. Meteor. Soc.*, **90**, 1519–1530, https://doi.org/10.1175/2009BAMS2815.1.

——, J. M. Krause, and A. V. Ryzhkov, 2016: Polarimetric radar characteristics of melting hail. Part III: Validation of the algorithm for hail size discrimination. *J. Appl. Meteor. Climatol.*, **55**, 829–848, https://doi.org/10.1175/JAMC-D-15-0203.1.

Orzel, K. A., and S. J. Frasier, 2018: Weather observation by an electronically scanned dual-polarization phase-tilt radar. *IEEE Trans. Geosci. Remote Sens.*, **56**, 2722–2734, https://doi.org/10.1109/TGRS.2017.2782480.

Otsuka, S., and Coauthors, 2016: Precipitation nowcasting with three-dimensional space–time extrapolation of dense and frequent phased-array weather radar observations. *Wea. Forecasting*, **31**, 329–340, https://doi.org/10.1175/WAF-D-15-0063.1.

Oue, M., P. Kollias, A. Shapiro, A. Tatarevic, and T. Matsui, 2019: Investigation of observational error sources in multi-Doppler-radar three-dimensional variational vertical air motion retrievals. *Atmos. Meas. Tech.*, **12**, 1999–2018, https://doi.org/10.5194/amt-12-1999-2019.

Palmer, R. D., and Coauthors, 2022: A primer on phased array radar technology for the atmospheric sciences. *Bull. Amer. Meteor. Soc.*, **103**, E2391–E2416, https://doi.org/10.1175/BAMS-D-21-0172.1.

Parker, M. D., 2023: How well must surface vorticity be organized for tornadogenesis? *J. Atmos. Sci.*, **80**, 1433–1448, https://doi.org/10.1175/JAS-D-22-0195.1.

Pazmany, A. L., J. B. Mead, H. B. Bluestein, J. C. Snyder, and J. B. Houser, 2013: A mobile rapid-scanning X-band polarimetric (RaXPol) Doppler radar system. *J. Atmos. Oceanic Technol.*, **30**, 1398–1413, https://doi.org/10.1175/JTECH-D-12-00166.1.

Potvin, C. K., A. Shapiro, and M. Xue, 2012a: Impact of a vertical vorticity constraint in variational dual-Doppler wind analysis: Tests with real and simulated supercell data. *J. Atmos. Oceanic Technol.*, **29**, 32–49, https://doi.org/10.1175/JTECH-D-11-00019.1.

——, L. J. Wicker, and A. Shapiro, 2012b: Assessing errors in variational dual-Doppler wind syntheses of supercell thunderstorms observed by storm-scale mobile radars. *J. Atmos. Oceanic Technol.*, **29**, 1009–1025, https://doi.org/10.1175/JTECH-D-11-00177.1.

Qiu, X., Q. Xu, C. Qiu, K. Nai, and P. Zhang, 2013: Retrieving 3D wind field from phased array radar rapid scans. *Adv. Meteor.*, **2013**, 792631, https://doi.org/10.1155/2013/792631.

Ray, P. S., C. L. Ziegler, W. Bumgarner, and R. J. Serafin, 1980: Single- and multiple-Doppler radar observations of tornadic storms. *Mon. Wea. Rev.*, **108**, 1607–1625, https://doi.org/10.1175/1520-0493(1980)108<1607:SAMDRO>2.0.CO;2.

Roberts, R. D., and J. W. Wilson, 1989: A proposed microburst nowcasting procedure using single-Doppler radar. *J. Appl. Meteor.*, **28**, 285–303, https://doi.org/10.1175/1520-0450(1989)028<0285:APMNPU>2.0.CO;2.

Rotunno, R., P. M. Markowski, and G. H. Bryan, 2017: "Near ground" vertical vorticity in supercell thunderstorm models. *J. Atmos. Sci.*, **74**, 1757–1766, https://doi.org/10.1175/JAS-D-16-0288.1.

Ryzhkov, A. V., M. R. Kumjian, S. M. Ganson, and P. Zhang, 2013: Polarimetric radar characteristics of melting hail. Part II: Practical implications. *J. Appl. Meteor. Climatol.*, **52**, 2871–2886, https://doi.org/10.1175/JAMC-D-13-074.1.

Salazar, J. L., and Coauthors, 2019: An ultra-fast scan C-band Polarimetric Atmospheric Imaging Radar (PAIR). *2019 IEEE Int. Symp. on Phased Array System and Technology (PAST)*, Waltham, MA, Institute of Electrical and Electronics Engineers, 1–5, https://doi.org/10.1109/PAST43306.2019.9021042.

Sandmæl, T. N., and Coauthors, 2023: The tornado probability algorithm: A probablistic machine learning tornadic circulation detection algorithm. *Wea. Forecasting*, **38**, 445–466, https://doi.org/10.1175/WAF-D-22-0123.1.

Satrio, C. N., D. J. Bodine, R. D. Palmer, and C. M. Kuster, 2021: Multi-radar analysis of the 20 May 2013 Moore, Oklahoma supercell through tornadogenesis and intensification. *Atmosphere*, **12**, 313, https://doi.org/10.3390/atmos12030313.

Saunders, C., 2008: Charge separation mechanisms in clouds. *Space Sci. Rev.*, **137**, 335–353, https://doi.org/10.1007/s11214-008-9345-0.

Scharfenberg, K. A., and Coauthors, 2005: The Joint Polarization Experiment: Polarimetric radar in forecasting and warning decision-making. *Wea. Forecasting*, **20**, 775–788, https://doi.org/10.1175/WAF881.1.

Schneider, M., D. J. Bodine, B. Cheong, and D. Schvartzman, 2023: Rapid-scan radar observations of two QLCSs during the PERiLS 2023 field campaign. *40th Conf. on Radar Meteorology*, Minneapolis, MN, Amer. Meteor. Soc., 102, https://ams.confex.com/ams/40RADAR/meetingapp.cgi/Paper/426268.

Schueth, A., C. Weiss, and J. M. L. Dahl, 2021: Comparing observations and simulations of the streamwise vorticity current

and the forward-flank convergence boundary in a supercell storm. *Mon. Wea. Rev.*, **149**, 1651–1671, https://doi.org/10.1175/MWR-D-20-0251.1.

Schultz, C. J., W. A. Petersen, and L. D. Carey, 2009: Preliminary development and evaluation of lightning jump algorithms for the real-time detection of severe weather. *J. Appl. Meteor. Climatol.*, **48**, 2543–2563, https://doi.org/10.1175/2009JAMC2237.1.

——, L. D. Carey, E. V. Schultz, and R. J. Blakeslee, 2015: Insight into the kinematic and microphysical processes that control lightning jumps. *Wea. Forecasting*, **30**, 1591–1621, https://doi.org/10.1175/WAF-D-14-00147.1.

Seimon, A., J. T. Allen, T. A. Seimon, S. J. Talbot, and D. K. Hoadley, 2016: Crowdsourcing the El Reno 2013 tornado: A new approach for collation and display of storm chaser imagery for scientific applications. *Bull. Amer. Meteor. Soc.*, **97**, 2069–2084, https://doi.org/10.1175/BAMS-D-15-00174.1.

Shapiro, A., P. Robinson, J. Wurman, and J. Gao, 2003: Single-Doppler velocity retrieval with rapid-scan radar data. *J. Atmos. Oceanic Technol.*, **20**, 1758–1775, https://doi.org/10.1175/1520-0426(2003)020<1758:SVRWRR>2.0.CO;2.

——, C. K. Potvin, and J. Gao, 2009: Use of a vertical vorticity equation in variational dual-Doppler wind analysis. *J. Atmos. Oceanic Technol.*, **26**, 2089–2106, https://doi.org/10.1175/2009JTECHA1256.1.

——, K. M. Willingham, and C. K. Potvin, 2010a: Spatially variable advection correction of radar data. Part I: Theoretical considerations. *J. Atmos. Sci.*, **67**, 3445–3456, https://doi.org/10.1175/2010JAS3465.1.

——, ——, and ——, 2010b: Spatially variable advection correction of radar data. Part II: Test results. *J. Atmos. Sci.*, **67**, 3457–3470, https://doi.org/10.1175/2010JAS3466.1.

Skolnik, M. I., 2001: *Introduction to Radar Systems*. 3rd ed. McGraw-Hill, 772 pp.

Smith, R. K., and L. M. Leslie, 1979: A numerical study of tornadogenesis in rotating thunderstorm. *Quart. J. Roy. Meteor. Soc.*, **105**, 107–127, https://doi.org/10.1002/qj.49710544308.

Snyder, J. C., and H. B. Bluestein, 2014: Some considerations for the use of high-resolution mobile radar data in tornado intensity determination. *Wea. Forecasting*, **29**, 799–827, https://doi.org/10.1175/WAF-D-14-00026.1.

——, and A. V. Ryzhkov, 2015: Automated detection of polarimetric tornadic debris signatures using a hydrometeor classification algorithm. *J. Appl. Meteor. Climatol.*, **54**, 1861–1870, https://doi.org/10.1175/JAMC-D-15-0138.1.

Soderholm, J. S., M. R. Kumjian, N. McCarthy, P. Maldonado, and M. Wang, 2020: Quantifying hail size distributions from the sky—Application of drone aerial photogrammetry. *Atmos. Meas. Tech.*, **13**, 747–754, https://doi.org/10.5194/amt-13-747-2020.

Souza, J. C. S., and E. C. Bruning, 2021: Assessment of turbulent intensity in different spots of lightning flash propagation. *Geophys. Res. Lett.*, **48**, e2021GL095923, https://doi.org/10.1029/2021GL095923.

Srivastava, R. C., 1987: A model of intense downdrafts driven by the melting and evaporation of precipitation. *J. Atmos. Sci.*, **44**, 1752–1774, https://doi.org/10.1175/1520-0469(1987)044<1752:AMOIDD>2.0.CO;2.

Stensrud, D. J., and J. Gao, 2010: Importance of horizontally inhomogeneous environmental initial conditions to ensemble storm-scale radar data assimilation and very short-range forecasts. *Mon. Wea. Rev.*, **138**, 1250–1272, https://doi.org/10.1175/2009MWR3027.1.

——, and Coauthors, 2013: Progress and challenges with warn-on-forecast. *Atmos. Res.*, **123**, 2–16, https://doi.org/10.1016/j.atmosres.2012.04.004.

Stough, S. M., L. D. Carey, C. J. Schultz, and D. J. Cecil, 2022: Supercell thunderstorm charge structure variability and influences on spatial lightning flash relationships with the updraft. *Mon. Wea. Rev.*, **150**, 843–861, https://doi.org/10.1175/MWR-D-21-0071.1.

Straka, J. M., D. S. Zrnić, and A. V. Ryzhkov, 2000: Bulk hydrometeor classification and quantification using polarimetric radar data: Synthesis of relations. *J. Appl. Meteor.*, **39**, 1341–1372, https://doi.org/10.1175/1520-0450(2000)039<1341:BHCAQU>2.0.CO;2.

Stratman, D. R., N. Yussouf, Y. Jung, T. A. Supinie, M. Xue, P. S. Skinner, and B. J. Putnam, 2020: Optimal temporal frequency of NSSL phased array radar observation for an experimental Warn-on-Forecast System. *Wea. Forecasting*, **35**, 193–214, https://doi.org/10.1175/WAF-D-19-0165.1.

Stuart, N. A., and Coauthors, 2022: The evolving role of humans in weather prediction and communication. *Bull. Amer. Meteor. Soc.*, **103**, E1720–E1746, https://doi.org/10.1175/BAMS-D-20-0326.1.

Sun, J., 2005: Convective-scale assimilation of radar data: Progress and challenges. *Quart. J. Roy. Meteor. Soc.*, **131**, 3439–3463, https://doi.org/10.1256/qj.05.149.

——, and Coauthors, 2014: Use of NWP for nowcasting convective precipitation: Recent progress and challenges. *Bull. Amer. Meteor. Soc.*, **95**, 409–426, https://doi.org/10.1175/BAMS-D-11-00263.1.

Supinie, T. A., N. Yussouf, Y. Jung, M. Xue, J. Cheng, and S. Wang, 2017: Comparison of the analyses and forecasts of a tornadic supercell storm from assimilating phased-array radar and WSR-88D observations. *Wea. Forecasting*, **32**, 1379–1401, https://doi.org/10.1175/WAF-D-16-0159.1.

Takahashi, T., 1978: Riming electrification as a charge generation mechanism in thunderstorms. *J. Atmos. Sci.*, **35**, 1536–1548, https://doi.org/10.1175/1520-0469(1978)035<1536:REAACG>2.0.CO;2.

Tanamachi, R. L., and P. L. Heinselman, 2016: Rapid-scan, polarimetric observations of central Oklahoma severe storms on 31 May 2013. *Wea. Forecasting*, **31**, 19–42, https://doi.org/10.1175/WAF-D-15-0111.1.

——, H. B. Bluestein, J. B. Houser, S. J. Frasier, and K. M. Hardwick, 2012: Mobile X-band, polarimetric Doppler radar observations of the 4 May 2007 Greensburg, Kansas, tornadic supercell. *Mon. Wea. Rev.*, **140**, 2103–2125, https://doi.org/10.1175/MWR-D-11-00142.1.

——, ——, M. Xue, W.-C. Lee, K. A. Orzel, S. J. Frasier, and R. M. Wakimoto, 2013: Near-surface vortex structure in a tornado and in a sub-tornado-strength convective-storm vortex 1934 observed by a mobile, W-band radar during VORTEX2. *Mon. Wea. Rev.*, **141**, 3661–3690, https://doi.org/10.1175/MWR-D-12-00331.1.

——, P. L. Heinselman, and L. J. Wicker, 2015: Impacts of a storm merger on the 24 May 2011 El Reno, Oklahoma, tornadic supercell. *Wea. Forecasting*, **30**, 501–524, https://doi.org/10.1175/WAF-D-14-00164.1.

Torres, S., and D. Wasiewlewski, 2022: The advanced technology demonstrator at the National Severe Storms Laboratory: Challenges and successes. *2022 IEEE Radar Conf. (RadarConf22)*, New York, NY, Institute of Electrical and Electronics Engineers, 1–6, https://doi.org/10.1109/RadarConf2248738.2022.9764231.

Toth, M., R. J. Trapp, J. Wurman, and K. A. Kosiba, 2013: Comparison of mobile-radar measurements of tornado intensity with corresponding WSR-88D measurements. *Wea. Forecasting*, **28**, 418–426, https://doi.org/10.1175/WAF-D-12-00019.1.

Trapp, R. J., and R. Davies-Jones, 1997: Tornadogenesis with and without a dynamic pipe effect. *J. Atmos. Sci.*, **54**, 113–133, https://doi.org/10.1175/1520-0469(1997)054<0113:TWAWAD>2.0.CO;2.

——, and C. A. Doswell III, 2000: Radar data objective analysis. *J. Atmos. Oceanic Technol.*, **17**, 105–120, https://doi.org/10.1175/1520-0426(2000)017<0105:RDOA>2.0.CO;2.

——, E. D. Mitchell, G. A. Tipton, D. W. Effertz, A. I. Watson, D. L. Andra Jr., and M. A. Magsig, 1999: Descending and nondescending tornadic vortex signatures detected by WSR-88Ds. *Wea. Forecasting*, **14**, 625–639, https://doi.org/10.1175/1520-0434(1999)014<0625:DANTVS>2.0.CO;2.

Vivekanandan, J., S. M. Ellis, R. Oye, D. S. Zrnić, A. V. Ryzhkov, and J. Straka, 1999: Cloud microphysics retrieval using S-band dual-polarization radar measurements. *Bull. Amer. Meteor. Soc.*, **80**, 381–388, https://doi.org/10.1175/1520-0477(1999)080<0381:CMRUSB>2.0.CO;2.

——, W.-C. Lee, E. Loew, J. L. Salazar, V. Grubisic, J. Moore, and P. Tsai, 2014: The next generation airborne polarimetric Doppler weather radar. *Geosci. Instrum. Methods Data Syst.*, **3**, 111–126, https://doi.org/10.5194/gi-3-111-2014.

Wakimoto, R. M., and V. N. Bringi, 1988: Dual-polarization observations of microbursts associated with intense convection: The 20 July storm during the MIST project. *Mon. Wea. Rev.*, **116**, 1521–1539, https://doi.org/10.1175/1520-0493(1988)116<1521:DPOOMA>2.0.CO;2.

——, and B. E. Martner, 1992: Observations of a Colorado tornado. Part II: Combined photogrammetric and Doppler radar analysis. *Mon. Wea. Rev.*, **120**, 522–543, https://doi.org/10.1175/1520-0493(1992)120<0522:OOACTP>2.0.CO;2.

——, and R. Srivastava, Eds., 2003: *Radar and Atmospheric Science: A Collection of Essays in Honor of David Atlas. Meteor. Monogr.*, No. 52, Amer. Meteor. Soc., 270 pp.

——, and Coauthors, 2016: Aerial damage survey of the 2013 El Reno tornado combined with mobile radar data. *Mon. Wea. Rev.*, **144**, 1749–1776, https://doi.org/10.1175/MWR-D-15-0367.1.

Wang, S., M. Xue, and J. Min, 2013: A four-dimensional asynchronous ensemble square-root filter (4DEnSRF) algorithm and tests with simulated radar data. *Quart. J. Roy. Meteor. Soc.*, **139**, 805–819, https://doi.org/10.1002/qj.1987.

——, Y. Wada, S. Hayashi, T. Ushio, and V. Chandrasekar, 2023: Signatures of vertical ice particles orientation before IC lightning flash initiation observed by X-band dual polarized phased array weather radar. *40th Conf. on Radar Meteorology*, Minneapolis, MN, Amer. Meteor. Soc., 10A.3, https://ams.confex.com/ams/40RADAR/meetingapp.cgi/Paper/426139.

Ward, N. B., 1972: The exploration of certain features of tornado dynamics using a laboratory model. *J. Atmos. Sci.*, **29**, 1194–1204, https://doi.org/10.1175/1520-0469(1972)029<1194:TEOCFO>2.0.CO;2.

Weber, M., J. Y. N. Cho, J. S. Herd, J. M. Flavin, W. E. Benner, and G. S. Torok, 2007: The next-generation multimission U.S. surveillance radar network. *Bull. Amer. Meteor. Soc.*, **88**, 1739–1752, https://doi.org/10.1175/BAMS-88-11-1739.

——, and Coauthors, 2021: Toward the next generation operational meteorological radar. *Bull. Amer. Meteor. Soc.*, **102**, E1357–E1383, https://doi.org/10.1175/BAMS-D-20-0067.1.

Weinheimer, A. J., and A. A. Few, 1987: The electric field alignment of ice particles in thunder-storms. *J. Geophys. Res.*, **92**, 14 833–14 844, https://doi.org/10.1029/JD092iD12p14833.

Weiss, C. C., 2009: The TTUKa mobile Doppler radar: Coordinated radar and in situ measurements of supercell thunderstorms during project VORTEX2. *34th Conf. on Radar Meteorology*, Williamsburg, VA, Amer. Meteor. Soc., 11B.2, https://ams.confex.com/ams/34Radar/techprogram/paper_155425.htm.

——, D. C. Dowell, J. L. Schroder, P. S. Skinner, A. E. Reinhart, P. M. Markowski, and Y. P. Richardson, 2015: A comparison of near-surface buoyancy and baroclinity across three VORTEX2 supercell intercepts. *Mon. Wea. Rev.*, **143**, 2736–2753, https://doi.org/10.1175/MWR-D-14-00307.1.

Wen, Y., T. Schuur, H. Vergara, and C. Kuster, 2021: Effect of precipitation sampling error on flash flood monitoring and prediction: Anticipating operational rapid-update polarimetric weather radars. *J. Hydrometeor.*, **22**, 1913–1929, https://doi.org/10.1175/JHM-D-19-0286.1.

Wheatley, D. M., K. H. Knopfmeier, T. A. Jones, and G. J. Creager, 2015: Storm-scale data assimilation and ensemble forecasting with the NSSL experimental Warn-on-Forecast System. Part I: Radar data experiments. *Wea. Forecasting*, **30**, 1795–1817, https://doi.org/10.1175/WAF-D-15-0043.1.

Wicker, L. J., and R. B. Wilhelmson, 1995: Simulation and analysis of tornado development and decay within a three-dimensional thunderstorm. *J. Atmos. Sci.*, **52**, 2675–2703, https://doi.org/10.1175/1520-0469(1995)052<2675:SAAOTD>2.0.CO;2.

Wienhoff, Z. B., H. B. Bluestein, L. J. Wicker, J. C. Snyder, A. Shapiro, C. K. Potvin, J. B. Houser, and D. W. Reif, 2018: Applications of a spatially variable advection correction technique for temporal correction of dual-Doppler analyses of tornadic supercells. *Mon. Wea. Rev.*, **146**, 2949–2971, https://doi.org/10.1175/MWR-D-17-0360.1.

——, ——, D. W. Reif, R. M. Wakimoto, L. J. Wicker, and J. M. Kurdzo, 2020: Analysis of debris signature characteristics and evolution in the 24May 2016 Dodge City, Kansas, tornadoes. *Mon. Wea. Rev.*, **148**, 5063–5086, https://doi.org/10.1175/MWR-D-20-0162.1.

Williams, E. R., and Coauthors, 1999: The behavior of total lightning activity in severe Florida thunderstorms. *Atmos. Res.*, **51**, 245–265, https://doi.org/10.1016/S0169-8095(99)00011-3.

——, M. E. Weber, and R. E. Orville, 1989: Relationship between lightning type and convective state of thunderclouds. *J. Geophys. Res.*, **94**, 13 213–13 220, https://doi.org/10.1029/JD094iD11p13213.

Wilson, J. W., 1986: Tornadogenesis by nonprecipitation induced wind shear lines. *Mon. Wea. Rev.*, **114**, 270–284, https://doi.org/10.1175/1520-0493(1986)114<0270:TBNIWS>2.0.CO;2.

——, R. D. Roberts, C. Kessinger, and J. McCarthy, 1984: Microburst wind structure and evaluation of Doppler radar for airport wind shear detection. *J. Climate Appl. Meteor.*, **23**, 898–915, https://doi.org/10.1175/1520-0450(1984)023<0898:MWSAEO>2.0.CO;2.

——, T. M. Weckwerth, J. Vivekanandan, R. M. Wakimoto, and R. W. Russell, 1994: Boundary layer clear-air radar echoes: Origin of echoes and accuracy of derived winds. *J. Atmos. Oceanic Technol.*, **11**, 1184–1206, https://doi.org/10.1175/1520-0426(1994)011<1184:BLCARE>2.0.CO;2.

Wilson, K. A., P. L. Heinselman, and C. M. Kuster, 2017a: Considerations for phased-array radar data use within the National Weather Service. *Wea. Forecasting*, **32**, 1959–1965, https://doi.org/10.1175/WAF-D-17-0084.1.

——, ——, ——, D. M. Kingfield, and Z. Kang, 2017b: Forecaster performance and workload: Does radar update time matter? *Wea. Forecasting*, **32**, 253–274, https://doi.org/10.1175/WAF-D-16-0157.1.

Wingo, S. M., and K. R. Knupp, 2016: Kinematic structure of mesovortices in the eyewall of Hurricane Ike (2008) derived from ground-based dual-Doppler analysis. *Mon. Wea. Rev.*, **144**, 4245–4263, https://doi.org/10.1175/MWR-D-16-0085.1.

Witt, A., D. W. Burgress, A. Seimon, J. T. Allen, J. C. Snyder, and H. B. Bluestein, 2018: Rapid-scan radar observations of an Oklahoma tornadic hailstorm producing giant hail. *Wea. Forecasting*, **33**, 1263–1282, https://doi.org/10.1175/WAF-D-18-0003.1.

Wood, V. T., and R. A. Brown, 1997: Effects of radar sampling on single-Doppler velocity signatures of mesocyclones and tornadoes. *Wea. Forecasting*, **12**, 928–938, https://doi.org/10.1175/1520-0434(1997)012<0928:EORSOS>2.0.CO;2.

Wu, L., Q. Liu, and Y. Li, 2018: Prevalance of tornado-scale vortices in the tropical cyclone eyewall. *Proc. Natl. Acad. Sci. USA*, **115**, 8307–8310, https://doi.org/10.1073/pnas.1807217115.

Wurman, J., 2002: The multiple-vortex structure of a tornado. *Wea. Forecasting*, **17**, 473–505, https://doi.org/10.1175/1520-0434(2002)017<0473:TMVSOA>2.0.CO;2.

——, and J. Winslow, 1998: Intense sub-kilometer-scale boundary layer rolls observed in Hurricane Fran. *Science*, **280**, 555–557, https://doi.org/10.1126/science.280.5363.555.

——, and S. Gill, 2000: Fine-scale radar observations of the Dimmitt, Texas (2 June 1995), tornado. *Mon. Wea. Rev.*, **128**, 2135–2164, https://doi.org/10.1175/1520-0493(2000)128<2135:FROOTD>2.0.CO;2.

——, and M. Randall, 2001: An inexpensive, mobile, rapid-scan radar. *30th Int. Conf. on Radar Meteorology*, Munich, Germany, Amer. Meteor. Soc., P3.4, https://ams.confex.com/ams/30radar/webprogram/Paper21577.html.

——, and K. Kosiba, 2018: The role of small-scale vortices in enhancing surface winds and damage in Hurricane Harvey (2017). *Mon. Wea. Rev.*, **146**, 713–722, https://doi.org/10.1175/MWR-D-17-0327.1.

——, J. M. Straka, and E. N. Rasmussen, 1996: Fine-scale Doppler radar observations of tornadoes. *Science*, **272**, 1774–1777, https://doi.org/10.1126/science.272.5269.1774.

——, Y. Richardson, C. Alexander, S. Weygandt, and P.-F. Zhang, 2007: Dual-Doppler and single-Doppler analysis of a tornadic storm undergoing mergers and repeated tornadogenesis. *Mon. Wea. Rev.*, **135**, 736–758, https://doi.org/10.1175/MWR3276.1.

——, P. Robinson, C. R. Alexander, K. A. Kosiba, and W. Lee, 2008: Rapid-scan mobile radar 3D GBVTD and traditional analysis of tornadogenesis. *24th Conf. on Severe Local Storms*, Savannah, GA, Amer. Meteor. Soc., P13.6, https://ams.confex.com/ams/24SLS/webprogram/Paper142176.html.

——, D. Dowell, Y. Richardson, P. Markowski, E. Rasmussen, D. Burgess, L. Wicker, and H. B. Bluestein, 2012: The Second Verification of the Origins of Rotation in Tornadoes Experiment: VORTEX2. *Bull. Amer. Meteor. Soc.*, **93**, 1147–1170, https://doi.org/10.1175/BAMS-D-11-00010.1.

——, K. Kosiba, and P. Robinson, 2013: In situ, Doppler radar, and video observations of the interior structure of a tornado and the wind–damage relationship. *Bull. Amer. Meteor. Soc.*, **94**, 835–846, https://doi.org/10.1175/BAMS-D-12-00114.1.

——, ——, ——, and T. Marshall, 2014: The role of multiple-vortex tornado structure in causing storm researcher fatalities. *Bull. Amer. Meteor. Soc.*, **95**, 31–45, https://doi.org/10.1175/BAMS-D-13-00221.1.

——, and Coauthors, 2021: The Flexible Array of Radars and Mesonets (FARM). *Bull. Amer. Meteor. Soc.*, **102**, E1499–E1525, https://doi.org/10.1175/BAMS-D-20-0285.1.

Xue, M., M. Tong, and K. K. Droegemeier, 2006: An OSSE framework based on the ensemble square root Kalman filter for evaluating the impact of data from radar networks on thunderstorm analysis and forecasting. *J. Atmos. Oceanic Technol.*, **23**, 46–66, https://doi.org/10.1175/JTECH1835.1.

Yao, D., Z. Meng, and M. Xue, 2019: Genesis, maintenance and demise of a simulated tornado and the evolution of its preceding descending reflectivity core (DRC). *Atmosphere*, **10**, 236, https://doi.org/10.3390/atmos10050236.

Yeary, M., R. Palmer, C. Fulton, J. Salazar, and H. Sigmarsson, 2021: Update on an S-band all-digital mobile phased array radar. *2021 IEEE Radar Conf. (RadarConf21)*, Atlanta, GA, Institute of Electrical and Electronics Engineers, 1–4, https://doi.org/10.1109/RadarConf2147009.2021.9455287.

Yoshida, S., T. Adachi, K. Kusunoki, S. Hayashi, T. Wu, T. Ushio, and E. Yoshikawa, 2017: Relationship between thunderstorm electrification and storm kinetics revealed by phased array whether radar. *J. Geophys. Res. Atmos.*, **122**, 3821–3836, https://doi.org/10.1002/2016JD025947.

Yoshikawa, E., T. Ushio, Z. Kawasaki, S. Yoshida, T. Morimoto, F. Mizutani, and M. Wada, 2013: MMSE beam forming on fast-scanning phased array weather radar. *IEEE Trans. Geosci. Remote Sens.*, **51**, 3077–3088, https://doi.org/10.1109/TGRS.2012.2211607.

Yu, T.-Y., D. Schvartzman, M.-D. Tzeng, D. J. Bodine, E. C. Bruning, V. C. Chimielewski, and M. Stock, 2023: High temporal resolution observations of cloud electrification with spectral polarimetry. *40th Conf. on Radar Meteorology*, Minneapolis, MN, Amer. Meteor. Soc., 43, https://ams.confex.com/ams/40RADAR/meetingapp.cgi/Paper/426167.

Yussouf, N., and D. J. Stensrud, 2010: Impact of phased-array radar observations over a short assimilation period: Observing system simulation experiments using an ensemble Kalman filter. *Mon. Wea. Rev.*, **138**, 517–538, https://doi.org/10.1175/2009MWR2925.1.

Zhang, F., C. Snyder, and J. Sun, 2004: Impacts of initial estimate and observation availability on convective-scale data assimilation with an ensemble Kalman filter. *Mon. Wea. Rev.*, **132**, 1238–1253, https://doi.org/10.1175/1520-0493(2004)132<1238:IOIEAO>2.0.CO;2.

Zhang, G., R. J. Doviak, D. S. Zrnić, R. Palmer, L. Lei, and Y. Al-Rashid, 2011: Polarimetric phased-array radar for weather measurement: A planar or cylindrical configuration? *J. Atmos. Oceanic Technol.*, **28**, 63–73, https://doi.org/10.1175/2010JTECHA1470.1.

Zhang, Y., F. Zhang, and D. J. Stensrud, 2018: Assimilating all-sky infrared radiances from *GOES-16* ABI using an ensemble Kalman filter for convection-allowing severe thunderstorms prediction. *Mon. Wea. Rev.*, **146**, 3363–3381, https://doi.org/10.1175/MWR-D-18-0062.1.

——, D. J. Stensrud, and F. Zhang, 2019: Simultaneous assimilation of radar and all-sky satellite infrared radiance observations for convection-allowing ensemble analysis and prediction of severe thunderstorms. *Mon. Wea. Rev.*, **147**, 4389–4409, https://doi.org/10.1175/MWR-D-19-0163.1.

Zrnić, D. S., and Coauthors, 2007: Agile-beam phased array radar for weather observations. *Bull. Amer. Meteor. Soc.*, **88**, 1753–1766, https://doi.org/10.1175/BAMS-88-11-1753.